# Decentralized Cross-layer Congestion Controls for DSRC-V2X and PC5-based Cellular-V2X Mode 4 in Crash Warning System

HIRAI Takeshi

# Abstract

Decentralized vehicle-to-everything (V2X) potentially supports various road traffic problems, like traffic accidents and traffic jams. Such V2X is applied to the crash warning system (CWS) to assist drivers in intelligent transportation systems (ITS) for *smart mobility*. In CWS, each node (e.g., a car or a pedestrian with V2X equipment) periodically broadcasts its data frames, including its location, speed, and direction. CWS warns the user based on its potential crash risks estimated from the received information. CWS requires reliable V2X communications to obtain enough frames for accurate warnings; in other words, the frame reception reliability of V2X plays a key role in using CWS practically. CWS can cover nodes in blind spots of existing sensors under the requirements, like radars and cameras. Thus, CWS improves mobility safety levels.

Two decentralized V2X standards have been actively studied: dedicated short range communications (DSRC) and PC5-based cellular-V2X mode 4 (called mode 4). These protocols have random access protocols in their medium access control (MAC) layer without any infrastructures, like base stations. This infrastructure-less characteristic strongly supports CWS in the early deployment stages because communication costs with base stations and implementing base stations are unnecessary to use the V2X technologies anywhere. DSRC implements a basic random access protocol, carrier sense multiple access with collision avoidance (CSMA/CA), and mode 4 implements an advanced random access protocol, sensing-based semi-persistent scheduling (SPS). Mode 4 provides more reliable communications than DSRC. In contrast, mode 4 commercially consumes higher costs than DSRC because the standard is still being developed. Practically, adopted technologies depend on industry requirements or every country's networks. For these reasons, advancing both protocols are necessary.

However, such V2X potentially experiences a channel congestion problem. Such a problem occurs in crowded environments, like intersections. The problem causes frame collision errors more frequently than in non-congested cases, and as a result, CWS may fail to satisfy its CWS requirements. Some related works focused on channel congestion as follows. Few related works have focused on the congestion problem considering the number of obtained frames required in CWS; in particular, no related works have evaluated the performance characteristics of mode 4 under its channel congestion by CWS requirements. Some related works also proposed the decentralized congestion control (DCC) for V2X. Unfortunately, most of the existing DCC methods reduce the number of transmitted frames to mitigate channel congestion. The mechanism efficiently decreases frame collision errors but also reduces the number of received frames per node. As a result, no related works have essentially addressed channel congestion in the use-cases of CWS. Mitigating channel congestion is necessary to use CWS practically.

The author studies the channel congestion problem of the decentralized V2X in this

paper. To this end, the author challenges the following three contents: proposing a congestion control for DSRC, evaluating the performance of mode 4 under channel congestion in CWS, and proposing a congestion control for mode 4. The proposed congestion controls focus on improving the random access mechanisms without decreasing the number of obtained frames, unlike the existing congestion control methods. The author then proposes cross-layer approaches for the congestion controls, i.e., decentralized cross-layer congestion controls; for example, the author focuses on application-MAC cross-layer approaches and physical-MAC cross-layer approaches for the V2X standards.

First, the author proposes a node-clustering method for DSRC, CLASES, which incorporates the application layer with the MAC layer. In CLASES, multiple nodes form a cluster, and then only each cluster head transmits frames of all the cluster members on behalf of members; data in frames of the members comply with estimated data from their past frames. The proposed method enables nodes to access the V2X channel efficiently and thus mitigates channel congestion. The simulation results highlighted that CLASES improved 27% better performance under channel congestion than the current DSRC. In summary, this research contributes to improving V2X performance without reducing the amount of information under the DSRC channel congestion through the efficient node-clustering method for CWS use-cases.

Second, this paper presents the performance degradation of mode 4 due to channel congestion. The author evaluates the performance in both fundamental and realistic node density, strongly related to the channel congestion. Through the simulations, mode 4 achieved 55% lower performance than the required performance at a large intersection. These results supported that mode 4 needs congestion controls. In summary, this study contributes to revealing performance characteristics under channel congestion and highlighting performance degradation of the current mode 4, compared with the CWS requirements.

Finally, the author proposes a method with the non-orthogonal multiple access (NOMA) for mode 4, called DB-NOMA, a physical-MAC cross-layer congestion control. DB-NOMA contains two methods. One of them is a frame relaying method using NOMA. In the proposed relaying method, each node broadcasts its own frame and the relayed frame of another node in a downlink NOMA manner. The other is a parallel transmission using NOMA, called SPS-NOMA. In SPS-NOMA, each node selects a spectrum resource based on sensing-based SPS, a suitable resource selection for NOMA. Then, multiple nodes simultaneously transmit their frames in an uplink NOMA manner. NOMA supports multiple nodes to access a spectrum resource at the same time and thus mitigates channel congestion. The proposed relaying method improved 94% better performance than the current mode 4. SPS-NOMA also boosted 38% better performance than the current mode 4. In summary, this research contributes to proposing NOMA for the decentralized V2X and mitigating the channel congestion problem of mode 4 while keeping the amount of information.

Through this paper, the author contributes to mitigating the congestion problem of CWS without decreasing the amount of information and extending decentralized congestion controls for both V2X standards to cross-layer congestion controls. First, the author demonstrated that the proposed methods supported more wide CWS use-cases without reducing the amount of information, unlike the existing DCC approach. Second, this paper strongly supports next-generation wireless networks, like the fifth-generation (5G) V2X networks, through studying advanced node-clustering method and decentralized NOMA. The proposed congestion controls are also expected to support other networks for *Smart city*.

# Contents

# Contents of Figures

# Contents of Tables

# I. Introduction

## 1. Background

Mobility and transportation have experienced various problems, including traffic accidents (or crashes) and road traffic jams [1]–[3]. These problems cause us to decrease the quality of life, like safety, relief, and comfort, in mobility and transportation. These problems have been seen over the world. For example, Reference [3] reported that traffic accidents caused 3500 deaths every day and 1.27 million deaths every year. Reference [1] also reported that traffic congestion caused a loss of US$2.8 billion per year economically. These reports have highlighted that we have faced serious problems for people over the world.

## 2. Intelligent Transportation Systems and Vehicle-to-Everything Communications

For solving such various road traffic problems, intelligent transportation systems (ITS) [4]–[7] have actively been developed in a part of *smart city*. *Smart city* is a concept to introduce information and communication technologies (ICT) in various situations. In ITS, vehicle-to-everything (V2X) plays a key ICT role in various systems [4], like Fig. 1. V2X strongly advanced *smart mobility*. For instance, driver assistance systems improve mobility and transportation [8]–[12]. Autonomous driving realizes safety and comfortable mobility. Here, V2X includes various communications, like vehicle-to-vehicle (V2V), vehicle-to-pedestrian (V2P), and vehicle-to-infrastructure (V2I).

One of the important ITS applications has been the crash warning system (CWS) with V2X [8]–[12]. In CWS, each node (e.g., a car or a pedestrian with V2X equipment) periodically advertises its state data (e.g., its location, speed, and direction) in broadcast mode. Each of the data is conveyed in a data frame (called a frame). After receiving

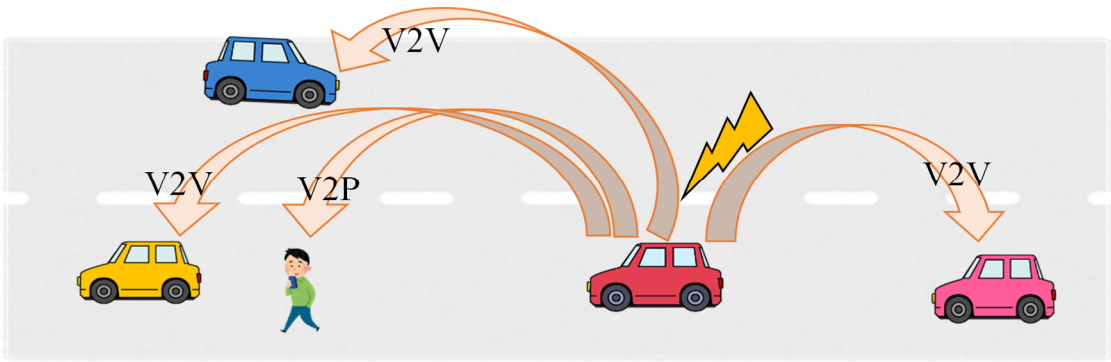


Fig. 1 A relationship between ITS and V2X and an example of V2X.

frames from a node, CWS calculates a potential crash risk between itself and the node. If the risk is higher than a threshold, CWS warns its user, such as drivers or pedestrians. In CWS, V2X can detect nodes in blind spots of sensors, like cameras or radars. These detections boost the safety of mobility. CWS requires enough amount of information to detect nodes in real-time. Some works have presented the requirements about the amount of information [9]–[12]; specifically, CWS needs a frame reception reliability, like 10 received frames per second for each node, or a frame reception ratio of 90% or more in 10 transmitted frames.

In V2X technologies, decentralized V2X plays a key role [13]–[40]. Such decentralized V2X supports device-to-device (D2D) communications without additional infrastructures, like base stations. Such decentralized V2X implements ITS applications earlier than centralized V2X [41] to require no additional infrastructures in wide areas. Decentralized V2X currently includes dedicated short range communications (DSRC) [13]–[21] [35] and PC5-based cellular-V2X mode 4 (C-V2X mode 4), called mode 4 in the followings [22]–[34] [36]–[40]. Each of these protocols has a random access protocol in its medium access control (MAC) layer. DSRC is one of the IEEE802.11 suites, i.e., wireless local area networks (WLANs). DSRC has carrier sense multiple access with collision avoidance (CSMA/CA) to access frequency resources. This random access protocol is one of the most fundamental mechanisms and supports lower implementation costs than other complex mechanisms. Mode 4 is an extended version of D2D cellular networks out of coverages of base stations, called mode 2 [42]. Mode 4 implements sensing-based semi-persistent scheduling (sensing-based SPS). This mechanism considers V2X communication characteristics to share spectrum resources, and thus, mode 4 has an advantage of V2X performance. Each advantage has attracted many researchers and engineers to study both of them. This paper also focused on each protocol to support its implementation cost and V2X performance; DSRC has an advantage of implementation costs, and mode 4 has an advantage of V2X performance. Practically, adopted technologies depend on industry requirements or every country's networks. For these reasons, the author motivates to extend both protocols in this paper.

# 3. Channel Congestion Problem of Decentralized V2X

Unfortunately, decentralized V2X potentially experienced a channel congestion problem. The problem occurs in crowded environments, such as intersections in urban areas. In such crowded environments, many nodes share a V2X channel, like Fig. 2; in other words, most portions of the channel are occupied. Then, both random access protocols yield frame collisions. At such frame collisions, a receiver fails to receive any frame or obtains at most a frame by *capture effect* [43] [44], depending on its signal-to-interference-and-noise ratio (SINR); such frame reception errors are called *collision errors*. For example, in Fig. 2, the red car receives two frames transmitted from a blue car and a pedestrian near the red car, and then, the frame from the blue car has a smaller SINR than another frame. Due to such collision errors, CWS satisfies none of the QoS

requirements; in other words, the node cannot collect enough information to recognize other nodes accurately. As a result, CWS cannot achieve to warn its user accurately, i.e., warning errors.

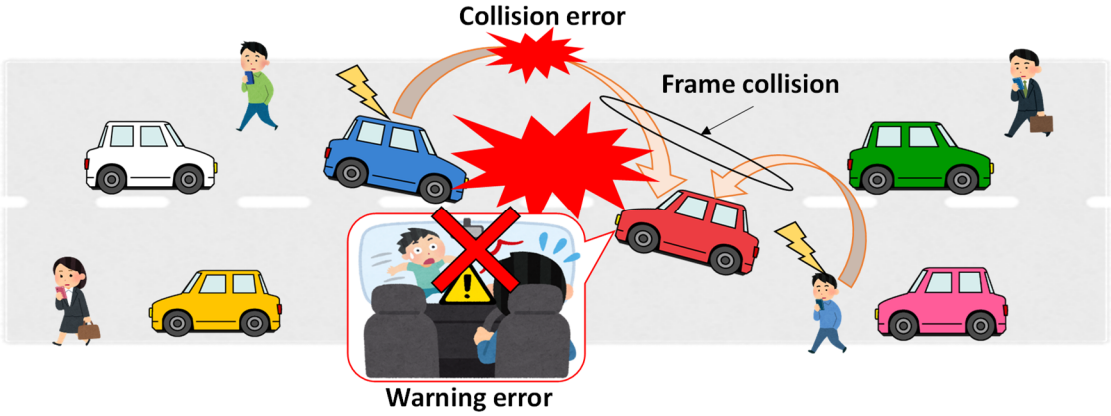


Fig. 2 V2X communications under channel congestion.

# 4. Related Works and Problems

Many researchers have focused on channel congestion of decentralized V2X [13]–[40], like Table 1. Some related works [13]–[16] [20] [21] evaluated the performance characteristics of DSRC, and other works [23]–[32] evaluated the performance characteristics of mode 4. These works emphasized a frame reception ratio, unlike the amount of information. Some works have actively studied a decentralized congestion control (DCC) approach to mitigate channel congestion directly. The approach mainly reduces the number of transmitted frames per node and thus reduces total frames in air. These related works effectively boost the frame reception ratio instead of decreasing the number of transmitted frames. For example, some works [17]–[19] focused on DCC methods for DSRC. The most fundamental method has been LIMRIC [17]. This method reduces in channel utilization metric called channel busy ratio (CBR); especially, such DCC suppressed only two transmitted frames per second in severe-congested environments. Two works [33] [34] have studied DCC methods for mode 4; mode 4 is a new technology, and mode 4 has had smaller related works about DCC than DSRC.

However, these related works have lost focusing on the required amount of information to detect nodes in CWS; in other words, the related works supported no CWS requirements, shown in Table 1. As a result, the following problems of related works have been highlighted;

1. The performance degradation of mode 4 considering the amount of information has been unknown under channel congestion, although some researchers have evaluated the performance of DSRC [20] [21];

2. Appropriate congestion controls for safety applications, like CWS, have remained

unknown in both DSRC and mode 4. The existing congestion controls, i.e., DCC, have been unsuitable for safety applications in terms of the amount of information, although DCC has been suitable for non-safety applications. As previously mentioned, DCC forces each node to transmit only two frames per second in congestion environments. In this case, each receiver obtains at most two frames; in other words, each node a location data every 500 milliseconds. At a node approaching a node at the relative speed of 120 km/h (i.e., each speed of 60 km/h), the distance between the two nodes reduces approximately 33 m per 500 milliseconds. Thus, each receiver cannot recognize surrounding nodes in real-time.

Table 1 Related works of performance evaluations and proposed congestion controls for both V2X protocols.

| V2X protocols | Contents | Amount of Information | Related works |
|---|---|---|---|
| DSRC | Evaluations | Unsupported | [13]–[16] |
| | | Supported | [20] and [21] |
| | Proposing congestion control | Unsupported | [17]–[19] |
| | | Supported | **Nothing** |
| Mode 4 | Evaluations | Unsupported | [23]–[32] |
| | | Supported | **Nothing** |
| | Proposing congestion controls | Unsupported | [33] and [34] |
| | | Supported | **Nothing** |

# 5. Challenges, Approaches, and Contributions

This paper aims to solve the two problems of related works, pointed out in the above sub-section. To this end, the author challenges to study the V2X performance evaluations under channel congestion in CWS and study congestion controls without decreasing the number of transmitted frames, unlike related works. First, the author needs to reveal the performance degradation due to channel congestion of mode 4 using CWS in related works. Additionally, the author needs to study congestion control methods for DSRC and mode 4 in the MAC layer instead of decreasing the traffic load proposed in related works. The challenges in this paper are summarized as follows;

1. The author studies a congestion control for DSRC for CWS to solve the problem-2 of DSRC;
2. The author investigates the performance characteristics of mode 4 under channel congestion in the use-cases of CWS to solve the problem-1;
3. The author studies a congestion control for mode 4 for CWS to solve the problem-2 of mode 4.

To approach the above challenges, the author evaluates the performance characteristics of mode 4 and introduce cross-layer technologies for efficient random access protocols, like [35]–[40]. In particular, this paper strongly focuses on the new cross-layer congestion controls, considering the characteristics of CWS. Cross-layer approaches incorporate the MAC layer with other layers, including their physical layer or application layer. The approaches enable the MAC protocol to share the channel efficiently.

For DSRC, the author proposes an application-MAC cross-layer approach [35] to keep an advantage of its low-complexity random access mechanism, as stated in the above section. The approach is a node-clustering method, named CLustering Algorithm with meSsage EStimation (CLASES) [35]. In CLASES, multiple nodes create a group (cluster). Only each cluster head in the cluster transmits frames of all the group members, including frames of the head on behalf of the members; then, the head estimates its members' data based on their past data. The key idea efficiently reduces the number of competitive nodes accessing spectrum resources. Thus, the method reduces frame collisions and mitigates channel congestion while keeping the MAC mechanism.

For mode 4, the author proposes a physical-MAC cross-layer approach [37] [38] [40] along to an advantage of V2X performance supported by the enhanced communication mechanism. In the approach, the random access protocol has the power domain non-orthogonal multiple access (called NOMA); specifically, the author proposes a concept of decentralized broadcast NOMA (DB-NOMA) [38]. DB-NOMA has the following two methods with NOMA: a frame relaying method with NOMA (RM) [38] and a parallel transmission method with NOMA (PTM or also called SPS-NOMA) [37] [38] [40]. NOMA has two types of existing cellular networks: uplink NOMA (UL-NOMA) and downlink NOMA (DL-NOMA). DB-NOMA includes both types. RM is based on DL-NOMA, and SPS-NOMA is based on UL-NOMA. DB-NOMA allows a node to receive multiple frames in a spectrum resource at the same time. The characteristic converts negative impacts due to frame collisions to positive impacts on V2X performance and is expected to mitigate channel congestion. In summary, the author focuses on the following approaches and presents the following contributions;

1. The author proposes a node-clustering method with location estimation, CLASES, for DSRC [35] in Section III. The new clustering approach provides an efficient random access protocol and thus mitigates the channel congestion problem without decreasing the amount of information;

2. The author evaluates the performance characteristics of mode 4 under channel congestion in CWS through simulations [36] [39] in Section IV. Through these performance evaluations, the author highlights the disadvantage of the current mode 4 under channel congestion and the difference between the performance and the QoS requirements;

3. The author proposes two NOMA methods with a frame relaying mechanism and a

parallel transmission mechanism for mode 4, called DB-NOMA [37] [38] [40] in Sections V and VI. The proposed methods successfully receive multiple frames in a slot and contribute to mitigating the channel congestion problem without reducing the number of transmitted frames.

The following sections are organized as follows. Section II shows related technologies (i.e., the current decentralized V2X standard protocols and the system model of CWS) and related works about this paper. Section III shows DSRC performance evaluation under channel congestion and describes a congestion control protocol, named CLASES, based on a node-clustering method. Section IV shows mode 4 performance evaluation under channel congestion. Section V introduces DB-NOMA for mode 4 and mainly focuses on the RM in the DB-NOMA. Section VI introduces SPS-NOMA or PTM in the DB-NOMA at the detail and confirms the performance characteristics. Finally, Section VII concludes this thesis. This paper is based on my three published open access papers [35]–[37] and my published conference paper [38]. The second and third papers give me their copyrights. Additionally, I denote the following copyrights to reuse the first paper [35] and conference paper [38]; 

# II. Related Technologies and Related Works

This section shows related technologies, i.e., decentralized V2X protocols and CWS, and related works for this paper. This section highlights the problem of these related works and the novelty of this paper. The following subsections provide related works of node-clustering methods, performance evaluations of mode 4 under channel congestion, and power domain NOMA in this order.

## 1. Decentralized V2X Standard Protocols

The current decentralized V2X standard protocols are divided into the following two protocols: DSRC and PC5-based C-V2X mode 4. Each protocol has a random access protocol. DSRC uses a basic CSMA/CA protocol. In contrast, mode 4 uses sensing-based SPS, which is different from the CSMA/CA protocol. In the following subsections, I briefly describe these protocols. These V2X protocols are typically deployed in broadcast networks and then have no acknowledgment (ACK), unlike unicast networks. Based on the characteristics, these protocols support no retransmissions.

### A) DSRC

DSRC uses IEEE802.11p in its MAC layer protocol [13]–[15]. IEEE802.11p is based on IEEE802.11a. Unlike IEEE802.11a, IEEE802.11p can use a lower data rate, i.e., 3 Mbps. IEEE802.11p complies with the basic CSMA/CA protocol, or distributed coordination function (DCF). This protocol tries to prevent nodes from using the busy channel by the following two steps. The first step is to sense the carriers. The step explores non-busy channels based on the received signal power. In the step, each channel is sensed during a pre-defined time, called DCF inter frame space (DIFS). At the sensing, its received power is lower than a pre-defined threshold, and then the process regards the channel as a non-busy channel. The second step is to wait back-off time associated with a contention window selected at random. This contention window is lower than sixteen to suppress the latency due to waiting time.

### B) PC5-based C-V2X mode 4

Mode 4 has an extended random access protocol, sensing-based SPS [22]–[25]. The protocol is more complicated than the CSMA/CA protocol. Mode 4 does not require any base stations to communicate with the other nodes, unlike other C-V2X standards such as Uu-based C-V2X and PC5-based C-V2X mode 3 (called mode 3) [41]. In the Uu-based C-V2X, each node must negotiate the transmission slots with a base station before transmissions. Subsequently, the node transmits data to the base station once, and then

the base station transmits the data to the other nodes. In contrast, mode 3 and mode 4 use PC5 interfaces to transmit data, i.e., sidelink. Fig. 3 shows a comparison between the characteristics of mode 4 and mode 3. Mode 3, the right figure in Fig. 3, requires negotiation for a transmission slot but directly transmits data through sidelink. In mode 4, the left figure in Fig. 3, each node autonomously selects a transmission slot and directly transmits data in the slot [22]–[25]. In summary, mode 4 has no additional infrastructures and no control signals, unlike mode 3; it reduces communication costs compared to the other C-V2X standards. We explain the algorithm of mode 4 as follows.

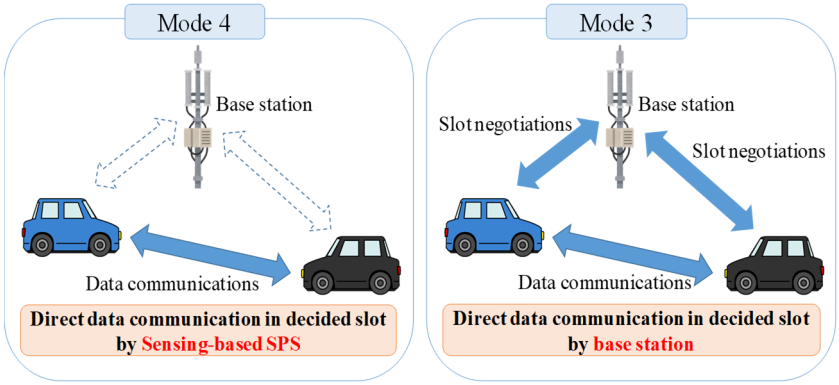


Fig. 3 The characteristics of mode 4, as compared to mode 3.

For communications without base stations, each node executes Sensing-based SPS, a new random access protocol. Sensing-based SPS has two different features from CSMA/CA as follows:

- Slot selection based on history: For selecting a good slot for the transmissions, each node uses the history of past slot utilization and estimates the interference of each future slot. The history includes the sensing information of all the slots, despite transmitting or not; that is, each node senses all the slots. This sensing information includes the received signal, the remaining number of slot utilization [23] (related to the next feature), and others.
- Semi-persistent slot utilization: For boosting the above estimation accuracy of the interference pattern, each node uses the same slot in a semi-persistent manner; in other words, each node successively uses the same frequency resource at specific times.

The basic procedure of the Sensing-based SPS has seven steps. The first four steps reduce the candidate slots using some carrier sensing mechanisms (Step 1–4). Specifically, each node filters the estimated slots with high interference in Steps 2–4. The last three steps operate successive transmissions (Step 5–7). We describe the steps in the following paragraphs.

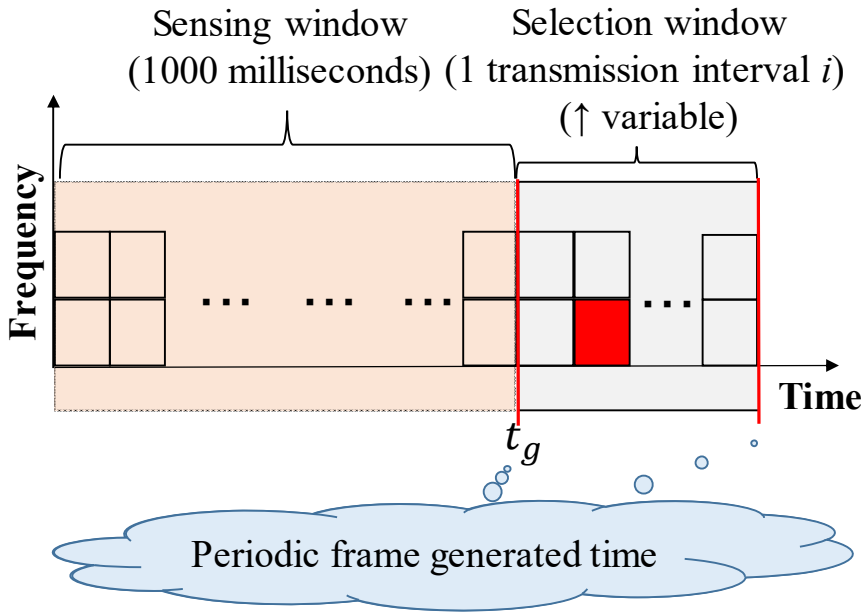


Fig. 4 The illustration of the sensing window and selection window.

**Step 1. Initialization:** When a frame is generated, each node initializes a set of candidate slots, $S_A$. The initial set includes all the slots during the *selection window*—as shown in the right part of Fig. 4. The selection window is during a transmission interval $i$, e.g., 100 milliseconds for ten frames/s, which is after its generated time $t_g$ of the periodic frames. In contrast, the sensing history includes all the slots during the sensing window—as shown in the left part of Fig. 4. As shown in Fig. 4, the length of this window is standardized at 1000 milliseconds.

**Step 2. Filtering 1 (half-duplex):** In this step, each node excludes non-sensed candidate slots during the sensing window from the initial set $S_A$. For example, each node cannot receive frames in the transmission slot. In these non-sense slots, nodes cannot infer the slot usage from the past slots due to the half-duplex. The updated $S_A$ passes to the next step.

**Step 3. Filtering 2 (Reference Signal Received Power (RSRP)):** In this step, each node excludes specific candidate slots by the RSRP conditions from $S_A$. The RSRP conditions are as follows;

- The first condition is that one or more nodes reserve the candidate slot in the sensing window. Each node refers to the remaining number of sensing information in the past slot. Note that the frame must be decoded successfully.
- The second condition is that the RSRP of the above slots, reserved by the other nodes, is higher than the threshold. Note that when the same transmitter reserves a transmission slot, the RSRP of the most recent slot is used.

From these two conditions, each node can exclude the candidate slots with

deterministically high interference in this step. Fig. 5 illustrates an example of Step 3. In Fig. 5, in the three past slots, the nodes reserve a candidate slot of time *t*. This step is iterated until the size of $S_A$ becomes 20% or higher of the initial size in order to ensure that a sufficient amount of candidate slots are handed over to the next step. With each iteration, the RSRP threshold is reduced by 3 dB of the standard.

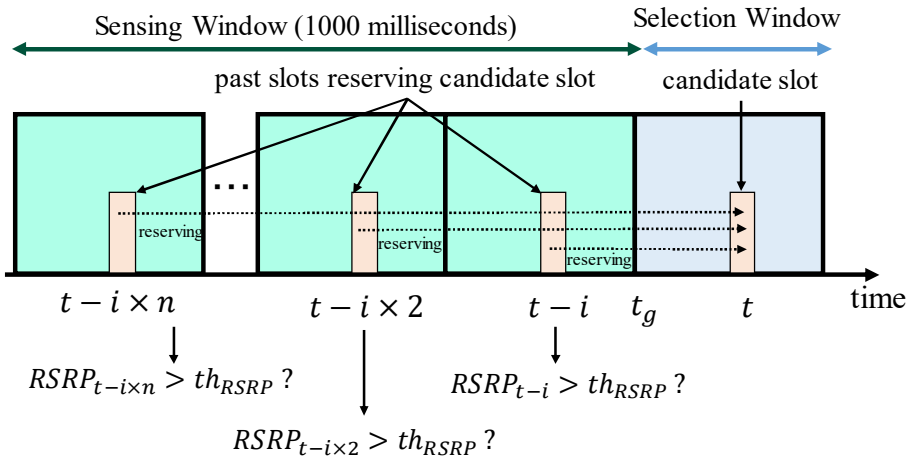


Fig. 5 The abstract image of the RSRP mechanisms at time $t_g$.

**Step 4. Filtering 3 (Received Signal Strength Indicator (RSSI)):** Each node excludes the candidate slots based on the average RSSI over the corresponding past slots. The corresponding past slots are defined as the slots traced back with the transmission interval from the candidate slot in the sensing window. Fig. 6 is an example of a node calculating the average RSSI. Then, an individual node puts the *N* top of the slots with the lowest average RSSI into the new set ($S_B$). The *N* is standardized as the value of 20% of the number of slots. This step estimates the interference, although the nodes cannot fully identify the interference. In other words, the nodes exclude the candidate slots with the estimated-high interference.

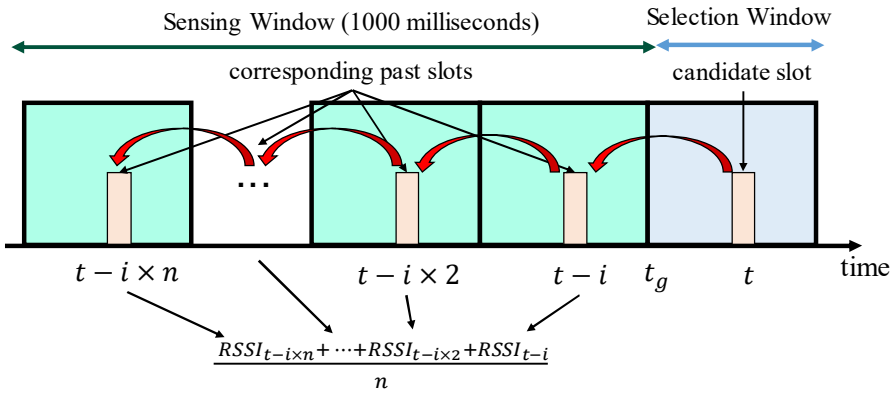


Fig. 6 The abstract image of the RSSI mechanism at time $t_g$.

**Step 5. Random Selection:** Each node randomly selects a transmission slot from $S_B$. This random selection prevents several nodes from selecting the same slot.

**Step 6. Configuration:** Each node randomly sets a reselection counter from a pre-defined range. Nodes reduce the counter by one every transmission. The node successively uses the same slot selected in Step 5 until the reselection counter becomes zero. The random selection of the counters is effective in avoiding simultaneous reselections with other nodes. As a result, the possibility of the node selecting the same slot with other nodes is decreased.

**Step 7. Successive transmissions and Reselection:** Each node successively uses the selected slot and probabilistically reselects the next slot after the reselection counter becomes zero. The node returns to Step 1 at a probability, called resource keeping probability. The probability is pre-defined in the range of 0–0.8; otherwise, each node maintains and uses the same slot.

# 2. Crash Warning System

## A) How to Warn

In CWS, each node advertises (broadcasts) its own state data periodically and calculates the crash risks in the near future (i.e., potential crash risks), based on the obtained state data from other nodes. Fig. 7 shows an example of a warning in CWS. The left illustration shows a periodical advertisement phase, and the right illustration shows a calculation phase.

In the periodical advertisement phase, each node broadcasts a frame, including its own state data in every transmission period. Each data includes the node's location, speed, direction, time, and other information related to its mobility. The data can be obtained from some sensors, such as GPSs and gyro sensors. In Fig. 7, node-A broadcasts its own state data to notify other nodes of its existence.

In the calculation phase, CWS calculates the node's potential crash risks in every received frame. Such a frame contains a node's location information, called node-A, and thus, CWS enables to calculate node-A's future location based on the physics laws. From the future location, CWS calculates such risks between the node-A and the node with the system. If the risks are higher than a pre-defined value, which depends on CWS, the system warns the user, such as the driver or pedestrian, with V2X equipment. In Fig. 7,

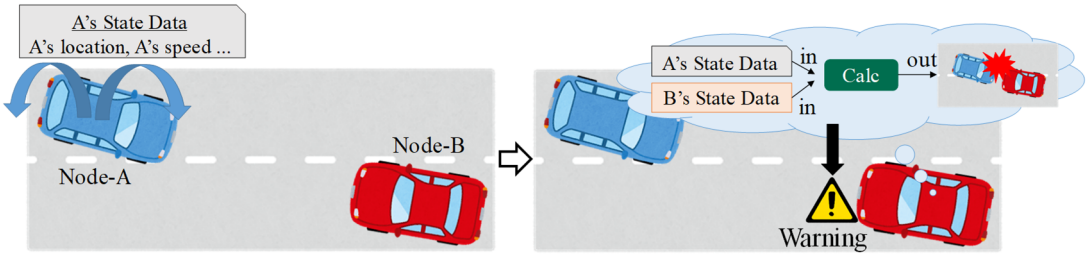


Fig. 7 The procedures of CWS: broadcast to surrounding nodes and warn the users.

the node-B detects the potential crash risks with node-A from the obtained frame and warns the driver. The warned driver may apply the break or operates the handle to avoid potential crashes. Note that this paper does not focus on the detailed calculation ways.

## B) QoS Requirements

CWS has the following three QoS requirements to detect *potential crash nodes*, which are likely to collide with other nodes. Fig. 8 illustrates an outline of the QoS requirements for the node-B to detect the node-A. Note that CPU processing is out of this paper's target.

*Frame reception reliability*: Potential crash nodes must receive frames at high reliability. The reliability is measured as either the following two metrics: the number of received frames or frame reception ratio (FRR). For the first metric, each potential crash node needs to meet ten frames/s from the corresponding potential crash nodes. Reference [10] standardizes the number of transmissions to 10 frames/s. This paper interprets this specification as a requirement concerning the number of received frames because receiving all of the transmitted frames is typically necessary and important in warning of potential crashes; namely, the nodes need to obtain enough information to predict their future location in a real-time manner accurately. In Fig. 8, the node-B needs to receive at least ten numbers of the node-A's frames per second. For the second metric, each potential crash node needs to satisfy a reception ratio of 90% or more at ten transmitted frames or more per second [11]. As well as the first metric, in Fig. 8, the node-B needs to receive frames from node-A's frames at a higher ratio than 90%.

*Warning period*: CWS can safely warn the user during this period. A guideline of the period [9] is during 2.5–9.5 s before potential crashes, i.e., during a time-to-crash within 2.5–9.5 s. In the guideline, the final warning opportunity is a time-to-crash of 2.5 s. For the opportunity, each potential crash node needs to satisfy the frame reception reliability during 2.5–3.5 s before its potential crash; for example, in Fig. 8, the node-B needs to detect the node-A during this final period at least. This requirement is reflected in the communication distance between potential crash nodes in our simulations. Such a longer distance decreases frame reception reliability more significantly. This paper does not focus on CPU processing time in the calculation phase and signal processing time.

Table 2 QoS Requirements of the CWS

| **Requirements** | **Required values** |
|---|---|
| Frame update frequency | 10 Hz or more [11]<br>(Every 100 milliseconds) |
| Frame reception reliability | (a) number of received frames: 10 or more [10]<br>(b) FRR: 90% or higher [11] |
| Warning period | 2.5–3.5 seconds [9] |
| Maximum end-to-end latency | 100 milliseconds [12] |

Configuring the warning period depends on individual differences of braking actions, including driver reaction and breaking, and thus, the guideline also tolerates such individual differences. This paper ideally assumes that such processing occupies enough short time for the individual differences through the above discussions.

*Maximum end-to-end latency*: Each data frame must reach the network layers of nodes within 100 milliseconds from generating the data [12] to guarantee the age of information. This paper focuses on only queueing latency because the latency mainly tends to be the most dominant to end-to-end latency in other kinds of contained latency, like signal processing latency, serialization latency, and propagation latency. The other latency is typically much smaller than queueing latency. End-to-end latency limits selecting transmission resources, especially for retransmissions, like relaying or transmitting by cluster head in node-clustering methods. Each frame regulates the latency requirement in our simulations.

In summary, according to the three QoS requirements, each potential crash node must satisfy requirements (a) or (b) for frames from the corresponding potential crash nodes during 2.5–3.5 s before the potential crashes. To link these requirements and the degree of channel congestion, the author introduces a *node accommodation capacity (NAC)*. NAC is the maximum number of nodes in the communication range when the potential crash nodes can satisfy these requirements. On average, the system can warn accurately when the number of nodes in the communication range is equal to or less than NAC. It is necessary to increase the NAC related to various factors, such as node density.

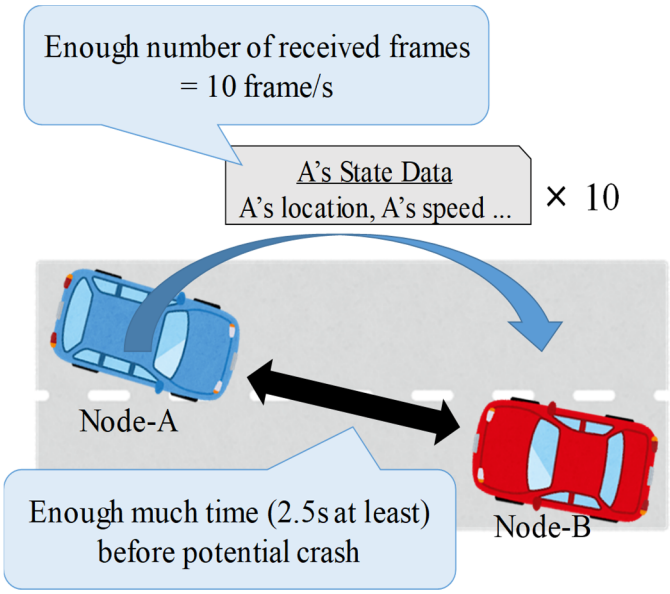


Fig. 8 An abstract image of the QoS requirements of CWS for the node-B to detect the node-A.

# 3. Related Works, Challenges, and Approaches

## A) CLASES

### a). Related Works of Node-clustering Methods

The conventional cluster-based methods usually use intracluster communications and intercluster communications. Fig. 9 describes an algorithm of typical conventional cluster-based methods. At first, by using intracluster communications, cluster heads collect data that the members wish to transmit (Fig. 9 (a)). After collecting all the data, if necessary, the data are compressed or fused with the other members' data, and then by using intercluster communications, the heads transmit the data on behalf of the members (Fig. 9 (b)). Note that the methods provide the following effects: interference mitigations by spatial reuses, routing overhead suppressions, hierarchical controls, and data compressions (fusions) in local nodes.

In conventional methods, intracluster and intercluster communications have been assigned to the different communication channels by time, frequency (spectrum), codes, and space. If clusters execute both of the communications on the same channels, the communications interfere with each other. Of course, there are methods for which the communications are executed on the same channel to obtain the above other gains rather than interference mitigation gains. Here, this section does not focus on the methods that obtain the other gains.

In methods that divide a bandwidth into intracluster communications and intercluster communications by time, each communication is assigned to different time slots. One of the methods has been proposed in [45]. The authors proposed a method that some heads cooperatively transmit their data through intercluster communications. The communication quality improves for time diversity gains.

The methods also allocate the two communications to different spectra. CBMMAC has been proposed as a TDMA-based medium access control [46], which assumes to use the multichannel of DSRC. Moreover, the approaches can effectively utilize multiple spectra and assign them to different channels. Thus, the methods are effective in data dissemination and Internet access. In [47]–[50], the authors also have proposed hybrid systems that use several wireless spectra; in other words, the authors added spectrums, like 4G and IEEE802.11p.

In methods that add bandwidth by codes, clusters use the different codes from each other. Thus, intracluster communications provide no interference with intercluster communications. The methods are usually used for saving the energy of sensor nodes in wireless sensor networks. In the networks, sensor nodes transmit data to sink nodes but are usually far away from sink nodes, so sensor nodes consume large transmission energies. The most popular method is LEACH (low-energy adaptive clustering hierarchy)

[51]. To obtain larger energy savings, LEACH has been improved [52]–[57].

In methods that divide the bandwidth into two communications by space, clusters can make spatial reuses by capture effects, as long as nodes do not need to obtain data transmitted from other clusters. In other words, nodes can more correctly receive their intracluster communications than intercluster communications. In the methods, researchers have focused on forming stable clusters. To form stable clusters, even in environments where nodes move dynamically, MOBIC has been proposed [59]. In the method, nodes whose relative locations are close to each other make a cluster. The following methods have managed clusters by using more complicated metrics of mobility (speed, direction, lane, and so on) than those of MOBIC [60]–[63].

### b). Challenge, Approach, and Contribution in Section III

The above conventional cluster-based methods include either of the following disadvantages in CWS.

- Existing methods consume frequency or time resources to divide the bandwidth into an intracluster channel and an intercluster channel. CWS data are exchanged on the channel for intercluster communications, but the channel becomes narrow. As a result, the number of accommodated nodes is limited.
- Existing methods use additional bandwidth to separate intracluster and intercluster channels. These methods use codes or add spectrums and thus require costs to add bandwidth.
- Existing methods efficiently reuse spaces to separate bandwidth of intracluster and that of intercluster communications. These methods are unsuitable for CWS because all clusters must listen to data transmitted from other clusters in CWS. Therefore, each member cannot conduct intracluster communications and intercluster communications in parallel.

To solve the above problems, the author proposes a new cluster-based communication method, CLASES [35], which suppresses smaller traffic loads for intracluster communications than existing methods. In the proposed method, cluster heads estimate the members' data and never regularly collect them. Members just broadcast their own data to correct data that the heads transmitted on behalf of the members. The idea allows each cluster to execute intracluster communications if necessary and thus enhances the quality of intercluster communications at a low cost. Section III presents the procedures and evaluates the performance while considering the impacts of various parameters. Finally, the contributions of Section III are as follows:

- The author proposes a new cluster-based method with a member's data estimation mechanism. The proposed method can suppress interference between intracluster communications and intercluster communications at a low cost and thus access

spectrum resources efficiently;

- The author significantly increases the NAC of the current DSRC in CWS through computer simulations. The simulation results mitigate the congestion problem without decreasing the number of transmitted frames.

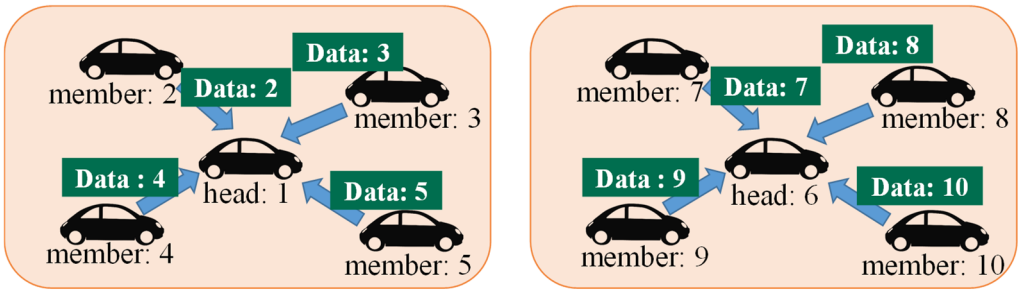


(a) **Intracluster Communication** for collecting members' data

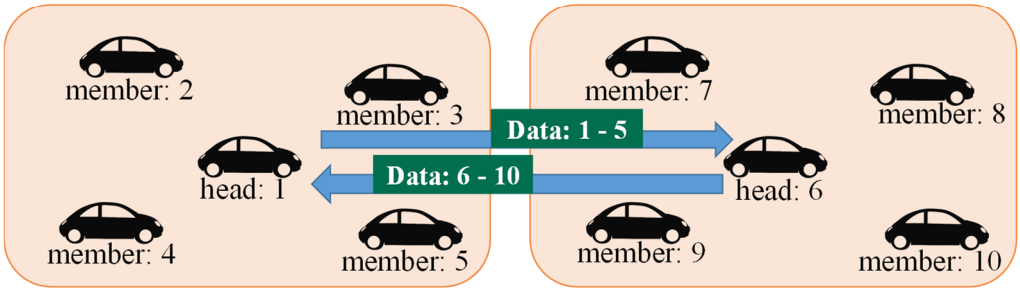


(b) **Intracluster Communication** for communicating with each other cluster

Fig. 9 The algorithm of the conventional cluster-based method.

## B) Performance Evaluations of Mode 4 in CWS under Channel Congestion

### a). Related Works of Performance Evaluations of Mode 4

Table 3 summarizes the existing works related to mode 4 [23]–[40]. Some works [23]–[32] evaluated the performance of PHY, MAC, or the application (such as cooperative awareness and platoon) layers of mode 4 rather than the performance in use-cases of CWS using mode 4. Our previous works [38]–[40] focused on the performance of mode 4 in CWS but did not cover feasibility. The following paragraphs briefly show the related works.

Some related works have focused on the performance of mode 4 in the PHY and MAC layers. The work in Reference [23] summarized the mechanism of mode 4. In Reference [23], the authors evaluated the packet delivery rates of the distance between a transmitter and a receiver. The study in Reference [24] simulated the performance of some mode 4 configuration parameters for slot selection. In Reference [25], the authors mathematically analyzed the performance of mode 4 in terms of the error and the distance between a

transmitter and a receiver. Reference [26] simulated the performance of mode 4 for frame sizes. In References [27] and [28], the authors also simulated the performance of mode 4 for its key configuration parameters. The work in Reference [29] enhanced the mechanisms of mode 4 to reduce collision errors by slot reselections.

The other works in References [30]–[40] evaluated the performance of mode 4 while considering the application layer. In References [30] and [31], the authors evaluated the performance of mode 4 in terms of cooperative awareness. The paper in Reference [30] revealed that mode 4 is characterized by greater delay and less packet delivery rates than those of IEEE802.11p. The work in Reference [31] concluded that it might be possible to utilize mode 4 for practical uses in terms of cooperative awareness by optimizing the modulation and coding scheme (MCS). In Reference [31], the authors simulated the performance of mode 4 in the platoon use cases and concluded that mode 4 outperforms IEEE802.11p in the use cases. The work considers traffic accidents in terms of platoon. However, the relative speed between platooned trucks is smaller than that in CWS. Our previous works [38]–[40] focused on CWS using mode 4. In References [38] and [40], the author proposed NOMA to overcome the congestion problem of mode 4. In Reference [39], the author investigated the behaviors of the slot selection mechanisms of mode 4. Our previous works did not cover investigations into the feasibility of mode 4 in various crash scenarios. The previous works focused on comparing communication systems rather than the feasibility evaluations of mode 4 in CWS.

Table 3 Summary of related works in terms of evaluated layers.

| Layer | | Crash Scenarios | Related works |
|---|---|---|---|
| PHY and MAC Layer | | Not assumed | [23]–[29] |
| Application Layer | Awareness | | [30] [31] |
| | Platoon | | [32] |
| | CWS | Not assumed | Our previous works [38]–[40] |
| | | Assumed | This work |

## b). Challenge, Approach, and Contribution in Section IV

According to the above discussions, the existing works have not investigated the feasibility of mode 4 in CWS. In Section IV, the author investigates the feasibility of CWS in terms of the congestion caused by crash scenarios. The author models crash scenarios in crowded intersections or high-speed vehicles and then evaluates the performance characteristics of mode 4 in the modeled scenarios. The former scenarios are mainly related to the density of the nodes. This section covers two densities: the uniform node distribution for revealing the performance limitations of mode 4 against the number of

nodes, i.e., NAC, and realistic node distributions for investigating the performance characteristics of mode 4 in realistic intersections. The latter scenarios depend on the relative speed of two nodes related to a potential crash, which is dominant to the performance limitations of mode 4. In summary, Section IV mainly contributes to investigating the NAC of mode 4 in various crash scenarios in CWS to show the feasibility of congestion conditions and highlights the performance degradation of the current mode 4 under channel congestion.

## C) DB-NOMA and Frame Relaying Method with NOMA

### a). Related Works of Power Domain NOMA

Section IV comprehensively focuses on the power domain NOMA in cellular networks, which effectively uses the power domain in a slot; Section V covers both UL-NOMA and DL-NOMA. Such NOMA technologies enable nodes to receive several frames in a transmission slot at the same time. In the NOMA, one or more transmitters superpose several signals at the transmitters' side; at the receivers' side, each receiver decodes the superposed signals by using SIC technologies [64]–[71]. The receiver must guarantee sufficiently high SINR in each SIC iteration.

The author categorizes the conventional NOMA technologies into centralized/decentralized and unicast/broadcast. Table 4 summarizes them. As shown in the following discussions and Table 4, the related studies have proposed no NOMA technologies for decentralized broadcast systems.

- NOMA for centralized unicasts: [64]–[66] has studied it in cellular networks. In this NOMA, a base station superposes several signals and transmit superposed signal. The base station controls the superposed transmission for a specific node to receive the superposed signal correctly because of unicast systems.
- NOMA for centralized broadcasts: [64] [67]–[69] have proposed it. In [64] and [68], a base station assigns several nodes to a transmission slot. In [69], a base station superposes several signals and transmits the superposed signal to all nodes within its cell. In [67], a car superposes two frames under a base station. In these methods, a base station manages all transmitters, and thus no collisions occur in the cell.
- NOMA for decentralized unicasts: [70] [71] has considered NOMA technologies for grant-free cellular networks. In the networks, each node does not need to send a request to acquire a transmission grant. In [70] [71], several nodes simultaneously send their frames to a base station, and as a result, signals are superposed.

Table 4 Summary of related works for the existing NOMA methods in cellular networks

| Index | | Related Work |
|---|---|---|
| Centralized | Unicast | [64]–[66] |
| | Broadcast | [64] [67]–[69] |
| Decentralized | Unicast | [70] [71] |
| | Broadcast | Only our work |

## b). Challenge, Approach, and Contribution in Section V

We cannot apply the existing NOMA technologies to mode 4 directly because mode 4 is the decentralized broadcast system. Mode 4 cannot use the existing centralized NOMA methods because mode 4 depends on no base stations managing all transmissions. Mode 4 cannot use the existing unicast NOMA methods because these algorithms focus on a single destination node. Additionally, we need to devise superposing signals to use NOMA in mode 4 by the two characteristics as follows. Due to the decentralized system, frame collisions coincidentally occur. Thus, the unexpected frame collisions significantly decrease NOMA performance; due to the broadcast system, many destination nodes need to sense high SINR of superposed signals. This constraint decreases the possibilities of signal superposition. We need a new NOMA that superposes signals suitably considering these constraints.

Considering the characteristics of mode 4, Section V proposes a new NOMA concept for decentralized broadcast cellular systems and applies it to mode 4. The author defines the concept as DB-NOMA. Then, the author proposes two methods using DB-NOMA for mode 4, called the enhanced mode 4. The first method is a parallel transmission method with DB-NOMA based on UL-NOMA, called PTM. The second method is a relay method using DB-NOMA based on DL-NOMA, called RM. The enhanced mode 4 can boost bandwidth utilization efficiency or can expand the high-quality broadcast range. Section V also analyzes the characteristics of the suitable signal superposition in the enhanced mode 4. Additionally, this section highlights that enhanced mode 4 increases the NAC of the original mode 4 by using suitable signal superposition parameters. In summary, the contributions of Section V are as follows;

- The author proposes a new concept, i.e., DB-NOMA, and basic design of an enhanced mode 4, i.e., two methods based on the concept, to improve CWS performance. The proposed method efficiently supports multiple frames at a spectrum resource on a NOMA basis in C-V2X mode 4.
- The author analyzes the performance characteristics of the two NOMA types. The

analysis is useful to design the detailed algorithm.

- The author demonstrates that the proposed method enables to increase the NAC of the current mode 4 and promotes the practical uses of CWS to suppress the channel congestion.

# D) SPS-NOMA

## a). Related Works of UL-NOMA

Section VI focuses on UL-NOMA in various networks. This subsection highlights the differences between Section VI and related works [68] [70]–[77], [38], and [40]. The related works are divided into two groups. The first group is unicast-based UL-NOMA [70]–[74]. The second group is broadcast-based UL-NOMA [68] [75]–[77], [38], and [40]. Table 5 summarizes the related works. This table emphasizes that the related works except for our works [38] and [40] have not focused on UL-NOMA in mode 4. In our previous works, the author proposed the concept of UL-NOMA in mode 4 in our conference papers. Section VI significantly extends the concept.

The first group is unicast-based UL-NOMA. The main topic of the group has been unicast cellular networks [70]–[74]. In the group, each of the unicast networks has a destination node, such as a BS or a D2D user. The authors [72] [73] proposed typical UL-NOMA systems in cellular uplink networks and evaluated the fundamental performance. The researchers [70]–[74] improved the SINR at each SIC iteration to boost the performance of UL-NOMA in the networks. The authors [70] proposed a layered user-pairing scheme. The scheme creates layers based on the distances between BSs and users. Selecting users in different layers provides the differences in BS–user distances, and thus, the scheme upgrades the SINR at each SIC iteration. The authors [71] used multiple antennas to improve the SINR. Providing space diversity by multiple antennas improved the SINR. The authors [74] proposed an effective algorithm for paring D2D users with cellular users to improve the spectrum utilization efficiency. Unlike these existing works, Section VI focuses on broadcast systems with multiple receivers in a wide area. Superposing many signals is challenging to provide high SINRs for such multiple receivers, and thus, the performance gains of UL-NOMA may be limited.

The other group is broadcast-based UL-NOMA. The main topic of this group has been V2X networks [68] [75]–[77]. The authors [68] proposed NOMA schemes for D2D-based V2X under the control of BSs. Other authors also investigated the schemes to boost the SINR at SIC iterations to improve the performance gains in broadcast networks as follows. The researchers [75] focused on IEEE802.11p with CSMA/CA and proposed using multiple antennas. The authors [76] proposed a distributed multiple access based on the distances between target receivers and target transmitters. The authors [77] focused on full-duplex NOMA (FD-NOMA) to enhance V2X performance, but the works did not focus on the slot selection mechanisms of mode 4. These works are strongly related to

Section VI but have not focused on mode 4. Sensing-based SPS in mode 4 is expected to boost the SINR at SIC iterations.

Finally, this section highlights the novelty compared with my previous works [38] [40]. In the previous works, the author proposed a basic concept of SPS-NOMA [38] and investigated the fundamental performance gains of SPS-NOMA in the uniform node distribution model [38] and realistic node distribution models [40]. However, the author has not focused on the key factors to improve the SINR at each SIC iteration, i.e., the slot selection mechanisms of sensing-based SPS, MCS, and RT.

Table 5 Summary of related works of UL-NOMA

| **UL-NOMA communication modes and wireless technologies** | | **Related works** |
|---|---|---|
| Unicast | Cellular uplink networks | [70]–[74] |
| Broadcast | IEEE802.11p-based V2X or D2D-based C-V2X (except for mode 4) | [68] [75]–[77] |
| | PC5-based C-V2X mode 4 (sensing-based SPS) | Only our works (Section VI and our previous works [38] [40]) |

## E) Challenge, Approach, and Contribution in Section VI

As previously discussed, related works have not focused on UL-NOMA in mode 4. Some related works [70]–[74] evaluated UL-NOMA for unicast networks. Unlike unicast networks, broadcast networks limit the performance gain of UL-NOMA because signals cannot be superposed for a specific receiver. Other works [68] [75]–[77] focused on broadcast networks in UL-NOMA, such as D2D-based V2X broadcast networks, except for mode 4. Unlike the other V2X standard, mode 4 implements sensing-based SPS. This mechanism may enhance the SINR at each SIC iteration, even in broadcast scenarios. Additionally, our previous works [38] [40] have not focused on the key factors to improve the SINR at each SIC iteration, i.e., the slot selection mechanisms of sensing-based SPS, MCS, and RT. We need to investigate the potential as an extension of mode 4 sufficiently.

Based on the discussions, in Section VI, the author proposes UL-NOMA in mode 4, named SPS-NOMA, and investigate the performance gains of SPS-NOMA compared with the current mode 4 (i.e., OMA). To this end, the author analyzes the performance characteristics for key factors to improve the SINR at each SIC iteration: the slot selection mechanisms, MCS, and redundant transmission (RT). Based on the analysis, the author evaluates the performance gains of SPS-NOMA in various node distribution models

through computer simulations. Through the simulation results, the author shows that the proposed method improves spectrum utilization efficiency. Finally, the contributions of Section VI are summarized as follows:

- The author proposes the detailed system design of the PTM of an enhanced mode 4, i.e., SPS-NOMA, as the next generation PC5-based C-V2X. The proposed method applies sensing-based SPS to NOMA to support an efficient physical-MAC cross-layer congestion control for decentralized V2X.
- The author presents the performance characteristics of SPS-NOMA for critical factors, such as the sensing-based SPS mechanisms, MCS, and RT.
- The author assesses the performance gains of SPS-NOMA in two kinds of node distribution models: the average gain in a uniform node distribution model and the practical gain in realistic node distribution models. The simulation results contribute to mitigating channel congestion and thus highlighting to support more diverse CWS situations through SPS-NOMA.

# III. CLASES for DSRC: Application-MAC Cross-layer Approach

Section III focuses on a new node-clustering method, CLASES, for DSRC as a decentralized application-MAC cross-layer congestion control.

## 1. CLASES: CLustering Algorithm with meSsage EStimation

CLASES introduces a data estimation mechanism instead of explicit intracluster communications. The mechanism suppresses intracluster communications and thus uses the vacant channel resources for intercluster communications. Hence, the effect of QoS improvement is more significant with intercluster communications.

Fig. 10 shows the algorithm of the proposed method. In the proposed method, nodes make a cluster and select the head. The head estimates the members' data (Fig. 10 (a)) and broadcasts them (Fig. 10 (b)). At the estimated data with an unacceptable error, the member transmits their own measured data (Fig. 10 (c)). The proposed method reduces traffic loads by comparing Fig. 9 and Fig. 10.

### A) Key Ideas of CLASES Method

The proposed method has two novel mechanisms for no using explicit intracluster communications: 1) data estimation and 2) unacceptable estimation error correction. Cluster heads use the data estimation mechanism from received past frames instead of collecting the members' data measured from GPS. Each member modifies the unacceptable estimation error by rebroadcasting its sensed data based on the unacceptable estimation error correction mechanism. The mechanism is executed at only members hearing unacceptable estimation errors in its frames from their cluster head. The limited rebroadcasting reduces the opportunity of intracluster communications more significantly than the existing methods. Note that the proposed method defines the range of unacceptable estimation errors based on CWS functions. The following subsections show the detailed procedures.

#### a). Data Estimation

The first idea is to introduce an estimation mechanism of the members' current data, which the nodes must transmit. Heads estimate the current data from the past data by some physics laws. The current data strongly correlate to the past data because the data

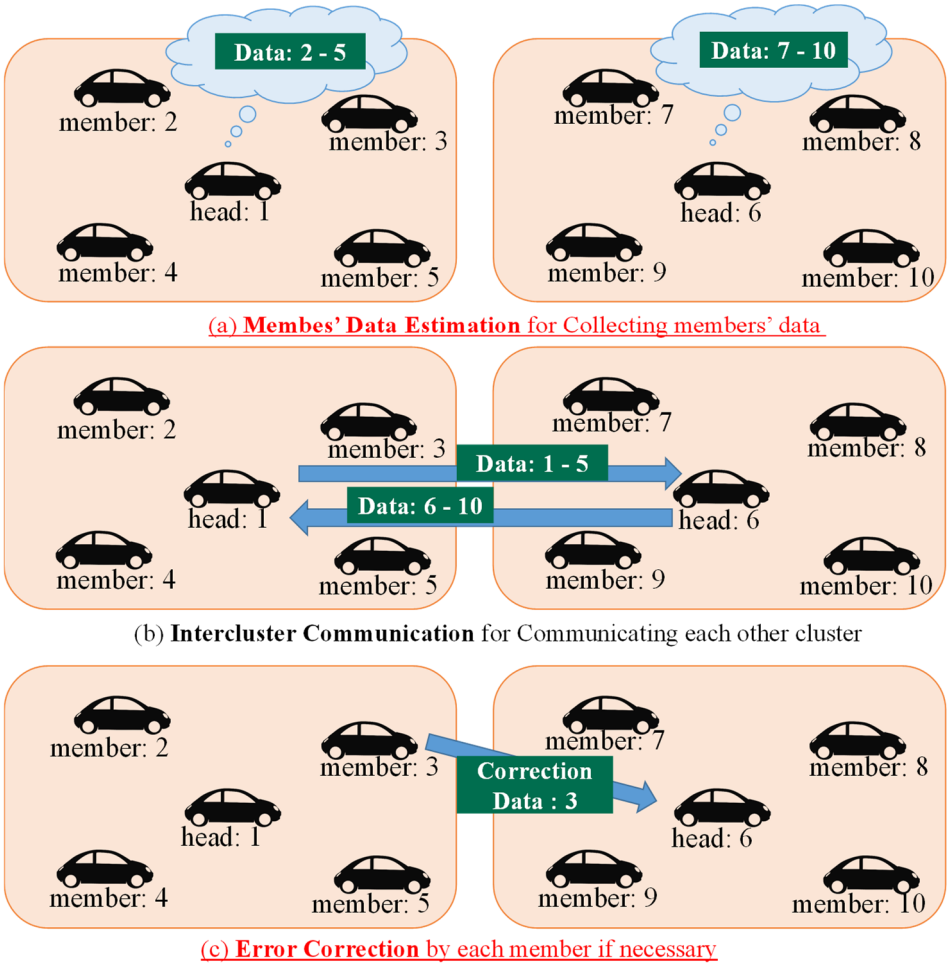


Fig. 10 The algorithm of the proposed method.

are the physics state data. For example, the nodes' location can be estimated by the past location and the current velocity. The velocity is estimated from the past velocity according to the past acceleration. These past data can be received without any additional costs because the data are broadcasted. The heads can also refer to the data that is further in the past, if necessary. Thus, the cluster heads can generate the members' current data. Confirm that any communications do not yield in this step.

After estimating the members' current data, the cluster heads broadcast on behalf of the members in addition to their own measured data, i.e., intercluster communications. Namely, the cluster head transmits the same number of frames as the cluster size. Let us discuss that a cluster head A estimates and broadcasts on behalf of the members (B and C). Fig. 11 shows estimations of B's data and unacceptable error corrections of B's data in the example. Let us consider the cluster head periodically changes to the other member, which becomes A, B, and C in order. During a period $t$, A transmits *Data(A, t)*, *Data(B', t)*, and *Data(C', t)*. *Data(A, t)* is measured by A; *Data(B', t)* and *Data(C', t)* are estimated by A from the past data *Data(B', t - 1)* and *Data(C', t - 1)*, respectively, which are transmitted at the previous period $t - 1$. If necessary, A may compute them by referring to

*Data(B, t - 2)* and *Data(C, t - 2)* at the further previous period *t – 2* as shown in Fig. 11.

Information ages of data do not decrease by the estimation mechanism because the estimation can be conducted fast, and the timing becomes right before frame generation. First, estimated data can be calculated from a formula that uses the location and velocity

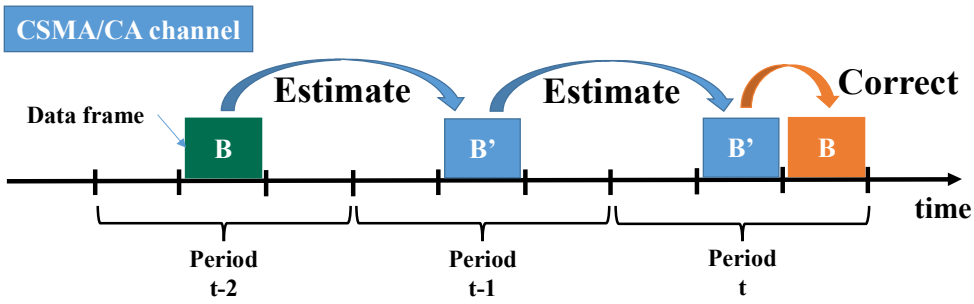


Fig. 11 Node B's data estimation and unacceptable error correction by node B.

of nodes, so the calculation finishes very fast. Second, estimations are conducted directly before the estimated data frame generation. From these two things, the real-time characteristic of estimated data becomes the same as that of general data frames in CWS.

Note that the proposed method needs no additional memory and CPU resources. CWS must analyze all nodes' location data and estimate their future nodes' location after a few seconds to detect potential crashes; that is, nodes monitor all surrounding nodes' motion. Therefore, nodes can store nodes' estimated future location data and others calculated from the past data. The proposed method can use the data without additional costs.

## b). Unacceptable Estimation Error Correction

The second idea is to correct unacceptable estimation errors by some members as necessary, as shown in Fig. 10. The heads' estimated data may sometimes include estimation errors. The significant errors prevent warning about crashes at high accuracy. The errors in the data exceed the predefined acceptable ranges. Therefore, members must replace data that include large errors from the correct data.

As soon as members detect unacceptable errors in their data estimated by the head, they newly broadcast their data measured by themselves. In the following sections, the frames are called *correction frames*. For the detection to include the unacceptable error in the head's broadcasted data, the members must hear the channel in intercluster communications; however, this is essential for CWS. In the above example and in Fig. 11, at B's data with an unacceptable error, B must transmit *Data(B, t)* during a period *t*; at an acceptable error in C's data, C transmits no frames during the period *t*. This step may yield some communications, but the traffic loads are much smaller than the conventional methods.

Cluster members in the same cluster can communicate with each other at high quality.

This is because the members are near each other than the distance between the members and nodes in the other clusters. Therefore, members can listen to the estimated data from cluster heads or the corrected data cluster members at high probability considering the capture effects.

The proposed method recovers nodes receiving corrections of members during a few transmission intervals. We can consider two cases about the procedure. The first case is that the next cluster head receives the corrections. In this case, the next cluster head sends the renewed data in the next transmission timing. Nodes can get chances for obtaining the correction data every transmission of the new cluster head. Thus, members successfully correct their data over long periods. The second case is that the next cluster head receives no corrections. In this case, the next cluster head transmits its data that takes over unacceptable errors in the data transmitted by the previous cluster head. As a result, the member transmits the correction again when the member receives the own data, including unacceptable errors. This case occurs at low probability because a member is typically near other members in the same cluster. Thus, the communication quality between such members is sufficiently strong to obtain the corrections. Incidentally, nodes may receive both estimated data and measured data. For addressing the incident, each node establishes a flag to its transmitted data, indicating the estimation data.

## B) Causes and Frequencies of Unacceptable Estimation Errors

Unacceptable estimation errors occur by (1) a large cluster size, (2) difficult estimations, (3) the number of estimations of the data of certain nodes, and (4) the narrow acceptable range of estimation errors. (1) As the cluster size is larger, the frequency of the estimations is larger. Inevitably, unacceptable errors are more likely to occur. (2) Typically, cluster heads can estimate members' current data from past data. This is because nodes (primarily vehicles) move according to physical laws. For example, nodes cannot sharply turn right/left. However, sharp driving operations, such as braking, accelerations, and turning right/left, may cause unacceptable errors because cluster heads cannot know such operations from the past data. (3) Cluster heads accumulate the data estimations several times without measured data, and then the data's errors become unacceptable. Even if the error in each estimation is slight, the accumulated errors may exceed the acceptable ranges in some instances. In (4), we can easily understand why unacceptable errors occur, and thus the author omits a description.

Unacceptable estimation errors infrequently occur. In the proposed method, heads estimate the members' states of the near future, i.e., the states that occur slightly after 100 ms. On the other hand, in CWS, all nodes estimate the other nodes’ states after 2.5 s–9.5 s. Based on CWS accuracy, the errors seldom occur, i.e., CWS always works precisely. Also, heads can obtain enough data about the states of the members. The above discussions show that the unacceptable errors occur only at most a few percentages.

## C) Data Frame in Intercluster Communications

Estimtaed frames comply with either the jumbo frame format or the single frame format. Users can select either of them according to the advantages and disadvantages. A jumbo frame composes of one header and all members' payloads. When a cluster head A makes a frame in a cluster formed by A–E as in Fig. 12, the payload size is five, which is the same as the cluster size. The advantage is improving QoS more substantially by reducing the same number of headers and DIFS slots as the number of members. The disadvantage is incurring some costs for changing the BSM standard.

A single frame composes of a header and a payload. The format follows the BSM standard. The heads make the same number of frames as the number of the members, which yields five frames, as shown in Fig. 12. The proposed method uses the format at a low cost because of the standard frame format. As a disadvantage, the format adds some headers and DIFS slots and thus decreases QoS improvement.

On the other hand, correction frames comply with the single frame format. The correction frames based on the jumbo frame consume additional channel resources. At transmitting jumbo frames and single frames simultaneously, the collisions wastefully consume the resources. The nodes that have correctly received the single frames wait for hearing the jumbo frames; in other words, the nodes can transmit nothing for a while.

Note that the payloads are not fused for CWS at high accuracy. By obtaining nonfused state data, nodes can correctly know the number of approaching nodes to themselves. Section III does not focus on further discussion about it.

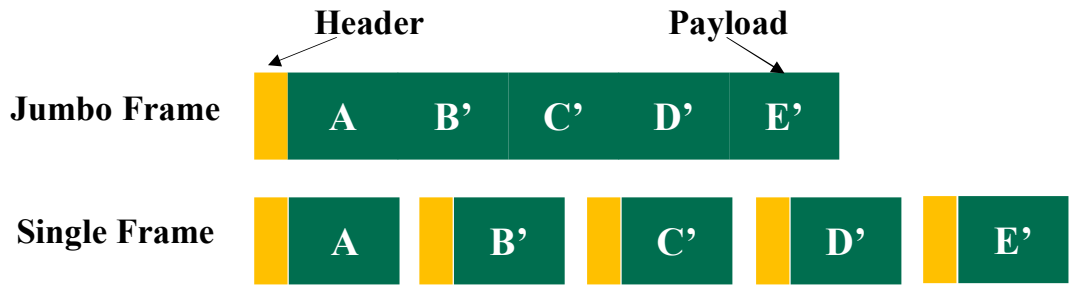


Fig. 12 Data frame composition (jumbo frame and single frame).

## D) Cluster Management Process

This section presents a simple cluster management process rather than the optimal one because the simple process does not occur frequently and finishes very fast. The process means a cluster formation and a cluster deformation. First, the process occasionally occurs since the cluster survives for a long time. The proposed method has no constraints about the cluster formation except that the members can communicate. As

long as the distances between the members are within the communication range, the cluster survives regardless of the locations of the members. For this reason, the management process occurs more infrequently than the periodic broadcasting of 100 ms. Clusters are formed by nodes whose locations and velocities are close to each other, as shown in [59]–[61] to avoid executing the management process. The above discussion is shown in some evaluations. Second, the process will finish during a short time; ideally, it will finish during just one period. The process is described in the following paragraphs.

Maybe, cluster members had better conduct to deform clusters when members are far away from each other because the performance of the proposed method decreases. This section focuses on the two simple triggers of deforming clusters rather than the optimal one. The first trigger is for members to receive no frames from the cluster heads many times. The second one is for members to know the members go away out of coverage of the current joining cluster. Incidentally, it may be better to provide a cluster deformation flag if you want to convey the meaning of cluster deformations correctly.

In the simple management process, each cluster head notifies the cluster management to all nodes through its broadcasted frames. Specifically, members are shown in the broadcasted frames. To identify the heads, members refer to the MAC address in the header. An example of notifications of two clusters is shown in Fig. 13. In the jumbo frame case, all nodes joining each cluster in a frame during a period are shown; in the single frame case, they are divided into multiple frames during a period. In either scenario, the nodes understand the members and the head that form the same cluster; in Fig. 13, A, B, and C are forming a cluster, and D, E, and F are forming a cluster.

For the cluster formation, a node transmits CWS frames containing the data of other nodes. The example of the cluster formation by node A–C is described as follows. During the first period $t$, each node transmits only its own data *Data(A, t)*, *Data(B, t)*, and *Data(C, t)* by itself. During the next period $t + 1$, for example, A wishes to form a cluster with B and C, and then A transmits *Data(A, t + 1)* by itself and transmits *Data(B', t + 1)* and *Data(C', t + 1)*, which A estimates. Then, B and C do not need to transmit their own data, as long as A's estimated data do not include unacceptable errors.

For the cluster deformation, a node transmits CWS frames containing only its own data. A sample of the cluster deformation is described by using the above example. During the next period $t + 2$, B transmits *Data(B, t + 2)* only; then, B intends to form a cluster that is only joined by itself. A and C listen to it, and then, for example, C transmits *Data(C, t + 2)* and *Data(A', t + 2)* without transmitting B's data. Note that the frames and correction frames are different. The correction frames are transmitted as soon as the periodic transmission occurs. Thus, nodes can understand whether each frame means cluster deformation or means error correction.

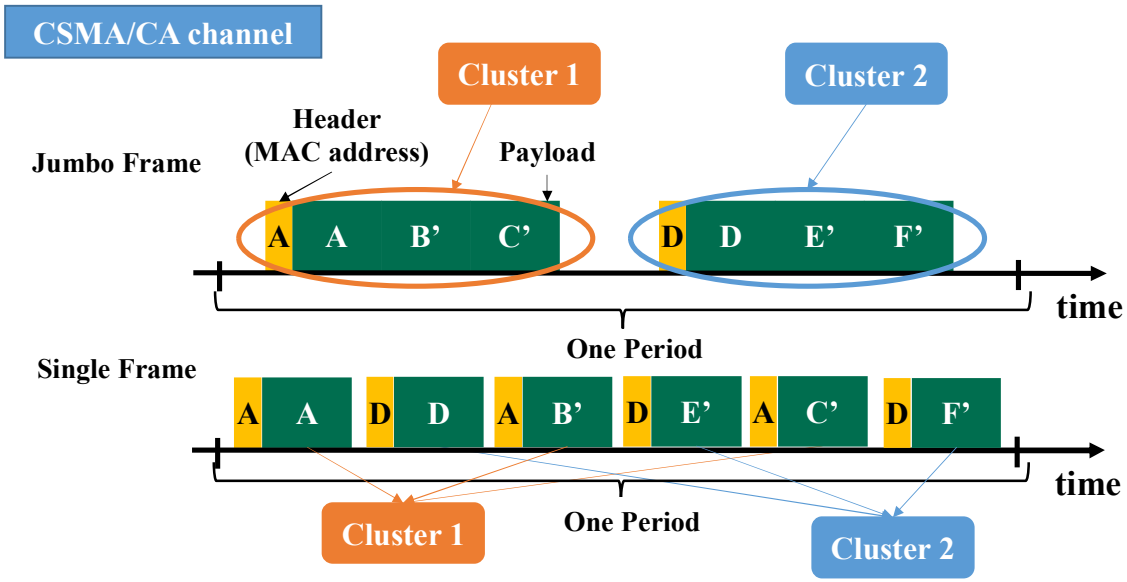


Fig. 13 Simple cluster management process through frames.

## E) Cluster Head Selection

This section focuses on two simple cluster head selections. The selection provides small impacts on performance if each member becomes cluster heads regularly (randomly). The priority of becoming heads is the same in all nodes except for the opportunity of the automatic error estimation. When a node becomes a cluster head, the node can automatically correct the accumulative estimation errors without transmitting correction frames. This is because heads can transmit their measured data. Let us consider that ten nodes create a cluster, and each node advertises its own data every 100 ms. In this case, the estimation errors are automatically corrected every 1 s. This section does not focus on which solutions are suitable and whether other solutions are better. Considering them will be worked in future studies.

The first way is that members know the next head through the order of the data in the head's transmitted frames. For example, a node shown in the first data is the current head, and a node shown in the second data is the next head. As seen in Fig. 14, even though either frame format is used, the next heads can be known, B and E. In the example of the above section, A transmitted *Data(B', t + 1)*, following with its own data during period *t + 1*. C also transmitted *Data(A', t + 2)*, following its own data during period *t + 2*. During the period *t + 2*, B removed A's cluster, and C knows it through B's frame; therefore, C becomes the next head instead of B. As in the successful examples, B's notification of the deformation is not listened to by A and C. In the cases, after B's head retried it several times, each node forms a cluster joining only itself again, if necessary.

In the way, members may receive incorrect information, which explicitly specifies the next cluster head. In other words, each member of a cluster receives the intended

information from the current cluster head. The event occurs when the members fail to receive frames due to frame errors. Incidentally, the event does not occur if members transmit correction frames to unacceptable estimation errors. Members identify correction frames by MAC address in the frame header, as mentioned in the above section. Therefore, members can know whether the frames are transmitted by members or by the head. Namely, they can know whether the frames are the correction frames or not.

The event causes several cluster members to become the next cluster heads or none of the cluster members to become the next cluster head. For example, the former occurs when the next cluster candidate, i.e., the member that the current cluster head specified as the next cluster head in frames, can correctly receive the frames. The other members cannot receive the frames. For example, the latter occurs when the next cluster candidate cannot correctly receive the frames, and the other members can the frames. In the case of using the single frame format, both of the events are likely to occur. Using the jumbo frame format, the former never occurs, but the latter is likely to occur.

A member sending a frame earliest becomes the cluster head in a first come first served manner to avoid the event. Several heads temporarily exist through this solution, but the situation is instantly resolved (in a few times). If members receive frames from several heads many times, i.e., the case seldom occurs and is the worst case, members transmit their own data by themselves, which means to deform the cluster. Next, the author explains a solution for selecting no cluster heads. At this event, none of the members transmits frames. Then, members deform the cluster as the solution because members receive no frames from the cluster head. Typically, cluster members are relatively near each other, and thus, these events may rarely occur as long as the members are near each other.

The second way is the decision based on the MAC address; specifically, members become the cluster head in descending or ascending order of their MAC address. Nodes need to memorize MAC addresses, but the head is correctly elected even if members fail

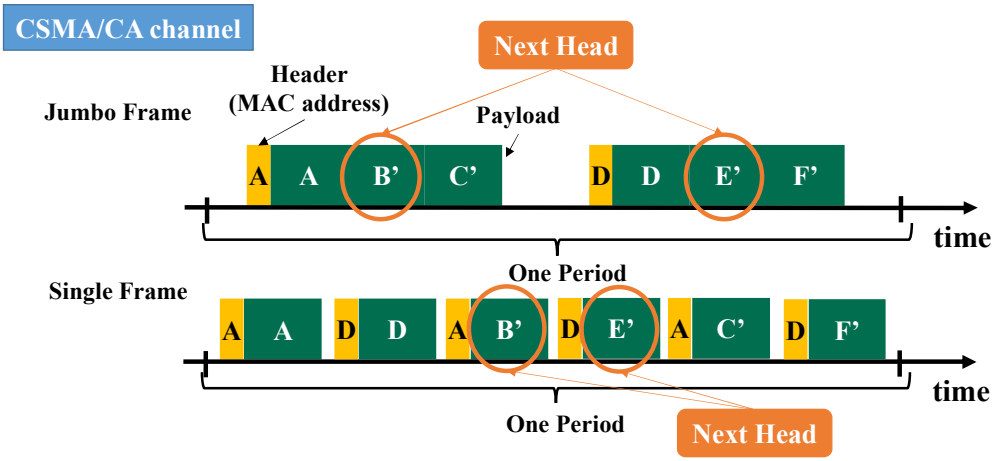


Fig. 14 Simple head selection process through frames.

to receive frames. If communications between members are frequently unable, i.e., members cannot receive frames from the cluster head in the pre-defined times, members deform the clusters. This is because members cannot detect estimation error corrections.

## F) Samples Operations of CLASES Method

Let us discuss five nodes (A–E) form a cluster along with the proposed method. The algorithm is divided into five steps. Here, *Data(X, t)* shows measured data that node X transmits at period *t*, and *Data(X', t)* shows estimated data of X at period *t*. Each cluster repeats Step 2 to Step 5.

1) Step 1: Cluster Management

First, A–E have not joined any clusters. Each node sends its own current data containing only its own state; namely, *Data(A, t)*, *Data(B, t)*, …, *Data(E, t)* are broadcasted by themselves. All nodes hear them and know that the nodes do not belong to any clusters. A sends *Data(A, t + 1)*, *Data(B', t + 1)*, *Data(C', t + 1)*, …, *Data(E', t + 1)* at the next period *t* + 1. Note that *Data(B', t + 1)*, *Data(C', t + 1)*, …, *Data(E', t + 1)* are the estimated values of *Data(B, t + 1)*, *Data(C, t + 1)*, …, *Data(E, t + 1)*, which A estimates in this case. All nodes know that A–E form a cluster because A sent these data. This process is repeated, if necessary.

2) Step 2: Cluster Head Selections

Then, a cluster elects a cluster head. Each node periodically becomes the head. Here, let us discuss the operations of the following steps when A is their cluster head.

3) Step 3: Data Estimation

In this step, cluster head A estimates the member's state data. At a period t, A estimates the state data of the members (B, C, D, E); namely, *Data(B', t)*, *Data(C', t)*, …, *Data(E', t)*. To estimate them, A can use their past state data such as data at period *t* - 1; namely, *Data(B, t - 1)*, …, *Data(E, t - 1)*. A can obtain them by listening to their frames before time t. Note that some estimated states are likely to contain unacceptable errors.

4) Step 4: Intercluster Communications

In Step 4, A broadcasts the frames conveying its own measured data *Data(A, t)* or members' estimated data *Data(B', t)*, …, *Data(E', t)*. All nodes, however, may still obtain state data with the remaining unacceptable errors in this step.

5) Step 5: Estimation Error Correction

In step 4, B–E must listen to A's broadcasted frames to correct their own data. For example, E's state data *Data(E', t)* contains an unacceptable error, and then E broadcasts *Data(E, t)* by itself.

## G) Characteristics of Performance of CLASES Method for Four Parameters

The communication performance of the proposed method mainly depends on the following four factors: 1) cluster sizes, 2) the occurring frequency of the unacceptable estimation errors, 3) the occurring frequency and the sustaining time of the clustering build-up phases, and 4) the total power of wireless interference. Here, the clustering build-up phases mean the phases, including cluster management.

### a). Cluster Sizes

As each cluster size is larger, the performance is higher at first and then becomes lower. The size affects a trade-off between the total power of interference and the possibility of parallel transmissions. First, a larger cluster size reduces interference power more significantly. Using a larger cluster size decreases the number of active nodes waiting for transmissions. As a result, the number of simultaneous transmitters decreases and thus decreases interference power. In contrast, decreasing the number of simultaneous transmitters involves decreasing the possibility of parallel transmissions by multiple cluster heads. Through the above discussions, the appropriate cluster size leads to maximizing the performance for improving the spatial uses of V2X communications. At

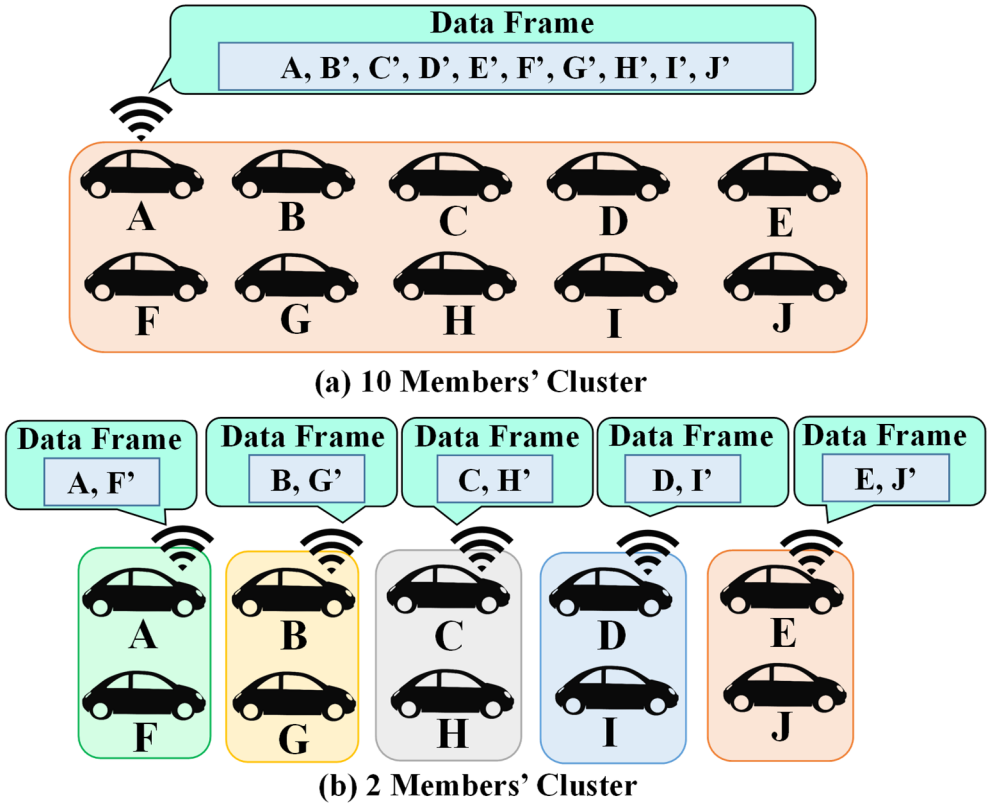


Fig. 15 The example of clusters with various cluster sizes.

severer channel congestion, the appropriate size is larger to avoid parallel transmissions more frequently. Fig. 15 shows the examples in which ten nodes make clusters in the proposed method. Fig. 15 (a) shows the cluster size is 10 in a cluster; Fig. 15 (b) shows the case where the cluster size is 2, and then 5 clusters are made. The number of active nodes in Fig. 15 (a) (i.e., one node) is smaller than that in Fig. 15 (b) (i.e., 5 nodes). In the case of Fig. 15 (a), mitigation of the total power of interference is more effective than parallel transmissions, especially. In contrast, we can observe the reverse characteristics in Fig. 15 (b) by capture effects.

### b). Unacceptable Estimation Errors

The occurrence frequency of the unacceptable estimation errors deteriorates the performance. The occurrence of the errors generates additional frames, i.e., correction frames. As a result, the total power of interference amplifies, so the performance deteriorates. The negative impacts are larger, as cluster sizes are larger. In cases where the jumbo frames are used, the negative impacts are larger. The above impacts were already described in the previous sections.

Also, the case that nodes cannot receive corrections occurs depending on the occurrence frequency of frame errors in the communications between nodes. In other words, nodes fail to receive correction frames more frequently as frame errors more frequently occur. However, nodes naturally fail to receive ordinary CWS frames, i.e., frames containing measured data, in the conditions that frame errors occur frequently. CWS frames yield larger errors than the corrections. On the other hand, when frame errors do not happen so frequently, corrections errors also seldom occur, so the impact is small.

### c). Clustering build-up phases

In this section, let us define unsuccessful communications between members in addition to cluster formations in progress as the clustering build-up phases. Both events cause to deform clusters. In this phase, members are likely to receive estimated frames from the cluster head unsuccessfully. As a result, members transmit frames containing their own data themselves. Also, if members cannot receive estimated frames from the head many times, members decide to deform the cluster. On the other hand, the clustering steady phases include the conditions in which communications between cluster members in the same clusters, which are not explicitly conducted, are necessarily successful.

During the clustering build-up phases, the performance slightly deteriorates because the cluster size during the clustering build-up phases is smaller than that during the clustering steady phases. In most cases, the proposed method with a small cluster size may not obtain high performance. The clustering build-up phases do not occur so frequently against transmission frequency. This is shown in the rough analysis in the following section. Hence, the performance deteriorates slightly. Note that the

performance in the proposed process does not deteriorate due to the management process's overheads, unlike the conventional methods. The proposed simple process finishes without any additional communications; the conventional processes must exchange some additional frames.

### d). Comparisons between QoS of CLASES and QoS of Other Methods

The proposed method provides higher performance than the non-cluster method by selecting a suitable cluster size. The proposed method is more effective for reducing the power of each interference source and the number of interference sources than the non-cluster method because of the spatial reuses. Based on the characteristics, as the total power of interference increases, the improvements increase and then decrease. Note that at environments with much weak interference, the proposed method cannot mitigate them further; at environments with high interference, the proposed method cannot also mitigate them further.

The performance is higher than that of the conventional cluster-based methods, as long as all the data include unacceptable errors. In the worst case, all cluster members transmit their data. Then, the channel resources are overused, and communication performance temporarily decreases sharply. The traffic load is the same as conventional cluster-based methods. As the advantage of the conventional ones, different intracluster and intercluster communication channels provide the irregularity of the frame sizes. The advantage leads the proposed method to provide slightly lower performance than the conventional ones. Typically, corrections occur much infrequently than the worst case. Nodes (especially vehicles) move according to physical laws; for example, nodes cannot sharply turn right/left. The author confirmed the characteristics based on the occurrence frequencies of the unacceptable estimation errors from the real node mobility data (i.e., Bologna data [82] [83]), and then the errors seldom occurred. Thus, the proposed method is typically higher performance than the conventional cluster-based methods.

## 2. Evaluation Models

This paper focused on both basic performance and practical performance through computer simulations; the basic performance evaluations used a stochastic node distribution model. The practical performance referred to models built with real data (Bologna data). These evaluations mainly highlighted the impacts of the cluster size and frequency of unacceptable errors. These results show performance improvements of the proposed method against the non-cluster method.

This section shows the evaluation models as follows. First, this section presents the common model and parameters: node models, wireless communication parameters, and CLASES method models. Then, the author derived an analysis model for the performance, including clustering build-up phases. Finally, the details of each evaluation are described.

## A) Node Model

This paper assumed the evaluation scenario in which two nodes approach each other at a relative speed of 60 km/h and then collide with each other head-on. The two nodes were called target nodes. As the distance between the nodes in the warning period is longer, NAC is smaller [78]. The distance of the head-on crash scenario is the longest of all scenarios, whereas the distance of the fastest node in the system is the longest of the other nodes. Here, NAC was based on the QoS of the node moving at the average speed. The average speed is approximately 30 km/h; namely, the average relative speed is 60 km/h.

Around the target nodes, other nodes were deployed according to the distribution models, called neighboring nodes. The nodes play a role in interference sources to the target nodes and compete with the opportunities of transmitting frames with the target nodes, according to CSMA/CA. The distributions are explained in the following sections.

## B) Wireless Communication Parameters

The wireless parameters complied with IEEE802.11p, and the MAC frame format complies with the BSM format [18] [79], used in CWS typically. The bandwidth was set to 10 MHz [14] [79]. The data rate was 3 Mbps for the broadcasting mode [14]. The header size of frames was 32 bytes, and the payload size was 250 bytes [18] [79]. Hence, the size of the jumbo frames was $32 + 250 \times N$ bytes, where $N$ indicates the cluster size. The maximum contention window was set to 15, fixed for the broadcasting mode [79]. The transmission power was 20 dBm [79].

Other parameters of the wireless communications were set to the following values. Nodes transmitted frames at slightly more than 10 per second as in [44]. All nodes used the same frequency. The threshold of SINR was set to 3.162 dB. This value was used frequently in some studies. The communication range was a circle of a radius of 300 m. The signal power followed a free radio propagation model within 300 m apart from a transmitter and then is zero; in other words, the signal power depended on only the distance between a transmitter and a receiver except for shadowing and fading. The radio propagation model is not effective for improvements. This is because the performance of both methods seems to deteriorate as well. The authors assumed no specific buildings to investigate fundamental performance. Note that the numbers and the materials are various in every location, and thus, general cases are difficultly modeled.

## C) Models of CLASES Method

First, the cluster formation complied with the following model. The cluster size of all clusters is the same for the following two reasons. First, the author evaluated the characteristics of the performance against it in a fundamental model. Second, clusters can

be formed at any cluster size in the dense cases. The readers are not interested in the communication characteristics of the sparse cases. The author also assumed that clustering build-up phases occur when members cannot correctly listen to each other's frames several times or a cluster head selection fails.

We have not accurately investigated the occurrence frequency of clustering build-up phases. It is out of this paper's scope, and the performance, including clustering build-up phases, is evaluated in further study in detail. Instead, we investigated the clustering build-up phases based on Bologna data and approximately evaluated the performance, including the clustering build-up phases. The clustering build-up phases' occurrence deeply depends on the distance between cluster members; namely, the clustering build-up phases occur more frequently as the distance becomes larger. Hence, we computed the duration that keeps the distance between two nodes smaller than a certain value from the real node mobility data (Bologna data). As a result, nodes can keep the distance of 20 m for approximately 133 seconds; namely, the duration is much shorter than transmission interval such as 100 ms. This comes only from Bologna data [82] [83], and the results depend on data sets and the number of nodes. To cover the negative points, the author evaluated the performance at a wide area of parameters about clustering build-up phases and used the performance degradation parameter such as 20% as the reference value of the tentative upper bound for our performance evaluations. The author also evaluated the performance at a wide area of parameters about clustering build-up phases to assume clustering build-up phases seldom occur in current road traffic mobility, but they may occur more frequently in future ones.

Second, unacceptable estimation errors probabilistically occurred. The ratio was called *error occurrence frequency (EOF)*. As a simple assumption, the errors homogeneously occurred for all nodes. The probability was also defined as the absolute occurrence frequency during 1 s that estimations of each member's data exceed a certain acceptable estimation range. Note that the absolute frequency is fixed with an increasing transmission frequency in the assumption. Note that EOF comprehensively expresses the occurrences of the errors by three factors in the above sections. The negative impacts against cluster sizes, which are written in the above section, are excluded as the cause of EOF. The negative impacts are larger when the cluster size is larger, as usual.

As well as the occurrence frequency of the clustering build-up phases, this paper approximately investigated the error occurrence frequency. Analyzing the frequency is out of this paper’s scope and will be evaluated in further study. From the real node distribution data, the author roughly calculated the expectation of EOF was 0.06; the performance evaluations hence referred to this value; unacceptable errors occurred at the EOF of 0.06 and fluctuated around this value every second per node on average. The calculation steps for expectations of the number of estimation errors between the estimated values and the true values are as follows. Firstly, we linearly extrapolated each location of a node after t seconds (t varies from 0.1 to 1.0 with 0.1 unit in the case of the transmission frequency of 10 frames /s) from the current location and velocity. Secondly,

we calculated estimation errors between the extrapolated locations and the true locations included in Bologna data. Thirdly, if the estimation errors are larger than 1 m, which are much smaller than the accuracy of the current market available GPS, we here defined that the estimations include unacceptable estimation errors. Fourthly, the author computed the estimation error probabilities corresponding to the number of estimation errors per node per second. Finally, the author selected the several nodes, computed the error expectations from their estimation error probabilities, and calculated the average of the error expectations, which was 0.06.

The estimation error expectations in the evaluations of this section are expected to be smaller than 0.06. The error expectations decrease as transmission frequencies increase. The value 0.06 was calculated in the transmission frequency of 10 frames/s. This section has evaluated the performance, including estimation errors at transmission frequencies of either 12 frames/s or 18 frames/s.

## D) Analysis Model of Performance including Clustering Build-up Phases of the CLASES Method

The author approximately evaluated the performance, including clustering build-up phases. Specifically, the author analyzed it based on the weighted summation (1) calculated from the duration of the clustering build-up phases and the performance of each phase.

$$I_{CLASES,all} = I_{CLASES,steady} \times r_{steady} + I_{CLASES,build-up} \times r_{build-up} \quad (1)$$

In Equation (1), $I_{CLASES,all}$ shows the performance improvement of the proposed method from the non-cluster method, including both clustering steady phases and clustering build-up phases. $I_{CLASES,steady}$ and $I_{CLASES,build-up}$ show the performance improvement with a comparison to the non-cluster method. $r_{steady}$, $r_{build-up}$ show the ratio of the duration of the clustering steady phases to overall and the ratio of the duration of the clustering build-up phases to overall.

$I_{CLASES,build-up}$ can be expressed as Equation (2) using $I_{CLASES,steady}$ and $r_{performance}$ that shows the performance during the clustering build-up phases to performance during the clustering steady phases. The performance decreases in comparison with clustering steady phases, so the value becomes small by a ratio $r_{performance}$.

$$I_{CLASES,build-up} = I_{CLASES,steady} \times r_{performance} \quad (2)$$

Moreover, $r_{steady}$ can be expressed using $r_{build-up}$ as Equation (3) because the cluster state is either of the clustering steady phases or the clustering build-up phases.

$$r_{steady} = 1 - r_{build-up} \quad (3)$$

Substituting Equation (2) and Equation (3) to Equation (1), we can obtain Equation

(4).

$$I_{CLASES,all} = I_{CLASES,steady} \times \left(1 - r_{build-up}\right) + I_{CLASES,steady} \times r_{performance} \times r_{build-up} \quad (4)$$

The author did not focus on revealing the ratio. In the previous section, the author explained that not all clusters are deformed simultaneously, and thus the ratio is expected not to be so small.

## E) Models and Parameters in Basic Performance Evaluations

In the evaluations, a performance evaluation metric is NAC, which is defined in Section 2. First, NAC in a clustering steady phase was evaluated while mainly changing the cluster size and EOF. Next, the performance, including clustering build-up phases, was evaluated according to an analysis model. In only the evaluation, the impacts of the additional two factors were evaluated, which the impact of the frame composition models and the impact of the frequency of periodic transmission. In real performance evaluation, the author evaluated the impacts of many real distributions rather than the impacts of the two factors.

In the evaluations, the neighboring nodes were uniformly distributed within a radius of 300 m; namely, a random node distribution model. The model is the most basic stochastic one. In the model, the author can easily change the number of nodes in the system while keeping the distribution. The model supported the general performance rather than that in certain distributions. The nodes were set to a slower speed than 30 km/h so that the target nodes become the fastest.

## F) Models and Parameters in Practical Performance by Realistic Node Distributions Evaluations

In the evaluations, nodes were deployed according to the real road traffic flow data. In addition to the basic ones, this paper focused on the impacts of cluster size, EOF, transmission frequency to performance, and clustering build-up phases. This paper focused on the various realistic distributions instead of evaluations of the impacts of the frame formats.

In the evaluations, a performance evaluation metric was the average number of the frames that a target node correctly receives during a period in which the traffic signal changes in seven intersections extracted from Bologna data [82] [83]. The realistic node distribution models allowed us to change no number of nodes freely. The data were collected in Bologna, Italy, in the project iTETRIS [82] [83]. The data are open data, and the URL is http://sumo.dlr.de/wiki/Data/Scenarios. The data include both road traffic

flows of vehicles and pedestrians, so they are suitable for evaluating the performance of V2X communication, including both V2V and V2P. Note that the data only include the locations, the speeds, and the angles, and so on. They do not include data about wireless communication. The data were collected over three days (from November 11 (Tue) to November 13 (Thu), 2008) with 636 detectors in Bologna; the data include peak hours in the morning. Therefore, many researchers have used the data for the simulation of V2X communications [80]–[83].

From the data, the author extracted seven intersections, and nodes within 300 m from the center of the intersections were deployed as neighboring nodes. The seven intersections are named A–G, as shown in Fig. 16. The set of intersections consists of four large-scale ones (A–D) and three small-scale ones (E–G). In the former, there are many vehicles; in the latter, there are many pedestrians. The author evaluated the performance of various distributions.

In each of the intersections, the author focused on the average number of frames during the five periods in which the traffic signal changes. During the periods, the node distribution largely changes. Note that the period of the intersections of no traffic signals is 112 s, which are the average periods of the other ones. The five periods for the evaluations are selected as follows. The number of nodes within 300 m from the center of the intersections is relatively large, at 3500 s in the data. Therefore, the author used data before and after the time; specifically, the author evaluated it during a period that started from 3500 s and from four periods that started from 2500 s, 3000 s, 4000 s, and 4500 s. A simulation time of a sample was 2 seconds, and the author evaluated samples of 2 seconds in about 1000 times. In a sample, the first 1 second was an initialization time and the last 1 second was an evaluation time. The first 1 second was used to exclude the

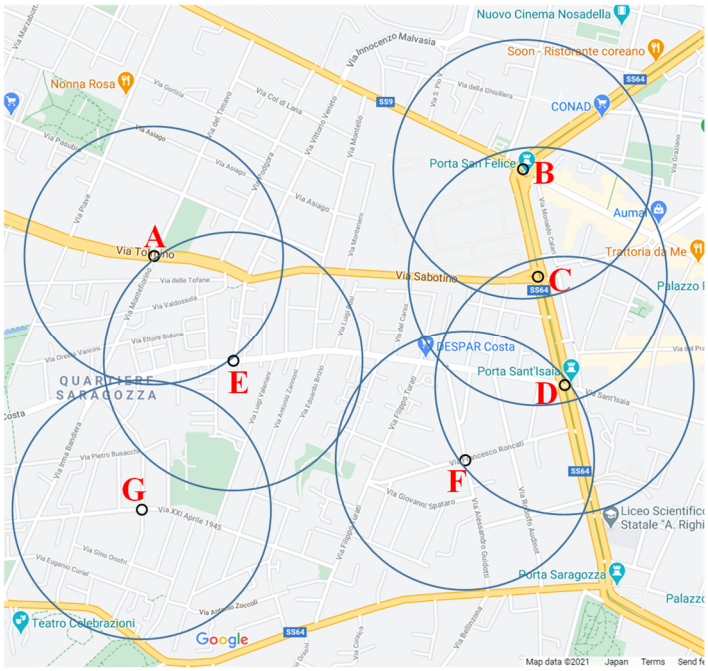


Fig. 16 Selected seven intersections (via google map).

DSRC transition duration. During the duration, the surrounding nodes stopped moving. The last 1 second was used for evaluating the DSRC performance. During the duration, the surrounding nodes moved along to the Bologna data; the number of the samples is different according to a period of traffic signals. Additionally, a simulation scenario was conducted in ten times. In CWS, evaluating the QoS between 2.5 and 3.5 seconds is important because it is the most recent warning period. The simulation time is sufficient enough to generate unacceptable estimation errors. CWS also uses broadcast communications, and the communications are stateless. This means that broadcast communication at one time and that at another time are independent.

The author roughly analyzed a relation between the node distributions and interference power in the locations. The author introduced system density and nearby density. A system density is the number of nodes within a circle with a radius of 300 m from an intersection center. A nearby density is the average number of nodes within the following circles from an intersection center; a circle is with an radius of 60 m and the other circle is with an radius 84 m. These nodes within the circles provided stronger interference than the SINR threshold before 2.5 seconds and 3.5 seconds prior to a potential crash, respectively.

Fig. 17 shows the relation between the average system density and the average nearby density of the five periods of traffic signals in each location. The horizontal axis expresses the average system density. The vertical axis expresses the average nearby density. The node distributions of A–F tend to be a higher nearby density than the random one; that of G tends to be a lower nearby density than the random one. A node in the former locations is interfered with more strongly from other nodes than in a random one when the location has the same system density as that of a random one. The author evaluated the impact of node distributions based on the analysis.

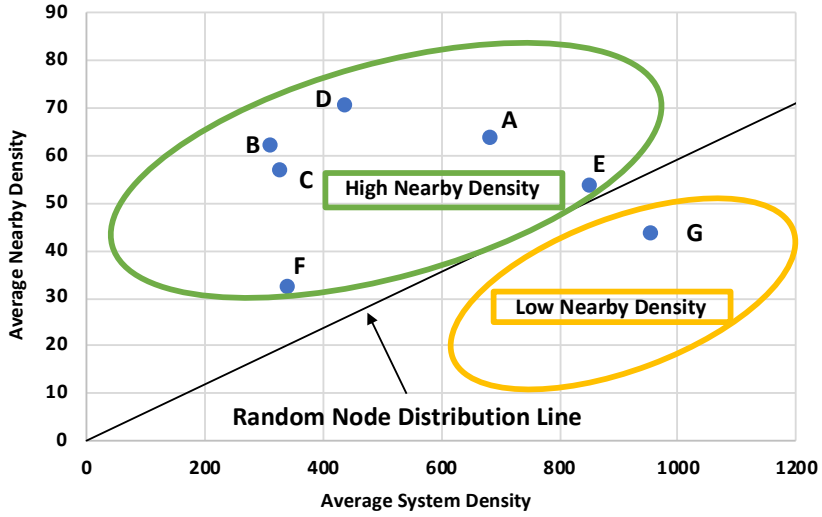


Fig. 17 The average nearby density against the average system density in each location.

# 3. Results of Basic Performance Evaluations

This section shows the performance of the proposed method in comparison with the non-cluster method in a stochastic node distribution model.

## A) Cluster Size and Transmission Frequency

Fig. 18 and Fig. 19 show a relation between NAC and cluster sizes at every transmission frequency. The graphs show the performance during a clustering steady phase in the case where unacceptable errors never occur. The horizontal axes express cluster sizes. The vertical axes express NAC. Each line expresses NAC against transmission frequency. Fig. 18 is a graph of the case using the jumbo frame format and Fig. 19 is a graph of the case using the single one. Note that the NAC of the non-cluster method shows the value in which cluster size is one. The black lines express it. These evaluations reveal the appropriate transmission frequency because of the characteristics of V2X communications, and the transmission frequency was utilized in the following evaluations.

The graphs show that the proposed method increases NAC by clustering nodes. Fig. 18 demonstrates that the proposed method using the jumbo frame format increases it by 30 % over that of the non-cluster one. The cluster size is eleven, and the transmission frequency is 18 frames/s. In Fig. 19, the author revealed that the proposed method using the single frame format increases NAC by 12 %. The cluster size is nine, and the transmission frequency is 18 frames/s. In the following two types of evaluations, the nodes transmitted frames at the frequency of 18 frames/s.

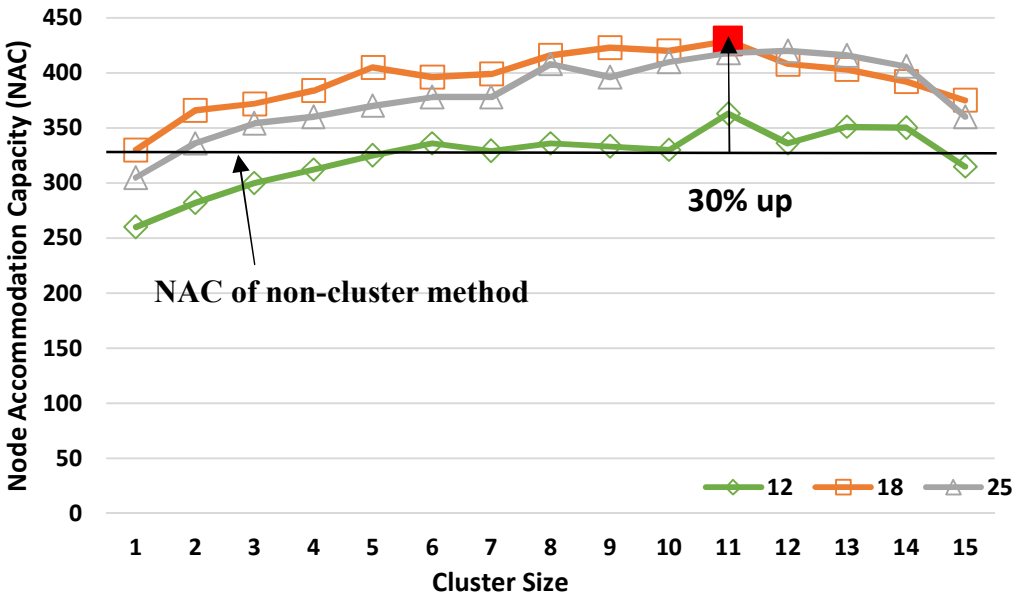


Fig. 18 A relation between cluster size and NAC in different transmission frequencies (jumbo frame format).

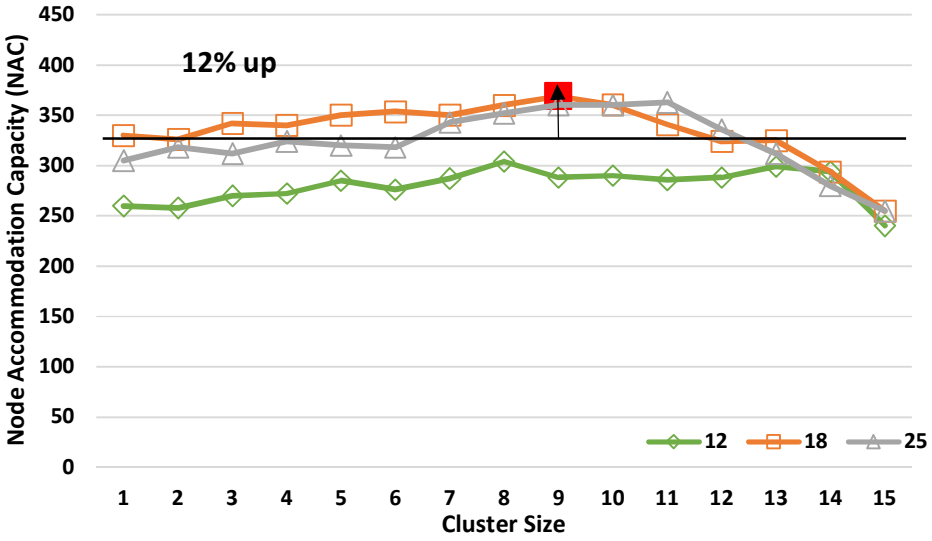


Fig. 19 A relation between cluster size and NAC in different transmission frequencies (single frame format).

## B) Unacceptable Estimation Errors

Fig. 20 and Fig. 21 show the performance in the case where unacceptable estimation errors occur. The horizontal axes express cluster sizes, and the vertical axes express NAC. Each line expresses a performance against EOF. Fig. 20 is a graph of the case using the jumbo frame format, and Fig. 21 is a graph of the case using the single one. As well as the above graphs, the black lines express the NAC of the non-cluster method.

The graphs show that even if the EOF is 0.06, the proposed method effectively increases NAC. Fig. 20 shows that the proposed method using the jumbo frame format increases NAC by 27 % when the EOF is 0.06. When the EOFs become 0.1 and 0.2, then

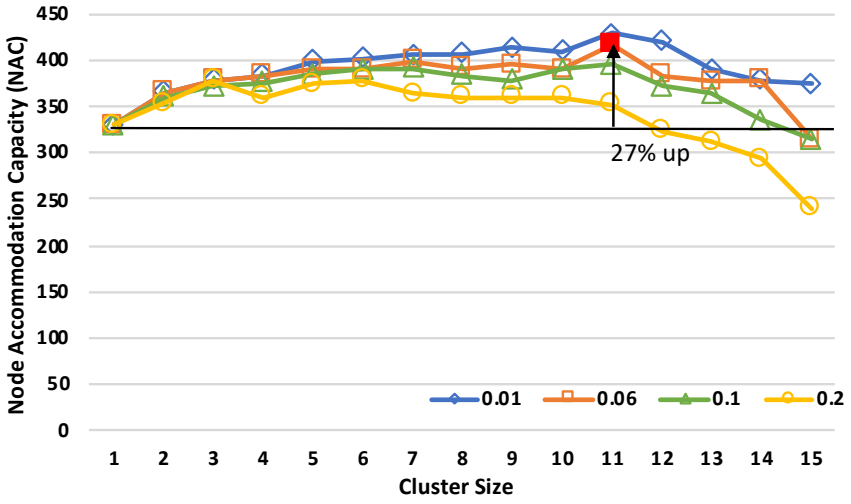


Fig. 20 A relation between cluster size and NAC in different EOF (jumbo frame format)

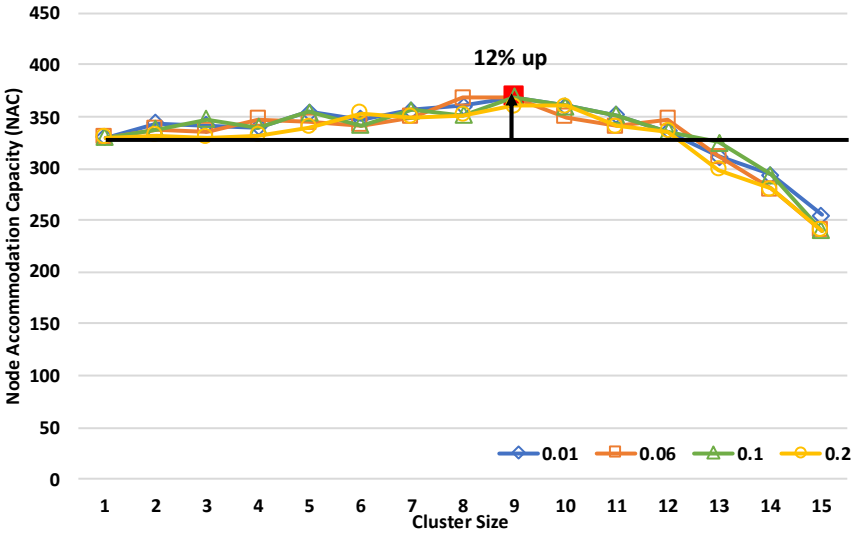


Fig. 21 A relation between cluster size and NAC in different EOF (single frame format).

the performance deteriorates from the above one. On the other hand, Fig. 21 shows that the proposed method using the single frame format increases NAC by 12 % when the EOF is 0.06. Also, the impact of the frequent errors on the performance is significantly small.

## C) Performance including Clustering Build-up Phases

Fig. 22 and Fig. 23 show the performance improvement ratio, including the clustering build-up phases of the proposed method under the maximum performance of the above section through the approximate evaluations in Section D). The horizontal axes express

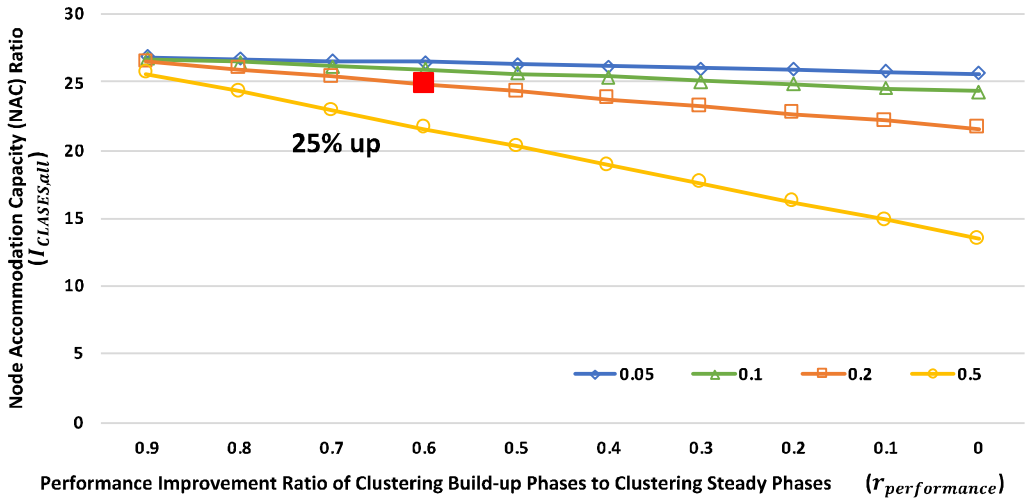


Fig. 22 The performance improvement ratio including clustering build-up phases (jumbo frame format).

the performance ratio of the clustering build-up phases to the clustering steady phases ($r_{performance}$), and the vertical axes express the NAC improvement ratio in comparison with the non-cluster method ($I_{CLASES,all}$). Each line expresses the occurrence ratio of clustering build-up phases. The graphs show the results using the jumbo frame format and the results using the single one. Each line in the following two graphs shows NAC improvement ratios compared with DSRC, unlike the above graphs.

Fig. 22 and Fig. 23 show that the proposed method sufficiently improves the QoS of V2X communications even when including clustering build-up phases. In the case using the jumbo frame, the proposed method increases NAC by 25 % (i.e., $I_{CLASES,all}$ is 25 %) when clustering build-up phases occupy 20 % of all phases (i.e., $r_{build-up}$ is 0.2) and the performance improvement ratio is 60 % (i.e., $r_{performance}$ is 0.6). In the case that uses the single one, the proposed method increases NAC by 11 % in the above parameters.

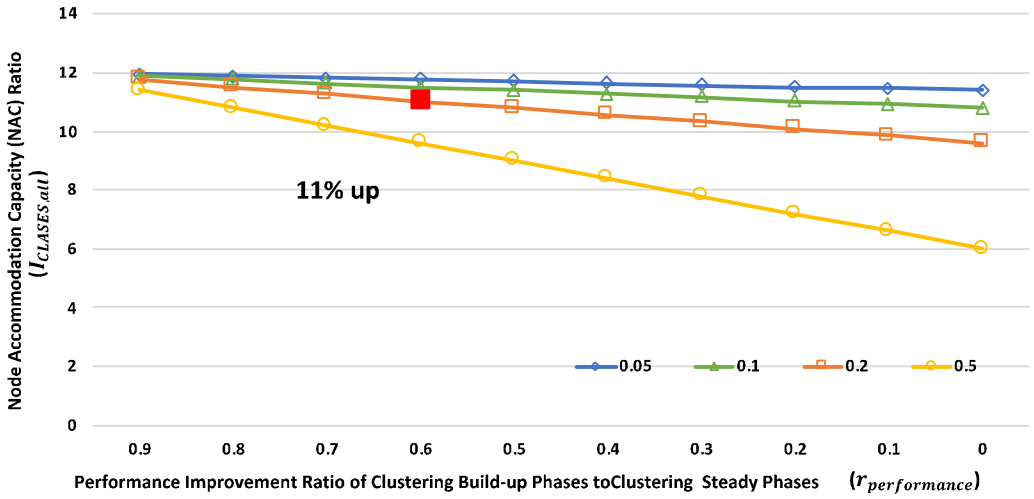


Fig. 23 The performance improvement ratio including clustering build-up phases (single frame format).

# 4. Results of Practical Performance by Realistic Node Distributions Evaluations

This section shows the performance of the proposed method compared to the non-cluster method in some specific node distribution models built with the real data.

## A) Cluster Sizes and Transmission Frequency

Fig. 24 shows the relation between the cluster size and the average number of received frames of all the locations (A–G) in various transmission frequencies. The horizontal axis expresses the cluster size, and the vertical axis expresses the average number of received frames. Each line expresses the results of various transmission frequencies. In the

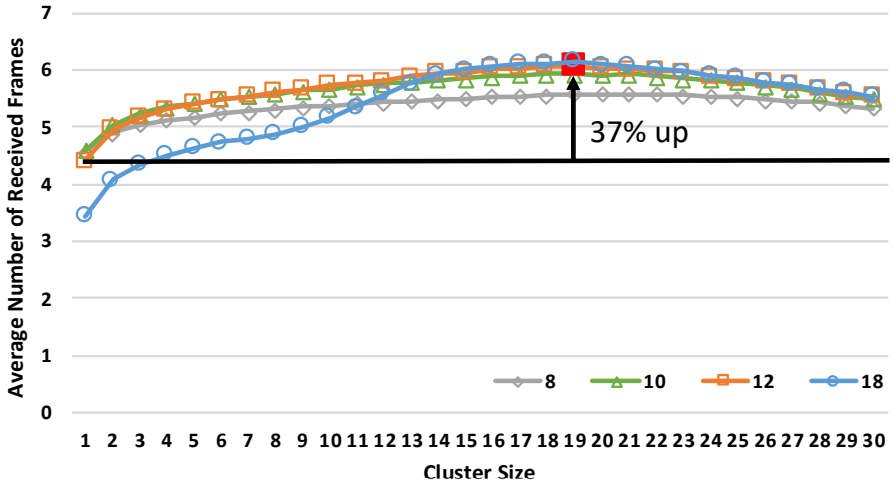


Fig. 24 A relation between cluster size and the average number of received frames against different transmission frequencies.

evaluations, unacceptable errors never occur. In the graph, the black line expresses the NAC of the non-cluster method. The evaluations also reveal the appropriate transmission frequency because of the characteristics of V2X communications, and the transmission frequency was utilized in the following evaluations.

The graph shows that the proposed method effectively improves the quality even in the realistic node distribution model. The average performance for which the cluster size varies from one to thirty was the highest in the transmission frequency of twelve. For this parameter, the proposed method increases the average number of received frames by 37 %. At the other frequencies, the proposed method increases it significantly. Note that the appropriate cluster size in the model is larger than that in the basic model because the power and the number of interference sources are larger. The graphs of the following sections show the performance in 12 frames/s.

Fig. 25 and Fig. 26 show the average number of received frames in the location of the highest value of nearby density and system density, respectively. The horizontal axes, the vertical axes, and the legends are the same ones as those of Fig. 24.

In both of the locations, the proposed method was effective for improving quality. In the location D, which is the highest nearby density, the proposed method increases the number of received frames by 57 % when nodes transmitted frames at the transmission frequency of 12 frames/s. In the location G, which is the highest system density, the proposed method increases it by 148 % in the same case. Additionally, in the cases of 8 frames/s in G, it was increased by 39 %.

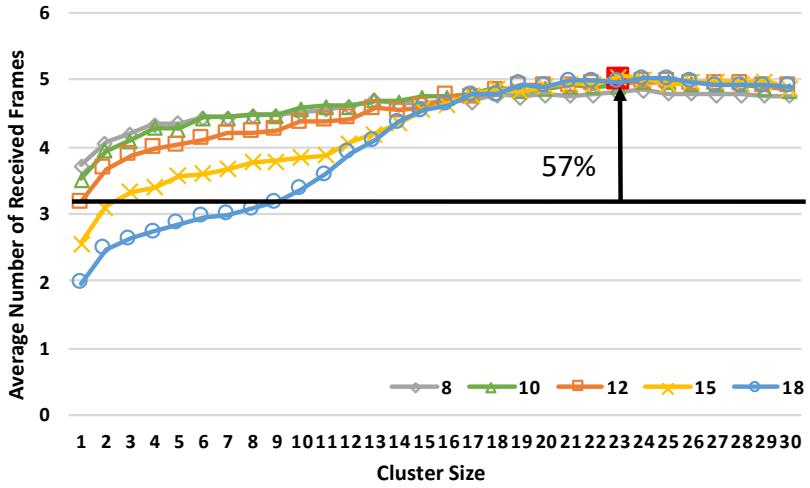


Fig. 25 The average number of received frames in location D (the highest nearby density).

## B) Unacceptable Estimation Errors

Fig. 27 shows a relation between the cluster size and the average of the received frames against EOF in the realistic node distribution model. The horizontal axis expresses the cluster size. The vertical axis expresses the average number of received frames. The legends are EOF.

Fig. 27 reveals that the proposed method improves the quality of V2X communications even when slight amounts of unacceptable errors occur in the realistic node distribution model. When unacceptable errors occur at the EOF of 0.06, the proposed method increases the average number of received frames by 20 %. Even when EOF is 0.1, at which the errors frequently occur, it increases by 16 %.

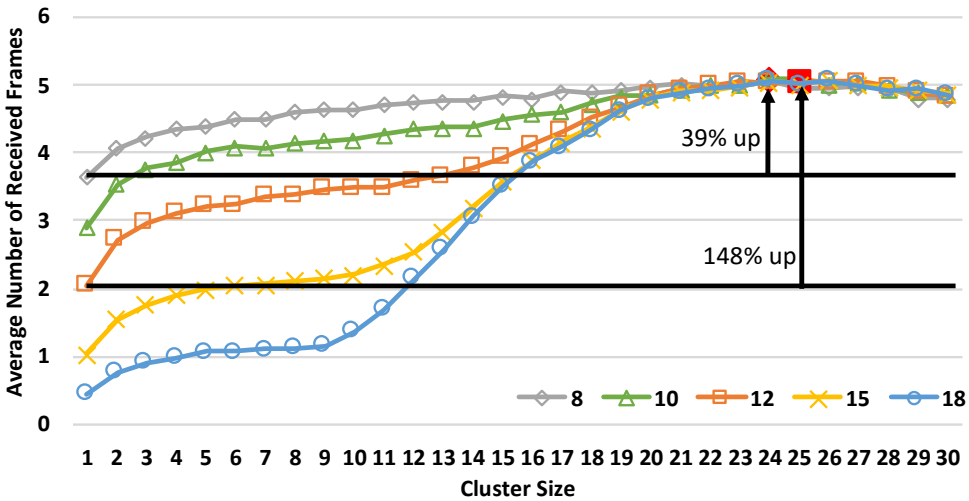


Fig. 26 The average number of received frames in the location G (the highest system density).

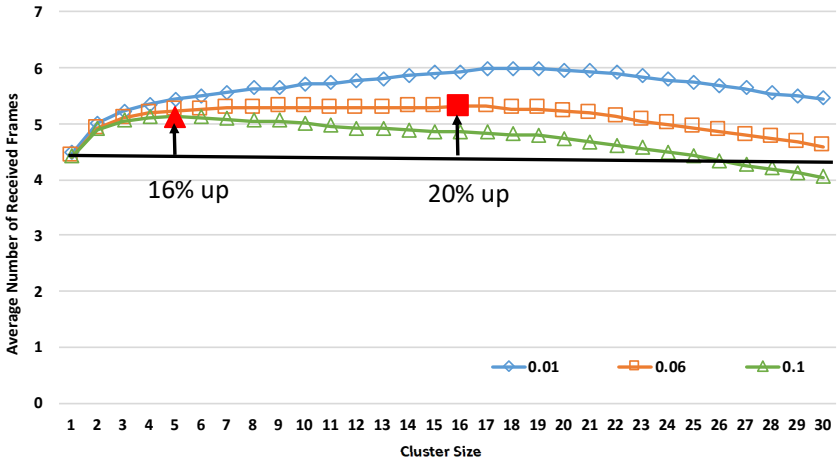


Fig. 27 A relation between cluster size and the average number of received frames against EOF.

Fig. 28 and Fig. 29 show the average number of received frames in the location of the highest value of nearby density and system density, respectively. The horizontal axes, the vertical axes, and the legends are the same ones as those of Fig. 27.

In both of the locations, the proposed method was effective for improving quality. In the location D, the proposed method increases the number of received frames by 32 % when EOF is 0.06. Additionally, it is increased by 21 % even when EOF is 0.1. In the location G, the proposed method increases it by 102 % and by 74 % when EOF is 0.06 and 0.1, respectively.

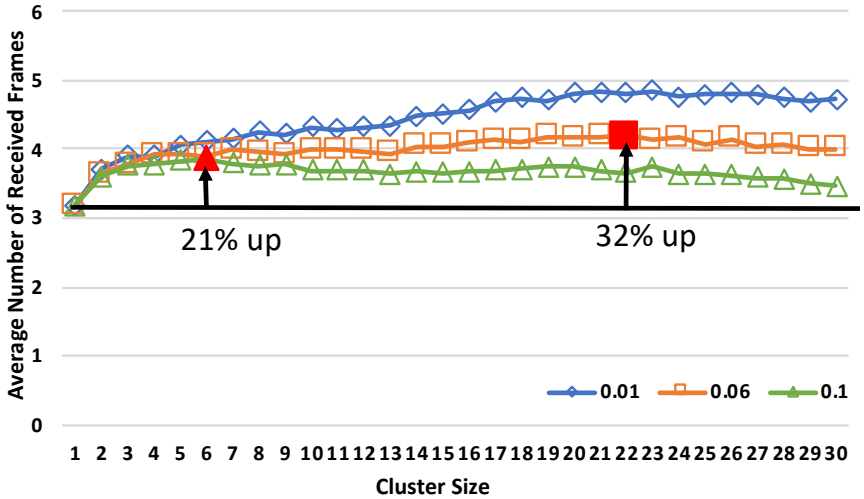


Fig. 28 The average number of received frames in location D (the highest nearby density).

## C) Performance including Clustering Build-up Phases

Fig. 30 shows the performance improvement ratio, including clustering build-up

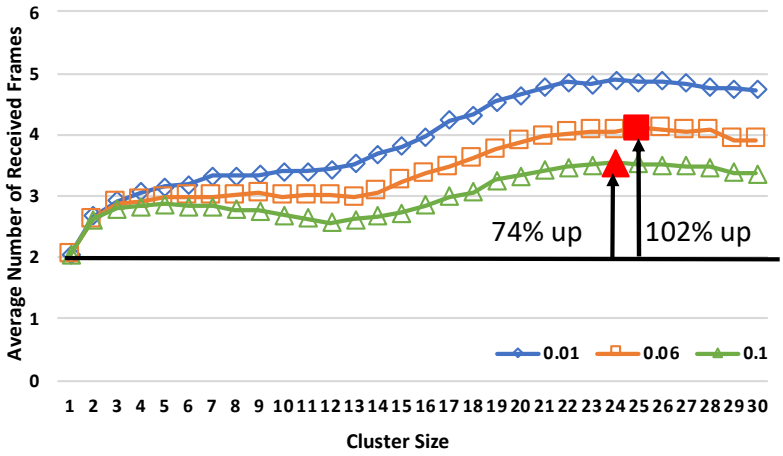


Fig. 29 The average number of received frames in the location G (the highest system density).

phases of the proposed method in the setting of the maximum performance of Fig. 27. The vertical axis expresses the ratio of the average number of received frames over the non-cluster method ($I_{CLASES,all}$). The horizontal axis and the legends are the same ones as that of Fig. 22.

The graph shows that the proposed method can improve the QoS even in including clustering build-up phases. The proposed method increases QoS by 18 % (i.e., $I_{CLASES,all}$ is 25 %) in the same parameters, as shown in Fig. 22. Additionally, the proposed method increases QoS by 16% even when both of the clustering build-up phases occupy 20 % of all phases (i.e., $r_{build-up}$ is 0.2) and the performance improvement ratio is 0 % (i.e., $r_{performance}$ is 0), and when clustering build-up phases occupy 50 % of all phases (i.e., $r_{build-up}$ is 0.5) and the performance improvement ratio is 60 % (i.e., $r_{performance}$ is 0.6).

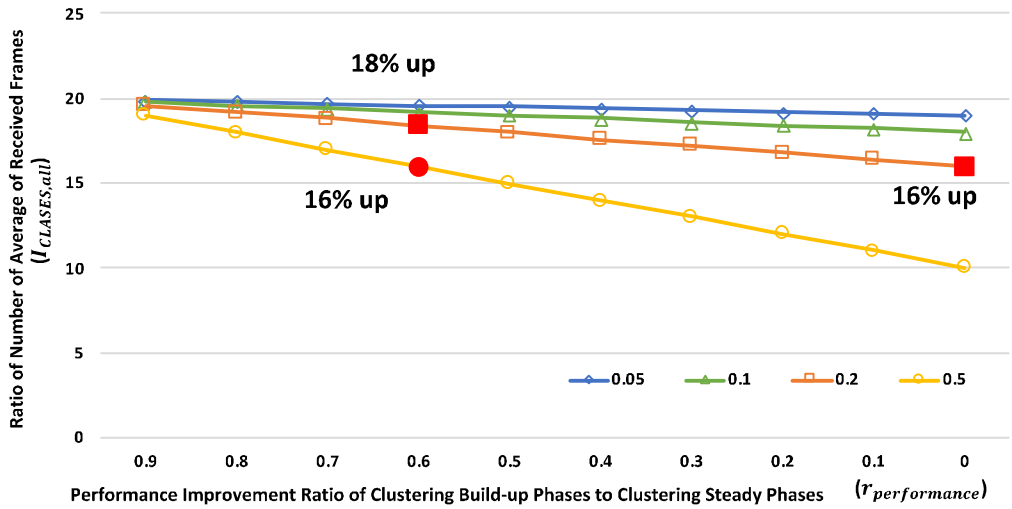


Fig. 30 The performance improvement ratio including clustering build-up phases

# 5. Conclusion in Section III

In this section, the author proposed a novel node-clustering method, CLASES, to improve the QoS of V2X communications for driving assistance with CWS. The proposed method can omit regular intracluster communications through a cluster members' data estimation and estimation error correction mechanism. The key idea supports intracluster communications while suppressing reducing the bandwidth for intercluster communications, unlike conventional cluster-based methods. The proposed method can operate a trade-off between interference power and parallel transmissions, and thus it improves the QoS of V2X communications. The drawback of the proposed method is that it amplifies interference due to the error correction mechanism involving the members' data estimation. The author evaluated the performance of the proposed method in various situations while changing various parameters. The evaluation results showed that the proposed method improves the QoS. The author also revealed that the proposed method could accommodate more nodes by 27 % than the non-cluster method even when the estimation errors occur at the realistic frequency.

# IV. Mode 4 Performance Evaluations under Channel Congestion in CWS

Section IV focuses on the performance characteristics of mode 4 in CWS under channel congestion. In this section, the author analyzes the performance characteristics in the following.

## 1. Performance Analysis of Mode 4 under Congestion

### A) Crash Scenarios and Congestion Problem

In this section, the author analyzes the performance of mode 4 in some crash scenarios. The following scenarios decrease communication performance;

Crowded intersection scenarios: crashes in crowded intersections.

High-speed scenarios: crashes with high-speed nodes, like emergency vehicles.

To discuss the relationships between the performance of mode 4 and the scenarios, the author considers an SINR during the warning period between two potential crash nodes: a transmitter *t* and a receiver *r*. Equation (5) denotes the SINR $\gamma_r$:

$$\gamma_r = \frac{S_{tr}}{I_r + N_0} \tag{5}$$

$N_0$ is noise power. $I_r$ is the interference power against the received signal at the receiver *r*. $S_{tr}$ is the received signal power from *t* to *r*. The received signal power is formulated as follows:

$$S_{tr} = P_t C_{tr} {d_{tr}}^{-\alpha} \tag{6}$$

$P_t$ is the constant transmission power. $d_{tr}$ is the distance between *t* and *r*. $C_{tr}$ is the fading gain between *t* and *r*. $\alpha$ denotes the path loss exponent. In the following subsections, the author discusses the performance characteristics of mode 4 in the two scenarios.

### B) Crowded Intersection Scenarios

Crowded intersections amplify the interference from other nodes. The interference is formulated as follows:

$$I_r = \sum_{i \in \mathcal{I}} S_{ir} \tag{7}$$

$\mathcal{I}$ denotes the set of other transmitters at the transmission opportunity of the transmitter *t*. $|\mathcal{I}|$ is the number of simultaneous transmitters. From Equations (6) and (7) is transformed as follows:

$$I_r = \sum_{i \in \mathcal{I}} P_t C_{ir} {d_{ir}}^{-\alpha} \tag{8}$$

The SINR in Equation (5) is transformed from Equation (8) as follows:

$$\gamma_r = \frac{S_{tr}}{\sum_{i \in \mathcal{I}} P_t C_{ir} {d_{ir}}^{-\alpha} + N_0} \tag{9}$$

From Equation (9), as $d_{ir}$ is smaller and/or $|\mathcal{I}|$ is larger, SINR is smaller. In crowded intersections, i.e., the density of the nodes is high, the number of nodes near the transmitter is, on average, larger than in non-crowded intersections. The trends of $d_{ir}$ and/or $|\mathcal{I}|$ decrease SINR, and as a result, the performance of mode 4 is downgraded in such intersections.

Additionally, $|\mathcal{I}|$ is related to the communication traffic load. Thus, the load is related to the number of transmissions per second (defined as NTS) is related to $|\mathcal{I}|$, in addition to the density of the nodes involved in the crash scenarios. Increasing NTS increases $|\mathcal{I}|$. Whereas increasing NTS is expected to improve SINR because of the redundant transmissions. The two impacts also operate the degree of congestion.

## C) High-Speed Scenarios

In high-speed crash scenarios, $S_{tr}$ is weaker than in low-speed scenarios. In the high-speed scenarios, potential crash nodes approach each other at high speeds. As nodes move at higher speeds, the relative speed $v_{tr}$ is higher. For example, emergency vehicles run at high-speeds. By using time-to-crash $t_{crash}$ and the relative speed, the communication distance during the warning period is shown as follows:

$$d_{tr} = v_{tr} t_{crash} \tag{10}$$

From Equations (6) and (10), the SINR is formulated as follows:

$$\gamma_r = \frac{P_t C_{tr} (v_{tr} t_{crash})^{-\alpha}}{I_r + N_0} \tag{11}$$

To recognize the potential crashes, the nodes need to receive frames during the warning period, i.e., $t_{crash}$ is 2.5–3.5 s, at least. As the relative speed is larger at time $t_{crash}$, the communication distance is larger. As a result, the SINR is lower than that of the low-speed scenarios.

# 2. Evaluation Model

## A) Crash Scenarios and Performance Metrics

Fig. 31 depicts an example of the simulations. The author investigated the number of received frames during the warning period at an evaluation target receiver from an evaluation target transmitter. The two target nodes were the potential crash nodes for each other; specifically, they frontally approached each other at a relative speed $v_{tr}$. This head-on crash scenario is the largest relative speed of the other scenarios, and thus, the communication distance is the largest in Equation (10). If the QoS requirements are satisfied in this scenario, the requirements are also satisfied in the other scenarios.

Around the target receiver, within 300 m, the other nodes were deployed, as shown in Fig. 31. All the nodes, including target nodes, shared spectrum resources in a multiple access manner. The manner causes the other nodes to play a role in the interference and competitors of slot selections for target nodes. Fig. 31 shows an example in which two nodes interfere with a frame from the target transmitter at the target receiver. The signal power was strong enough at the target receiver within 300 m.

Next, the author explains the dynamic ranges of the parameters modeling the crash scenarios. For crowded intersection scenarios, two kinds of densities (i.e., node distribution models) were given. The first kind of model is the uniform distribution model. This model is the most fundamental stochastic model. The model provides us with average performance. Additionally, the stochastic model allows us to change the number of nodes in order to boost the density of the nodes. The two reasons provide an average upper limit of the number of nodes, i.e., NAC. The second one is the realistic distribution model. The model is built by Bologna data [82] [83], which is the realistic mobility data for cars and pedestrians. From Bologna data, the author modeled three intersections: large, medium, and small intersections, named A–C, respectively. The next section explains the details of the data. The NTS of each node depends on the degree of channel congestion. In our simulations, NTS was also given 10–30 frames/s. Considering high-speed scenarios, the author set $v_{tr}$ at 120–240 km/h. For the scenarios, the author assumed that emergency vehicles run at high speeds in urban areas. In our models, the target nodes approach at a given relative speed.

The author showed the number of received frames during 2.5–3.5 seconds and NAC as a performance metric. The first metric was compared to the QoS requirements. For one of the references of NAC, the author computed the *average number of nodes (ANN)*, which is an average value over the number of nodes used in the three realistic intersections from Bologna data. ANN had 488 nodes. The number of received frames were averaged over 300 iterations in the uniform node distribution model and over 3 iterations × 1 period for the traffic signal. The period of A is 105 s. B and C have no traffic signals, so the author defined 112 s as the period because the duration is averaged over other traffic signals in the data. The metric was simulated by a simulator that the author made. In our investigations, the author could not find suitable mode 4 simulators with the system-level performance in the context of CWS. The author confirmed that the simulator outputted values along with the characteristics of mode 4.

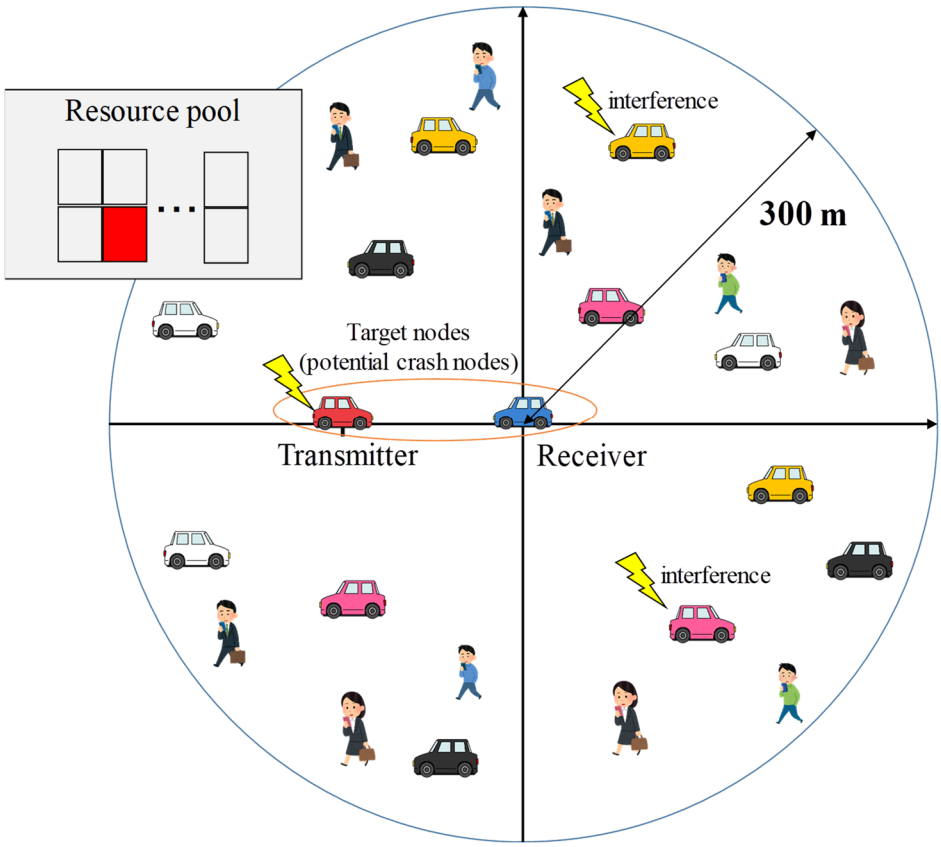


Fig. 31 The abstract image of the simulation model of CWS: the transmitter and receiver are potential crash nodes.

## B) Bologna Data and Realistic Node Distribution Models

Bologna data is the open data in iTETRIS [82] [83] (http://sumo.dlr.de/wiki/Data/Scenarios). The Bologna data was collected over three days from November 11 (Tue) to November 13 (Thu) in 2008 with 636 detectors in Bologna,

Italy. The data includes peak hours in the morning. This data includes mobility data of pedestrians. The data is suitable to evaluate V2X performance, including Vehicle-to-Pedestrian. The author obtained the mobility data from the Bologna data by Simulation of Urban MObility (SUMO) [84].

From Bologna data, the author extracted three intersections (A–C) × 9 periods. Fig. 32 (a) illustrates the geographical map of the target intersections. These densities varied with time. To analyze the characteristics of the densities with time, the author introduced two densities: *central density* and *system density*. The former is defined as the number of nodes within 100 m of the center point; the range was within the time-to-crash of approximately 3 s at the relative speed of 120 km/h. As the central density is large, $d_{ir}$ in Equation (4) is, on average, small. System density represents the number of nodes within 300 m. As the density is large, $|\mathcal{I}|$ in Equation (3) is also, on average, large. Fig. 32 (b) provides the average densities of each period. The trends of the system density and central density are proportional to the size of the intersections. Additionally, the system density is at its peak at 3500 s compared to the other times. The highest central densities were 3000 s at A, 1000 s at B, and 3500 s at C. In these periods, the performance is likely to be degraded.

## C) Wireless Parameters

First, the communication system model complied with the mode 4 standard [23]. A carrier frequency of 5.9 GHz was used as standard. The bandwidth was 10 MHz. The frame size was set to 190 bytes. The author assumed that each frame conveyed accurate data that were sufficient to provide a warning. Additionally, the author simply modeled the sub-channel of mode 4. To guarantee enough resources to transmit a frame of 190 bytes, mode 4 can have two sub-channels. Mode 4 has 1000 sub-frames/s at standard, and thus, the total number of slots was 2000 slots/s. Also, all the nodes were synchronized with GNSS.

Second, transmitted frames were correctly decoded when the SINRs were equal to or more than the threshold, as in References [43] [44]. The threshold was set to 5 dB **[35]**. As for SINR, radio propagation complied with the WINNER+ model [85], as recommended by METIS [86]. The author used the LOS model to investigate the fundamental model and did not bind specific NLOS environments. The propagation loss included a log-normal shadowing loss with a deviation of 3 dB, as established in Reference [23]. The author calculated the independent and identically distributed (i.i.d) shadowing loss between nodes. In the propagation model, the antenna height of all the nodes was 1.5 m, as was used in Reference [29]. The noise power was set to –110 dBm [30].

Third, Sensing-based SPS was configured as follows. The initial reselection counter was calculated at random but within a range. The range was configured so that it continued to use a slot within 0.5 s–1.5 s for NTS $n_t$; for example, at ten frames/s, the range was from 5 to 15. The standard determined the NTSs of 10, 20, and 50 frames/s.

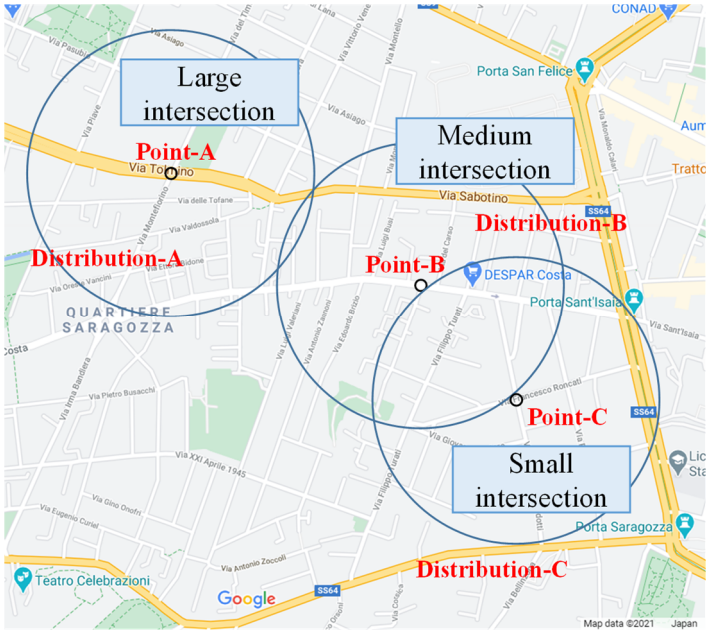


(a) Location and size of the three intersections (A–C)

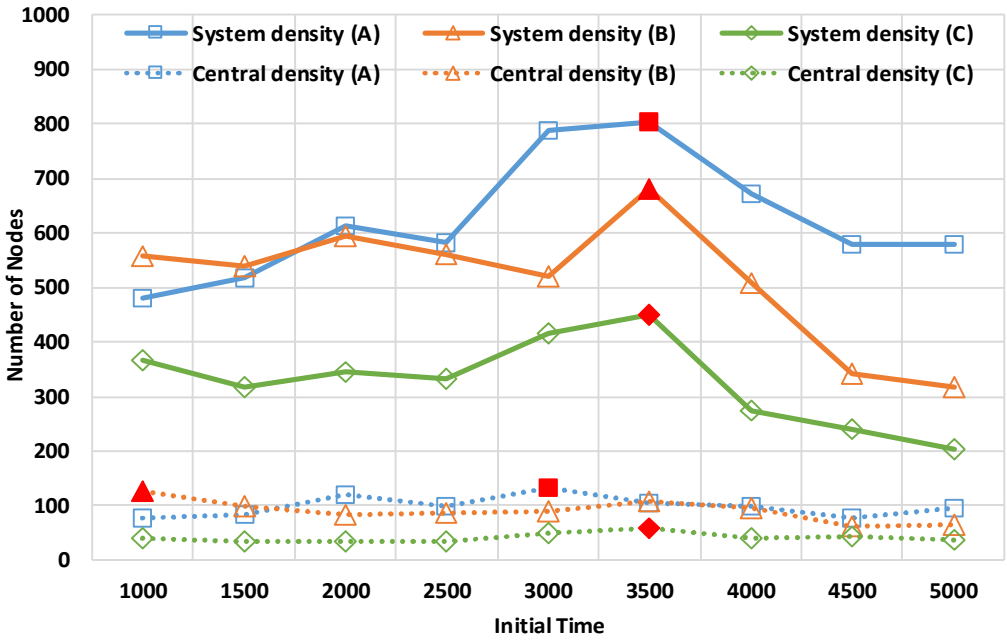


(b) The system density and central density in three intersections (A–C).

Fig. 32 The three extracted intersections (A–C) and the statistic information about system density and central density.

The ranges except for the standard NTS (from $R_{lower}$ to $R_{upper}$), were set to linear values, based on the range of 10 frames/s, as in Equation (12).

$$\begin{cases} R_{upper} = \lfloor n_t \times 1.5 \rfloor \\ R_{lower} = \lfloor n_t \times 0.5 \rfloor \end{cases} \tag{12}$$

The initial RSRP threshold was set to –110 dBm, which was the same as the noise power. The resource keeping probability was set to zero because of the most fundamental setting [23]. In other words, the nodes always reselected the next slot when the counter became zero. These parameters are summarized in Table 6.

Table 6 Key parameters in simulations.

| Crash scenario Parameters | Values |
|---|---|
| NTS | 10–30 frames/s |
| Node distribution model | Uniform, Realistic |
| Relative speed | 120 km/h–240 km/h |
| **Wireless Settings** | **Values** |
| Carrier frequency | 5.9 GHz |
| Bandwidth | 10 MHz |
| Frame size | 190 bytes |
| Radio propagation model | WINNER+ (LOS) B1 |
| Shadowing deviation | 3 dB (i.i.d) |
| Noise power | −110 dBm |
| SINR threshold | 5 dB |
| **Configuration Settings** | **Values** |
| Reselection counter range | Linear Average |
| Initial RSRP threshold | −110 dBm |
| Resource keep probability | 0 |

# 3. Number of Received Frames and NAC in Two Crash Scenarios

This section presents the performance characteristics of mode 4 in crowded intersection crash scenarios and high-speed crash scenarios.

## A) Crowded Intersection Scenarios

### a). Uniform Node Distribution Models

Fig. 33 shows the number of received frames for the number of nodes at a relative speed of 120 km/h. The horizontal axis is the number of nodes, and the vertical axis is the number of received frames. The legends in Fig. 33 represent the NTSs. In the evaluations, all the nodes were uniformly distributed.

First, the author explains the performance characteristics of the NTSs. In particular, at the NTS of 30 frames/s, the author can observe the performance trend explained in the above section. At the NTS, the number of received frames was the largest until reaching 220 nodes because of the redundant transmissions. However, it was the lowest at 500 nodes due to overloading frames. The performance sharply drops as the traffic load increases. In contrast, at the NTS of 15 frame/s, the number of received frames was the largest at 420 nodes, although it was the second-lowest at 300 nodes. Therefore, configuring the NTS depends on the degree of the congestion situation.

In terms of CWS, Fig. 33 demonstrates that mode 4, on average, provides less

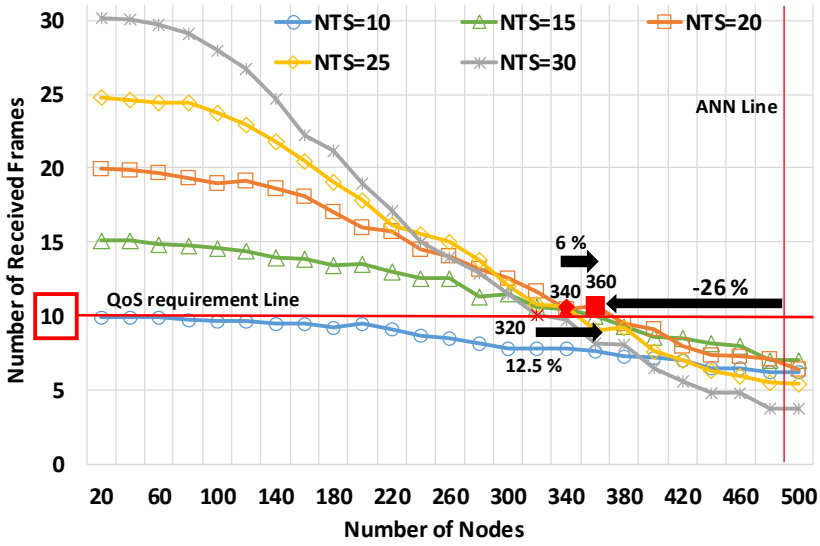


Fig. 33 The number of received frames for the number of nodes in the uniform node distribution model at a relative speed of 120 km/h.

performance than the QoS requirements. In Fig. 33, using the NTS of 20 frames/s provided the best performance of the five NTSs; specifically, the NAC was 26% less than the ANN (i.e., 488 nodes). The NAC at the NTS exceeded the NAC at the other NTSs, like 15 frames/s or 25 frames/s, by 6%. It was also 12.5% above the NAC at the NTS of 30 frames/s. Therefore, the author highlighted that mode 4 showed the best performance at the NTS of 20 frames/s but was not able to satisfy the requirements.

## b). Realistic Node Distribution Models

Fig. 34–Fig. 36 depict the number of received frames in the large–small intersections at the five NTSs, respectively. The horizontal axes are the initial times of the periods of the traffic signal in each intersection. The vertical axes are the numbers of received frames. In the simulations, the relative speed of the target nodes was 120 km/h, which is to be assumed in urban areas.

Fig. 34 demonstrates that the number of received frames did not satisfy the CWS requirements at any initial time in the large intersection at any NTS. From the results, using 10 frames/s and 15 frames/s showed better performance than performance at the other NTSs because the scenarios had many nodes, as compared to the other scenarios. At the initial time of 3000 s, using the NTS of 10 frames/s provided the best performance, and the number of received frames was 55% less than the QoS requirements. At the initial time of 3500 s, the suitable NTS was 15 frames/s, and the number of received frames was 52% less than the QoS requirements. The results emphasized that mode 4 failed to satisfy the requirements in the large intersection.

Fig. 35 shows that mode 4 failed to satisfy the QoS requirements during many periods in the medium intersection. In particular, the performance at the initial time of 1000 s or 3500 s was lower than the performance at the other periods. In the former period, mode 4 suppressed 42% fewer numbers of received frames than the QoS requirements. In the

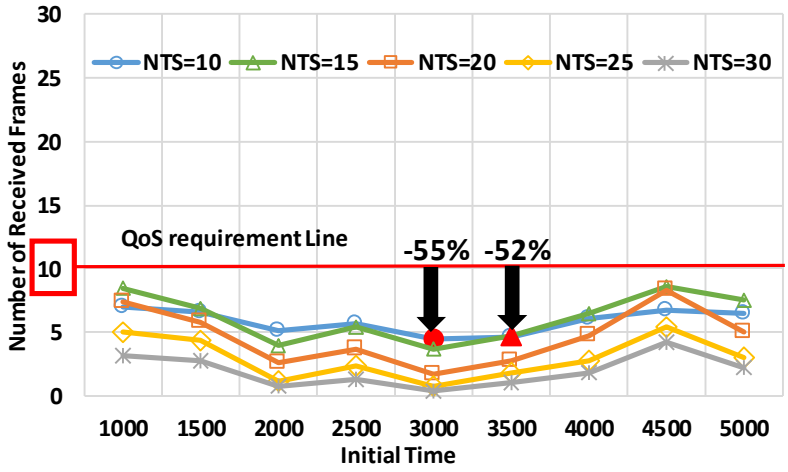


Fig. 34 The number of received frames in the large intersection.

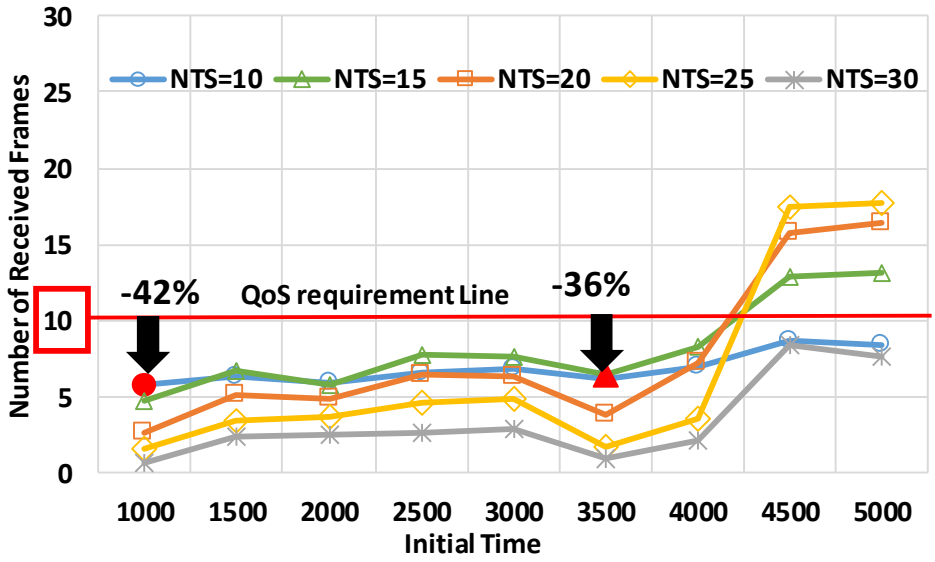


Fig. 35 The number of received frames in the medium intersection.

latter period, using the NTS of 15 frames/s provided the best communication quality, but the number of received frames was 36% less than the QoS requirements. At the periods of the initial time of 4500 or 5000, mode 4 showed enough performance to satisfy the requirements at the NTSs of 15, 20, and 25 frames/s.

As observed in Fig. 36, the target node satisfied the QoS requirements at many periods at the small intersection. At periods except for the periods of the initial time of 3000 s or 3500 s, the number of received frames exceeded 10 frames/s. At the initial time of 3500 s or 3000 s, the target node did not receive a smaller number of frames than 10 frames at any NTS. In particular, at the initial time of 3500 s, the optimal NTS was 15 frames/s,

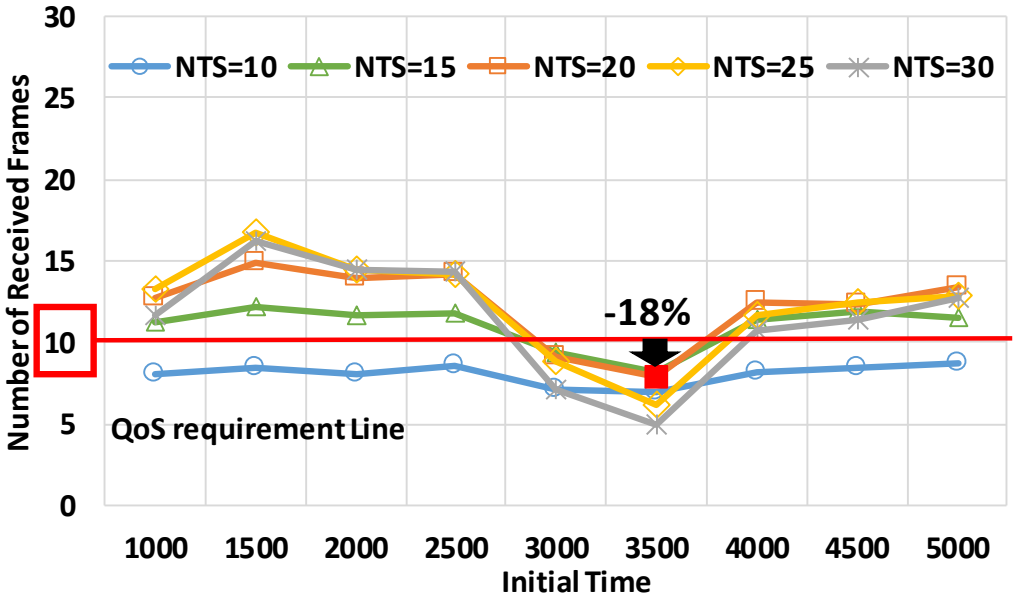


Fig. 36 The number of received frames in the small intersection

and the number of received frames was 18% less than the QoS requirements. Therefore, the author showed that mode 4 needed to improve the performance even in the medium and small intersections.

## B) High-Speed Scenarios

Fig. 37 and Fig. 38 depict the performance characteristics in high-speed scenarios. Fig. 37 shows the number of received frames for the number of nodes at a relative speed of 240 km/h. The horizontal axis, vertical axis, and legends are the same as in Fig. 33. Fig. 38 provides NAC characteristics for the relative speed between the target nodes. The horizontal axis is the relative speed, and the vertical axis is NAC. These results were evaluated in the uniform node distribution model to observe the average performance.

The two graphs highlight that the performance of mode 4 was sharply downgraded in high-speed scenarios. At first, Fig. 37 shows that the NAC was significantly less than the ANN. The most effective NTS for NAC was 15 frames/s, and the NAC was, at most, 140 nodes. The resultant NAC was 71% less than ANN. After the number of nodes was 160, the best NTS was 10 frames/s, but the performance was much below the QoS requirements. Therefore, high-speed scenarios were provided to decrease performance. Fig. 38 demonstrates that the performance sharply dropped as the relative speed increased. At the NTS of 15 frames/s, the NAC at 240 km/h was 43% below that at 120 km/h. Therefore, concerning high-speed nodes, like emergency vehicles, it is necessary to significantly improve the performance of mode 4 for effective crash warning.

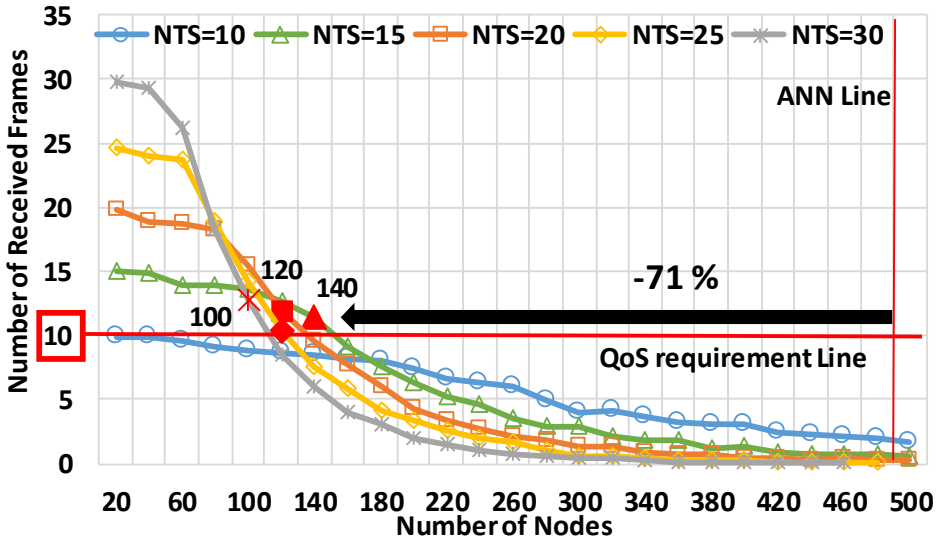


Fig. 37 The number of received frames for the number of nodes at the relative speed of 240 km/h in the uniform node distribution model.

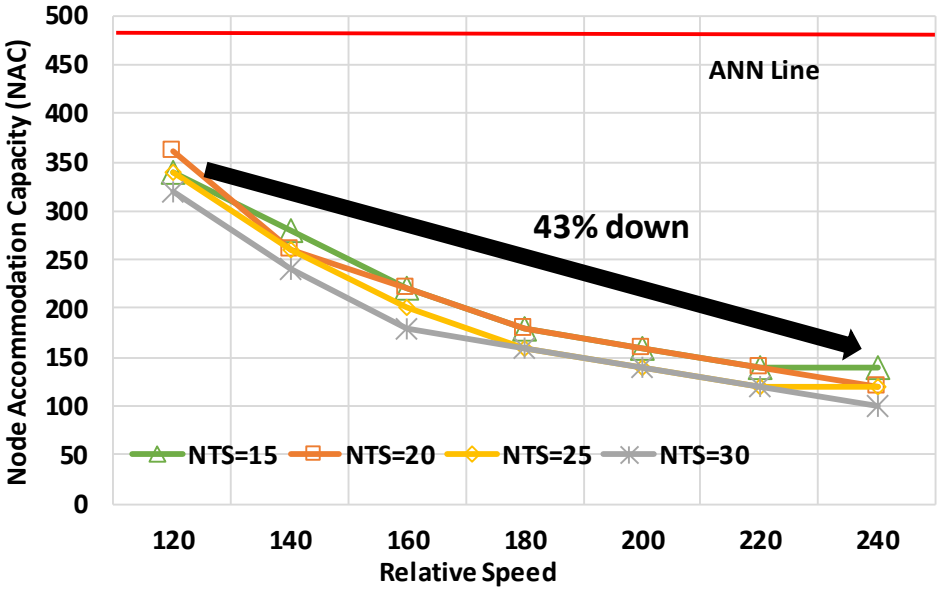


Fig. 38 NACs for relative speed in the uniform distribution model.

# 4. Conclusion in Section IV

This section investigated the feasibility of mode 4 in modeled crash scenarios in performance under congestion conditions. The evaluation results highlight that mode 4 failed to satisfy the QoS requirements in many crash scenarios. At first, in crowded intersection scenarios, mode 4 provided low-reliable communications. In the uniform node distribution model, which evaluated average performance, the results demonstrated that NAC was 26% lower than the ANN. As well as the average performance, the author evaluated more practical performance in the realistic node distribution model built by Bologna data. In the realistic large intersection, the number of received frames was 55% smaller than the QoS requirements. The high-speed scenarios, like emergency cars in urban areas, also cause congestion. When nodes collided with each other at a relative speed of 240 km/h, the NAC was 71% below the ANN. Our feasibility evaluations highlight the necessity to improve communication performance of mode 4 by new mechanisms like Decentralized Congestion Control to use CWS in the real world.

# V. Decentralized Broadcast NOMA and Frame Relaying with NOMA for Mode 4: Physical-MAC Cross-layer Approach

Section V comprehensively proposes DB-NOMA for mode 4 as a decentralized physical-MAC cross-layer congestion control. Notably, this section focuses on the performance characteristics of the RM with NOMA.

## 1. Enhanced Mode 4 with DB-NOMA

The author proposes DB-NOMA, which is a concept that applies NOMA to the decentralized broadcast system. To apply the concept in practice, the author proposes the enhanced mode 4 with two NOMA methods. Unlike the existing NOMA methods, the concept and proposed methods try to superpose broadcasted signals autonomously. The following subsections describe the overview, ideas, basic designs, and characteristics.

### A) Overview of Enhanced Mode 4

Fig. 39 shows the flow chart of the enhanced mode 4. The enhanced mode 4 has a parallel transmission method (PTM) and a relay method (RM). (1) Each node decides whether to act as a relay node according to some conditions by RM. One of the necessary conditions is to relay only frames transmitted from potential crash nodes because the author needs to improve the QoS while suppressing the overflowing of relay frames. Each node can detect potential crash nodes from the transmitted advertisements. (2) After a relay node generates its own advertisement, the node superposes the relay and the advertisement by RM. (3) Each node broadcasts the superposed signal (its advertisement signal if the node does not relay any frames) by PTM.

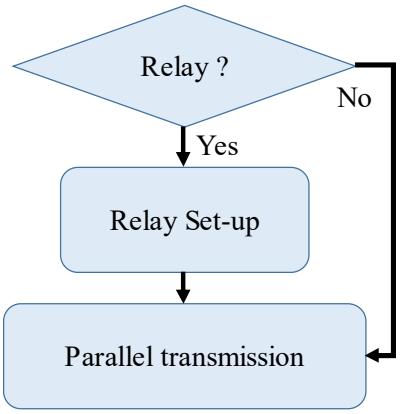


Fig. 39 The flow chart of DB-NOMA.

# B) Parallel Transmission Method using DB-NOMA (PTM)

## a). Key Idea and Basic Design of PTM

In PTM, multiple transmitters autonomously use the same slot, and each receiver decodes the superposed signal by SIC; all nodes apply SIC to all received frames. Fig. 40 illustrates the example of PTM. In Fig. 40, node-A and node-B use the same slot, and as a result, a signal of node-A's advertisement and a signal of node-B's advertisement are superposed at the receiver side.

PTM may improve the spectrum utilization efficiency to boost the number of nodes using a slot by suitable decentralized signal superposition, unlike the conventional NOMA methods. The decentralized signal superposition depends on the decentralized slot selection in which many destination nodes sense the SINR of superposed signals high. Additionally, PTM can resolve the two constraints by the decentralized slot selection mechanism. To explore the suitable mechanism, the author discusses the characteristics in the following subsection.

## b). Performance Analysis of PTM

To investigate the characteristics of the slot selection strategy, the author focus on the SINR in the following equation (13). In the SINR, two nodes (node-A and node-B) simultaneously use a slot, and a receiver *j* senses node-A's signal larger than node-B's signal. $P_t$ denotes a transmission power, and all nodes use the same power in mode 4. $N_0$ is noise power. $PL_{ij}$ is a radio propagation loss from a transmitter *i* to a receiver *j*. Here, *i* denotes node-A (*A*) and node-B (*B*).

$$\mathrm{SINR} = \frac{P_t \times PL_{Aj}}{P_t \times PL_{Bj} + N_0} \tag{13}$$

To analyze the SINR simply, the author considers the propagation loss as the only path loss. The author assumes that $PL_{ij}$ is a decrement function for the distance between *i* and *j* as the following equation (14). *C* denotes a constant coefficient of the path loss model, and $n$ denotes a path loss exponent. By substituting Equation (14) to Equation (13), Equation (15) is obtained.

$$PL_{ij} = C \cdot {d_{ij}}^{-n} \tag{14}$$

$$\mathrm{SINR} = \frac{P_t \times C \cdot {d_{Aj}}^{-n}}{P_t \times C \cdot {d_{Bj}}^{-n} + N_0} \tag{15}$$

The performance is dominated by the difference between the distances ($d_{Aj}$ and $d_{Bj}$). The difference is yielded due to the decentralized slot selection. A better slot selection strategy is that each node selects a slot used by moderately far away nodes from itself. At first, the author discusses the case where node-A and node-B are near each other, and then they use the same slot. Unfortunately, this simultaneous transmission causes many receivers to sense a small SINR of Equation (15) to receive both frames incorrectly. Whereas the author discusses the case where node-A and node-B are too far from each other, and then they use the same slot. In this case, many receivers obtain sufficiently high SINR, but the improvements in spectrum utilization efficiency become small. The most naive slot selection method is Sensing-based SPS, though this method does not fully select a slot to use NOMA effectively.

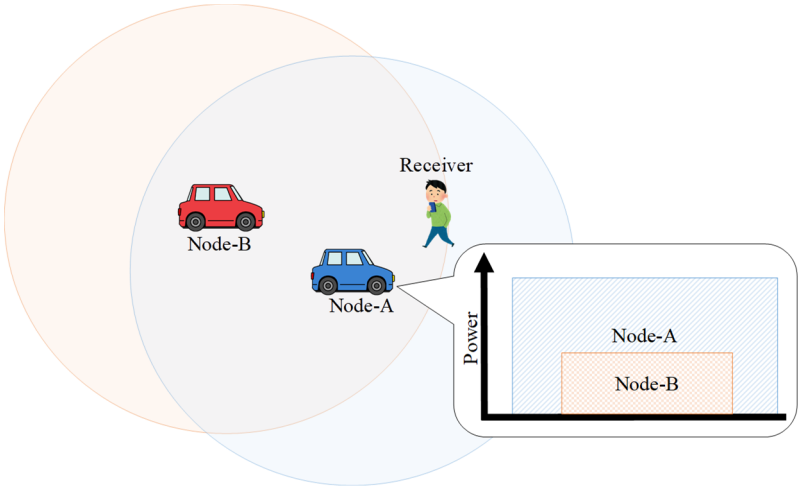


Fig. 40 The example of PTM and the superposed signal by PTM.

## C) Relay Method applying DB-NOMA (RM)

### a). Key Idea and Basic Design of RM

In RM, a relay node autonomously superposes its own advertisement signal and the received advertisement signal from a potential crash node. Then the node broadcasts the superposed signal. The receiver uses SIC for all received frames; then, the receiver does not identify the relay frames. Fig. 41 is an example of RM. In Fig. 41, a relay node superposes the two advertisements (orange and blue circles).

RM may expand the broadcast ranges of potential crash nodes without consuming additional slots of relays by suitable decentralized relay with signal superposition. Whereas, RM has a negative impact that decreases the advertisement range of relay nodes due to decreasing transmission power for its own advertisement. From the above discussions, the suitable signal superposition is defined as maximizing the QoS improvements under suppressing the negative impact. The key mechanisms are the autonomous superposed transmission power distribution and relay node decision. Additionally, RM guarantees SINRs for broadcasting by introducing relay and the first

algorithm and resolves the decentralized constraints by the two algorithms. To explore the suitable algorithms, the author analyzes the characteristics in the next subsection.

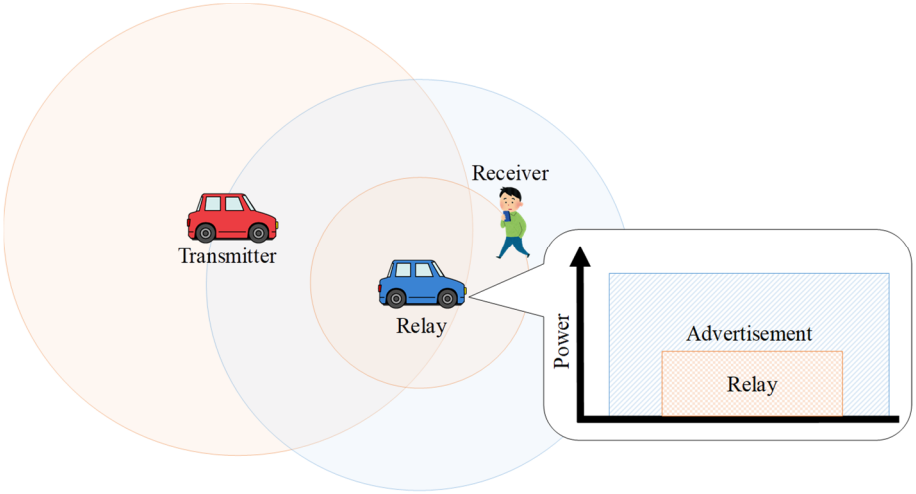


Fig. 41 An example of a superposed signal by RM.

## b). Performance Analysis of RM

The author investigates the characteristics of the two algorithms from two SINRs of Equations (16) and (17), in which Equation (14) is substituted. Equation (16) shows the SINR of the advertisement of the relay node, and Equation (17) shows that of the relay frame of the relay node, in both of which the only relay node transmits a superposed signal. Equations (16) and (17) use the same parameters as Equation (15). Here, $i$ denotes the relay node $r$. $\alpha$ shows a relay power ratio to the total power, and thus, $\alpha \cdot P_t$ is the relay power, and $(1-\alpha) \cdot P_t$ is the advertisement power.

$$SINR_{ad} = \frac{(1-\alpha) \cdot P_t \times C \cdot {d_{rj}}^{-n}}{\alpha \cdot P_t \times C \cdot {d_{rj}}^{-n} + N_0} \tag{16}$$

$$SINR_{relay} = \frac{\alpha \cdot P_t \times C \cdot {d_{rj}}^{-n}}{N_0} \tag{17}$$

From Equations (16) and (17), the performance depends on $\alpha$ and $d_{rj}$. The two parameters are dominated by the following two mechanisms.

- $\alpha$: This value is operated by a superposed transmission power distribution mechanism, in which relay nodes autonomously distribute the available transmission power.
- $d_{rj}$: This value is operated by the relay node decision mechanism, in which nodes

judge to relay a received frame in a distributed manner.

Suitable α improves performance. α dominates the tradeoff between enhancing $SINR_{relay}$ and deteriorating $SINR_{ad}$. As this algorithm applies large α, $SINR_{relay}$ improves, but $SINR_{ad}$ deteriorates. Besides, α is dominated by the following two constraints (a) and (b). (a) Each node needs to use small α enough to guarantee high $SINR_{ad}$. (b) The relay node needs to set up so high α that $SINR_{relay}$ becomes more than $SINR_{trans}$, of which is direct communication from the transmitter to the receiver as Equation (18). $d_{tj}$ is the distance between the transmitter *t* and the receiver *j*.

$$SINR_{trans} = \frac{P_t \times C \cdot {d_{tj}}^{-n}}{N_0} \tag{18}$$

$d_{rj}$ also fluctuates the performance. $SINR_{relay}$ becomes small even though a relay node is too close to the transmitter or too near the receiver. When a node near the transmitter relays the frame, $SINR_{relay}$ is likely to become less than $SINR_{trans}$. When a remote node from a transmitter relays the frame, the receiver is also likely to receive the original frames, i.e., the relaying is not needed. Therefore, selecting suitable relay nodes maximizes the SINR of the transmitter.

# 2. Evaluation Models

This section investigates the fundamental characteristics and impacts of the enhanced mode 4 with DB-NOMA. Table 7 summarizes the key parameters.

## A) Evaluation Metrics

- The number of received frames: The author investigated the two kinds of it. (1) The author evaluated the average number of received frames of a specific node (target receiver) from a specific node (target transmitter), called *target metric*. The two nodes are no different from other nodes except for potential crash nodes and the target of the proposed relay method. (2) The author evaluated the average number of received frames of a node from the relay node, called *relay metric*. The author compares the relay metric with the target metric without relays to evaluate the demerits of RM. The relay metric is evaluated in the same case as the target metric, such as the distance between the two target nodes.
- NAC: The author evaluated the upper number of nodes that the target metric is 10 frames or more.

## B) Node Distributions

The target transmitter was put at 100 m apart from the target receiver as Fig. 42. This distance is before 3 seconds prior to a potential accident in the case that the two nodes frontally approach at a relative speed of 120 km/h. This duration is the middle of the last 1 second during the required warning period.

The author uniformly deployed nodes as the center of the target receiver within the radius of communication range, i.e., 300 m, as shown in Fig. 42. This distribution is one of the most fundamental stochastic. Furthermore, the author assumed that pedestrians also exist in various locations, unlike vehicles. All deployed nodes periodically advertise their own location and play the role of the interference source. All nodes did not move from the initial position to simplify the model.

The author simply assumed that relays are introduced only for the target transmitter, and a node undertakes all relays. The relay node is put on somewhere between the two target nodes, as shown in Fig. 42. The relay node also periodically transmits its advertisement. The node superposed its own advertisement and a relay when the node received the target transmitter's advertisements.

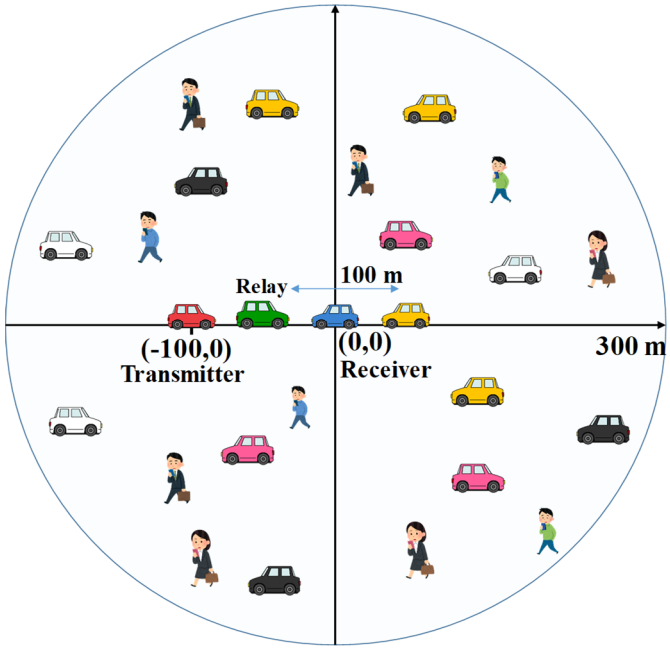


Fig. 42 The abstract of the node distribution of simulations.

## C) Wireless Parameters

The author used the standard parameters of mode 4. The settings of the physical layer were the same as other researches [24] [25]. The carrier frequency was 5.9 GHz. The channel bandwidth was 10 MHz. The frame size was 300 bytes. Besides, the remaining

parameters of Sensing-based SPS complied 3GPP standard. In particular, the transmission frequency was set to 20 frames/s, and hence, the number of same slot utilization was selected in 10–30 at random [25]. Setting 20 frames/s is because nodes achieve to receive 10 frames/s even if they incorrectly receive some frames due to collision error. Additionally, all nodes used the same transmission power (i.e., 23 dBm [25]) for broadcasting.

The frame reception and radio propagation model was set as follows. A frame was assumed to be correctly received when the SINR is the threshold or larger. The threshold was set to 5 dB [35]. The radio propagation model was WINNER+ LOS (B1) model [85] [86], which was recommended by 3GPP. The author did not incorporate the propagation model into shadowing to exclude the impacts. Noise power is −110 dBm as [30].

Table 7 Key Parameters

| **Basic settings** | **Values** |
|---|---|
| Distance between target nodes | 100 m |
| Transmission Frequency | 20 frames/s |
| SINR threshold | 5 dB |
| Radio propagation model | WINNER+ (LOS) B1 |
| **Enhanced mode 4 settings** | **Values** |
| Superposed relay power ratio to total power α | 1/5–1/60 |
| Distance to the relay node from target transmitter $d_{rj}$ | 12.5–87.5 m |

## D) Models and Parameters of Enhanced Mode 4

For PTM, the author just adopted Sensing-based SPS. Sensing-based SPS can select a slot with relatively low interference. Therefore, each node can transmit frames with relatively remote nodes from itself. The author modeled RM as follows. At first, the author used superposed relay signal power to the total power of 1/5–1/60, and the denominator increment is 5. Next, the distance to the relay node fluctuates from 12.5 m to 87.5 m from the target transmitter to a unit of 12.5 m. In this model, the relay node near the target transmitter frequently receives frames from the transmitter and relays them because the same node relays frames. This setting averagely reduces the advertisement power of the relay node and shrinks the range of its advertisements. To use NOMA, the author needs to add reference signals to know Channel State Indicator (CSI) of each signal [71]. The author assumed to enable to substitute of the reference signals of mode 4 for it.

# 3. Number of Received Frames and NAC

This section presents three graphs about the performance characteristics of the enhanced mode 4. The first graph shows the performance for the number of nodes, and the other graphs show the performance characteristics for the two parameters of RM.

## A) Performance for Number of Nodes

Fig. 43 shows the number of received frames for the number of nodes. The horizontal axis is the number of nodes in the communication range, and the vertical axis is the number of received frames. The legends of Standard, PTM-only, and PTM+RM denote original mode 4 without NOMA, a method using only PTM, and the enhanced mode 4 with PTM and RM, respectively. Besides, the color points show the target metrics, and the white points show the relay metrics. The enhanced mode 4 uses two sets of parameters; one set is a suitable one in which the relay power ratio is 1/20, and the distance from the target transmitter to the relay node is 75 m. The other set is an unsuitable one in which the ratio is 1/5, and the distance is 50 m.

Fig. 43 demonstrates that our enhanced mode 4 increased the NAC of Standard by 119% without the analyzed negative impacts by suitable parameters. The breakdowns are as follows. By comparing the red point of Standard (the blue line) with PTM-only (the orange line), the contribution of PTM was 13%; by comparing the red point of PTM+RM with the suitable set (the yellow line with the white square) and PTM-only, RM boosted the NAC of PTM-only by 94%. In PTM+RM with the suitable set, no demerits of relay node were observed. Specifically, the relay metric (the yellow line with the white square) was 12% more than the target metric in Standard, though the relay metric was 15% less than the target metric in PTM-only. Unfortunately, the proposed methods using the

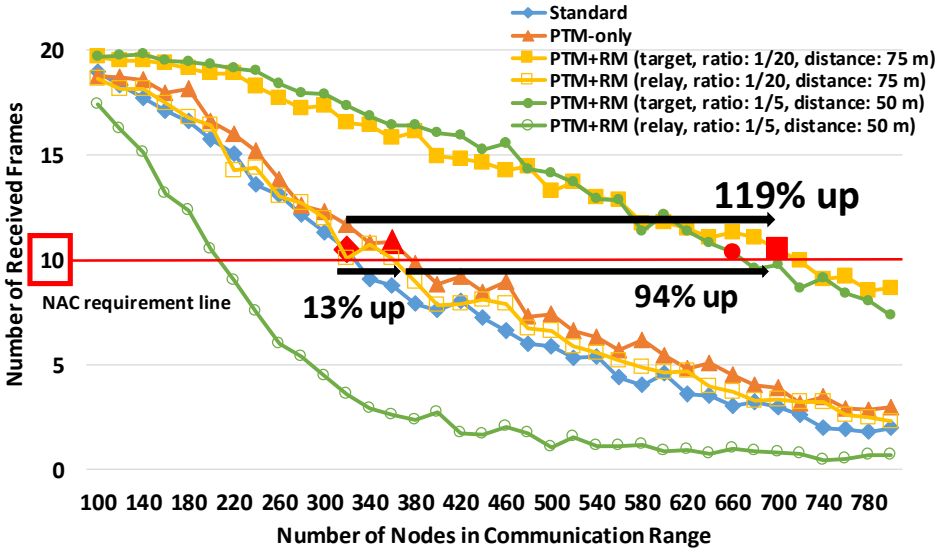


Fig. 43 The number of received frames for the number of nodes.

unsuitable set significantly decreases the relay metric by comparing the green line with the white circle with the other line. In summary of the above results, the author points out the enhanced mode 4 significantly outperformed Standard though the author suitably set to the parameters.

## B) Performance for Superposed Relay Power Ratio

Fig. 44 shows the number of received frames for the superposed relay power ratio to the total power. The horizontal axis is the ratio. The vertical axis, legends, and points are similar to Fig. 43. Fig. 44 shows the results in the distance to the relay node from the target transmitter of 75 m.

Fig. 44 demonstrates that the suitable ratio significantly boosted the QoS of advertisements of the relay node while improving that of the target transmitter. From Fig. 44, the author can observe the relay metric (the white square) increases, and the target metric (the yellow square) decreases, as the ratio decreases, as analyzed in the above section. Then, the suitable ratio was 1/20 for the following reasons. In the white square, the relay metric in 1/20 increased by108% over that in 1/5, though the target metric decreased by 9%. Additionally, from 1/20, the relay metric became nearly equal to the target metric in PTM-only, which is the maximum improvement.

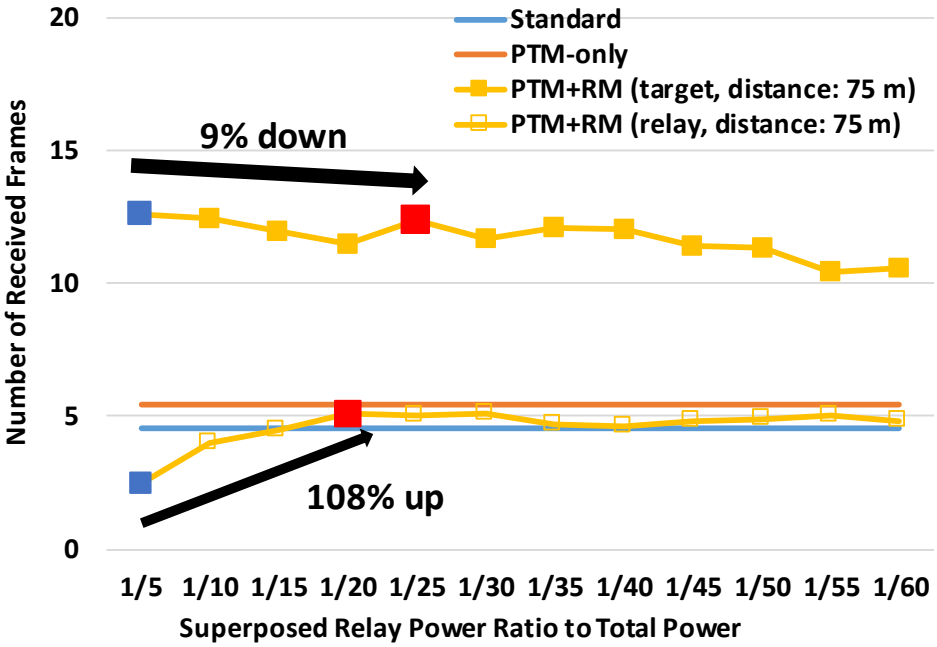


Fig. 44 The number of frames for the superposed power ratio.

## C) Performance for Distance to Relay Node

Fig. 45 shows the number of received frames for the distances to the relay node from the target transmitter. The horizontal axis is the distance. The vertical axis and legends

are similar to Fig. 43. Fig. 45 shows the results of the typical superposed relay power ratio to the total power of 1/20.

Fig. 45 demonstrates that suitable relay nodes significantly improved the QoS of the target transmitter's advertisements. From Fig. 45, the author can observe the target metric (the yellow square) increases and then decreases, as the distance increases, as described in the above section. In this simulation, the suitable distance is 75 m for the following reasons. In the yellow line with the yellow square, the target metric of PTM+RM in 75 m was 115% larger than that in 12.5 m; it was 27% more than that in 87.5 m. Additionally, the author can observe the relay metric became nearly equal to that in PTM-only. Therefore, the suitable distance (i.e., selecting the suitable relay node) of RM successfully improves the QoS of advertisements of both of the nodes.

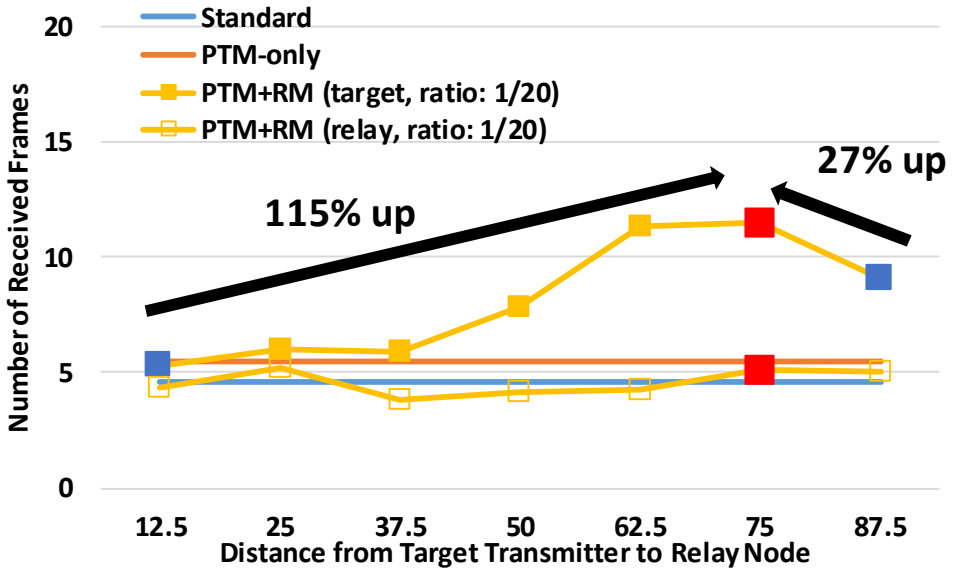


Fig. 45 The number of received frames for the distances to the relay node from the target transmitter.

# 4. Conclusion in Section V

The author proposed a novel concept, DB-NOMA, for decentralized broadcast systems and mainly evaluated the performance characteristics of the proposed RM in CWS. The enhanced mode 4 with DB-NOMA includes a relay method and a parallel transmission method. Our analysis demonstrated that the enhanced mode 4 improves the performance by using suitable signal superposition parameters. Our simulations highlighted that the enhanced mode 4 increased the NAC by 119% over that of the current mode 4 by the suitable parameters. In further studies, the author considers the detailed procedures based on our analysis and evaluations to provide high performance.

# VI. SPS-NOMA for Mode 4: Physical-MAC Cross-layer Approach

Section VI extends PTM or SPS-NOMA based on UL-NOMA in DB-NOMA, a part of a decentralized physical-MAC cross-layer congestion control. In the following sections, the author discuss the system model.

## 1. Sensing-based SPS with UL-NOMA (SPS-NOMA)

In this section, the author describes the system design of SPS-NOMA in the first subsection and then discusses the performance in the next subsection.

### A) System Design of SPS-NOMA

The proposed system aims to support SIC effects by sensing-based SPS. This system complies with the standard sensing-based SPS to select slots and transmit frames. The system also uses SIC decoders to decode frames in addition to sensing-based SPS procedures.

#### a). Step 1: Sensing-based SPS-aided Slot Selection

First, the author explains the slot structure of SPS-NOMA. The main structure is the same as the standard of mode 4. Each slot contains a piece of sidelink control information (SCI) and a transport block (TB) occupied by several resource block pairs (RBPs). Every SCI includes the MCS index and the slot utilization counter; each TB conveys a CWS frame.

An RBP has four symbols in a time domain for reference signals. Initially, the reference signals are used for nodes to select slots and estimate channel gains for decoding frames. In addition to the roles at sensing-based SPS, the signals play roles in detecting simultaneous transmitters and estimating the channel gains for SIC decoding. For the new roles, the reference signals need to be orthogonal sequences between simultaneous transmitters. Methods, such as References [71] [87], can create such sequences. For example, the author can assume using Zadoff-Chu sequences for reference signals based on [71]. The sequences are used in cellular networks. The author can deploy the sequences in time and/or frequency domains, reusing the existing symbols used for reference signals of mode 4. The proposed method requires to prepare them enough to avoid collisions of them, at which multiple nodes share a reference signal. The collisions increase channel estimation errors and thus degrade SIC performance. Note that how to deploy orthogonal sequences in detail is out of scope.

Next, the author briefly describes the slot selection mechanisms. The mechanisms use a history of past slots based on sensing-based SPS. The history is stored sensing information during the past 1000 milliseconds. At the beginning of the mechanisms, each node initializes the set of candidate slots to all the slots within the *selection window* (called SW), e.g., 100 milliseconds for 10 Hz. Subsequently, the node executes the following two mechanisms to exclude slots with estimated high interference from the candidate slots.

- RSRP mechanism: This mechanism excludes slots that satisfy both the following two conditions. (a) The decoded SCI of any past slot within SW reserves the slots. Here, $\mathcal{M}$ shows the set of reserved slots. (b) The average RSRP over RBPs of any slot in $\mathcal{M}$ is higher than the threshold $P_{th}$. The behavior is shown as:
  The mechanism has been repeated until the number of non-excluded slots becomes

$$^{\exists}P_{RSRP}^{m} > P_{th} \qquad m \in \mathcal{M}. \tag{19}$$

  20% of the SW or more to guarantee the number of candidate slots. At every next iteration, the threshold increases by 3 dB. This mechanism passes the non-excluded slots to the following mechanism.

- Received signal strength indicator (RSSI) mechanism: This mechanism filters slots with high average RSSI over the corresponding past slots. The corresponding past slots are traced back from a candidate slot at a unit of the transmission period, e.g., 100 milliseconds. The average RSSI $\tilde{P}_{RSSI}$ is written as:

$$\tilde{P}_{RSSI} = \frac{1}{|\mathcal{K}|}\sum_{k\in\mathcal{K}} P_{RSSI}^{k}, \tag{20}$$

where $\mathcal{K}$ shows the set of the corresponding past slots. The RSSI in a past slot $k$ is represented by $P_{RSSI}^{k}$. Based on the average RSSI of candidate slots, this mechanism sorts the candidate slots in ascending order. Finally, it selects a slot from the top 20% of the sorted slots at random.

In addition to selecting the slot, the node selects a reference signal to transmit with data. The history helps to avoid collisions of the reference signals. The node uses the history and selects a sequence unused by other simultaneous transmitters.

### b). Step 2: Sensing-based SPS-aided Transmission

Every node uses the selected slot in a semi-persistent manner. The slot utilization counter was selected randomly from a range of 5–15 [22] for 10 Hz as a standard. The value decreases by one after every transmission. After using the slot in the selected times, the node reselects a new slot by Step 1.

In SPS-NOMA, nodes can optionally use RT, a potential extension of the retransmission mechanism of mode 4. The RT is inspired by Reference [89] and the retransmissions. In the reference, nodes alternately used two slots at 10 Hz. Our system uses two independent slots at 20 Hz. In other words, a node has two SPS process of 10 Hz. Unlike the retransmissions, both slots are selected by the SPS mechanism. Fig. 46 shows the behavior of the RT. In Fig. 46, node-A uses the two reserved slots. The node alternately uses the first reserved slot and the second reserved slot every 100 milliseconds. The RT provides nodes with selection diversity to improve the SINR by retransmissions based on the SPS mechanism, and nodes send their up-to-date location data more frequently. Unfortunately, the congestion level also increases. The characteristics are shown in detail in the following sections.

### c). Step 3: SIC-aided Reception

Transmitted signals are superposed at each receiver. The mixed signal $y_j^{(1)}$ at receiver $j$ is expressed as:

$$y_j^{(1)} = \sum_{i \in \mathcal{I}^{(1)}} \sqrt{P_t} g_{ij} s_i + n, \tag{21}$$

where $P_t$ is the transmission power, which is the same power in all the nodes because of advertising. $\mathcal{I}^{(1)}$ is the set of simultaneous transmitters at the first SIC iteration. Each of the transmitters $i$ in $\mathcal{I}^{(1)}$ transmits the signal $s_i$. $g_{ij}$ is the channel gain between $i$ and $j$. $n$ is the additive white Gaussian noise at $j$ with the spectral power density of $N_0$.

Receivers use SIC and try to decode several signals in the superposed signal. The SIC decoder iterates the signal reception and interference cancellation. An example of the SIC decoding is as below. First, receiver $j$ tries to decode the strongest signal in the superposed signal by the capture effect, in which the signal is correctly decoded under the SINR is sufficiently strong for decoding; here, the receiver $j$ successfully decodes the signal from a transmitter $x$. Subsequently, the receiver estimates the channel gain from the reference signals. The estimated gain is denoted as $\tilde{g}_{xj}$. By re-modulating the decoded signal with the estimated gain, the receiver creates the replica signal. Then, the receiver subtracts the replica signal from the mixed signal. The subtracted signal is written as:

$$y_j^{(2)} = y_j^{(1)} - \sqrt{P_t} \tilde{g}_{xj} s_x \approx \sum_{i \in \mathcal{I}^{(1)} \setminus \{x\}} \sqrt{P_t} g_{ij} s_i + n. \tag{22}$$

Repeatedly, the receiver tries to decode the strongest signal in $y_j^{(2)}$ by the capture effect. With these procedures, receivers obtain multiple signals, including weaker signals than the strongest signal. Note that the author may observe channel estimation errors practically, for example, due to collisions of reference signals. In such cases, channel

estimation errors cause every SIC iteration to accumulate residual interference in Equation (22). As a result, the SIC performance degrades. Thus, the proposed method requires the number of available reference signals enough to avoid the collisions of reference signals, although the SPS mechanism supports to avoid the collisions.

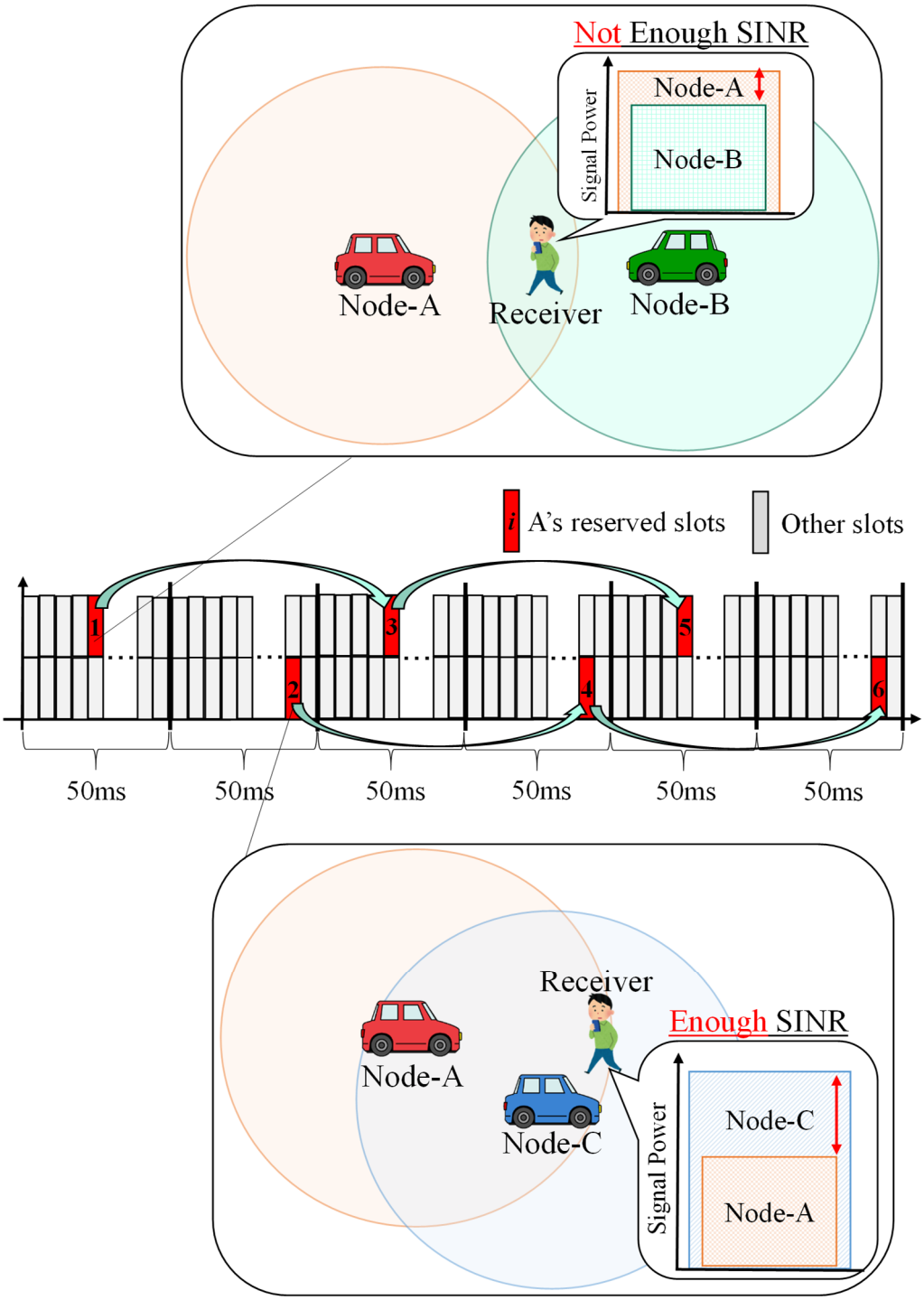


Fig. 46 An example of the RT of SPS-NOMA.

## B) Performance Analysis of SPS-NOMA

In this section, the author analyzes the performance of SPS-NOMA compared with the current mode 4. To the end, the author discuss the number of successful SIC iterations per transmission, denoted as $L$; in other words, $L$ is the number of received signals at each slot. The performance of SPS-NOMA becomes $L$-times as large as that of the current mode 4.

$L$ depends on the SINR at each SIC iteration. The SINR at the $l$-th SIC iteration is represented as:

$$\gamma_j{}^{(l)} = \frac{P_t \left|g_{xj}\right|^2}{\sum_{i \in \mathcal{J}^{(l)} \setminus \{x\}} P_t \left|g_{ij}\right|^2 + N_0}, \tag{23}$$

where the received signal from transmitter $x$ is the strongest power at receiver $j$. In Equation (23), $\mathcal{J}^{(l)}$ shows the set of simultaneous transmitters at the $l$-th SIC iteration. $\left|\mathcal{J}^{(l)}\right| = \left|\mathcal{J}^{(1)}\right| - (l-1)$. Given the channel gain as:

$$\left|g_{ij}\right|^2 = c_{ij} d_{ij}{}^{-\alpha}, \tag{24}$$

From Equation (24), Equation (23) is transformed as:

$$\gamma_j{}^{(l)} = \frac{P_t c_{xj} d_{xj}{}^{-\alpha}}{\sum_{i \in \mathcal{J}^{(l)} \setminus \{x\}} P_t c_{ij} d_{ij}{}^{-\alpha} + N_0} \ . \tag{25}$$

$d_{ij}$ is the distance between $i$ and $j$. $c_{ij}$ is the coefficient between $i$ and $j$. $\alpha$ is the path loss exponent. Given a frame reception model [43] [44] with the SINR threshold $\gamma_{th}$, $L$ satisfies the following condition:

$$\left(\bigwedge_{l=1}^{L} \gamma_j{}^{(l)} > \gamma_{th}\right) \wedge \left(\gamma_j{}^{(L+1)} < \gamma_{th}\right). \tag{26}$$

Based on the above discussions, $L$ depends on the following parameters: the channel gains of simultaneous transmitters to a receiver $g_{ij}$, the number of simultaneous transmitters $\left|\mathcal{J}^{(l)}\right|$, and the SINR threshold $\gamma_{th}$. In SPS-NOMA, these parameters are mainly operated

by the slot selection mechanisms, MCS, and RT. In the following subsections, the author discusses the relationship between these parameters and the key factors in SPS-NOMA.

## a). Sensing-based SPS-aided Slot Selection

The first key factor is the slot selection mechanisms of sensing-based SPS. The mechanism operates $g_{ij}$ and $\left|\mathcal{J}^{(l)}\right|$. Based on Equation (25), the author analyze the mechanisms and $L$ below.

- RSRP mechanism

This mechanism assesses the power contribution of the strongest signal in the candidate slots. A node $z$ senses the following average RSRP when the transmitter $x$ in Equation (25) reserves a candidate slot in a past SCI under ${\gamma_z}^{(1)} > \gamma_{th}$:

$$P_{RSRP} = P_t \hat{c}_{xz} {d_{xz}}^{-\alpha}, \tag{27}$$

where $\hat{c}_{xz}$ is the average $c_{xz}$ over reference signals in used RBPs. From Equation (19) and Equation (27), the filtering condition of this mechanism is written as:

$$P_t \hat{c}_{xz} {d_{xz}}^{-\alpha} > P_{th} \leftrightarrow {d_{xz}}^{-\alpha} > \frac{P_{th}}{P_t \hat{c}_{xz}} \leftrightarrow d_{xz} \ < \sqrt[\alpha]{\frac{P_t \hat{c}_{xz}}{P_{th}}}. \tag{28}$$

From Equation (28), this mechanism excludes slots that $x$ near $z$ uses. At such a slot, the channel difference between $g_{xj}$ and $g_{zj}$ is small at receiver $j$, and thus, ${\gamma_j}^{(l)}$ is also small. As $P_{th}$ increases, this effect also increases. In contrast, a $P_{th}$ that is too small limits $\left|\mathcal{J}^{(l)}\right|$. $L$ depends on the two impacts.

Unfortunately, this mechanism does not cover slots with the non-decoded SCI, even if the slots provide higher interference than the other slots. As collision errors increase, the contributions of the mechanism decrease.

- RSSI mechanism

This mechanism assesses the expected interference at the future slots, based on the RSSIs at the past slots. A node $z$ senses the following RSSI at the corresponding past slot $k$:

$$P_{RSSI}^{k} = \sum_{i \in \mathcal{I}^{(1)}} P_t c_{iz} {d_{iz}}^{-\alpha} + N_0. \quad (29)$$

By this mechanism, z uses a slot with a relatively lower RSSI than other slots. At such a slot, the number of simultaneous transmitters is likely to be smaller, and the number of transmitters near z is likely to be smaller than the other slots. As a result, ${\gamma_j}^{(l)}$ is expected to decrease on average.

Unfortunately, this mechanism refers to no reservations. Positively, the behavior covers the assessments of the collided slots, which the RSRP mechanism does not support. Negatively, the average RSSI of this mechanism in Equation (20) may include RSSIs of past slots unrelated to future slots; in other words, $\mathcal{K}$ may include nodes that do not reserve the candidate slot. For example, transmitters in a slot may not use the same slot after 1000 milliseconds. In such cases, this mechanism incorrectly predicts the interference, and thus, nodes may not select a better slot for SPS-NOMA. When the positive effect is more dominant than the negative impact of this behavior, the mechanism enhances *L*.

### b). MCS

The second key factor is MCS. It operates the trade-off between the SINR threshold $\gamma_{th}$ and the average interference level. At first, low-index MCSs allow nodes to decode signals more reliably than high-index MCSs. In a threshold-based model, the effect means that the SINR threshold $\gamma_{th}$ decreases. Decreasing the SINR threshold is effective for every SIC iteration in Equation (26).

However, low-index MCSs convey fewer data bits per symbol than high-index MCSs. This characteristic decreases the number of slots, increasing the number of simultaneous transmitters $\left|\mathcal{I}^{(l)}\right|$ per slot at each SIC iteration. Increasing $\left|\mathcal{I}^{(l)}\right|$ means to amplify the interference in ${\gamma_j}^{(l)}$. Based on these two impacts, low-index MCSs provide larger *L* than high-index MCSs when decreasing the SINR threshold is more dominant than amplifying the interference.

### c). Redundant Transmission

The third key factor is RT. The RT provides the trade-off between the SINR selection diversity and the average interference level. As the positive impact, using multiple slots boosts selection diversity for interference and fading in the time and frequency domains. This diversity provides to increase the SINR ${\gamma_j}^{(l)}$. Fig. 46 illustrates the diversity effects. In Fig. 46, node-A uses the first slot with node-B and the second slot with node-C. In the first slot, node-A cannot obtain a sufficiently large SINR for the receiver due to transmitting frames with node-B. In the second reserved slot, node-A obtains enough

SINR for the SIC decoding. High-index MCSs are more effective than low-index MCSs in terms of the number of available slots.

As the negative impact, RT becomes twice as many frames as nothing of RT. The increase involves increasing the number of simultaneous transmitters $\left|\mathcal{I}^{(l)}\right|$ at each slot on average, i.e., the interference is amplified on average. As the number of nodes is more, the negative impact of the redundancy is more dominant. Although the number of frames increases in proportion to the number of nodes originally, the redundancy doubles the increasing ratio. Thus, $L$ increases when the selection diversity is more dominant than amplifying the interference.

# 2. Evaluation Model

The author focused on CWS scenarios because the system has been one of the most important V2X applications. The author implemented SPS-NOMA in our system-level simulator [38] [40] and simulated the behaviors of SPS-NOMA in the CWS in crash scenarios. The simulator computed the system-level performance based on the simulated SINRs. In the first subsection, the author describes the performance metrics and the CWS scenarios considering the QoS requirements, summarized in Table 2. In the second subsection, the author explains the wireless parameters. Note that the QoS requirements in Table 2 are similar to the other V2X applications. The numerical results can also support the performance of the proposed method in other applications.

## A) Performance Metrics and Crash Scenarios (CWS Model)

The author used the following two performance metrics and used another metric for the RT in addition to the two metrics. The first metric is the frame reception reliability per time window of 100 milliseconds during the warning period, defined as *frame receivability (FR)*. In other words, this metric indicates the probability that a receiver correctly receives one or more frames from a transmitter during a time window. The time window reflects the first requirement in Table 2 because the target system essentially requires reliably periodic frame reception per time window. The warning period included ten windows, and thus, the FR $p_{FR}$ was computed as:

$$p_{FR} = \frac{n_{success}}{10}, \tag{30}$$

where $n_{success}$ is the number of success windows per second and is divided by the total number of windows per second (i.e., ten windows). This metric provides system-required performance. This metric is based on the concept of the packet delivery ratio (PDR) used in many studies [23] [24]. Note that a packet is the same meaning as a frame. The PDR $p_{PDR}$ indicates the reception reliability per frame, i.e., the probability, as:

$$p_{PDR} = \frac{n_{rece}}{n_{trans}}, \tag{31}$$

where $n_{\mathrm{rece}}$ and $n_{\mathrm{trans}}$ are the number of received frames and the number of transmitted frames, respectively. The FR provides similar characteristics to the PDR at transmissions of 10 Hz because a node transmits a frame during a time window of 100 milliseconds. At the RT, the FR shows different trends from the PDR. Based on the requirement of periodic frame reception of 10 Hz, using the FR is better to observe the system-required performance than using the PDR. In contrast, the PDR provides direct SIC gains. From the above discussions, the author presented both metrics only at using the RT and focused on only the FR in the other evaluations.

The second metric was NAC. Based on the FR, the author redefined it as the maximum number of surrounding nodes under $p_{FR} \geq 0.9$. This metric shows the

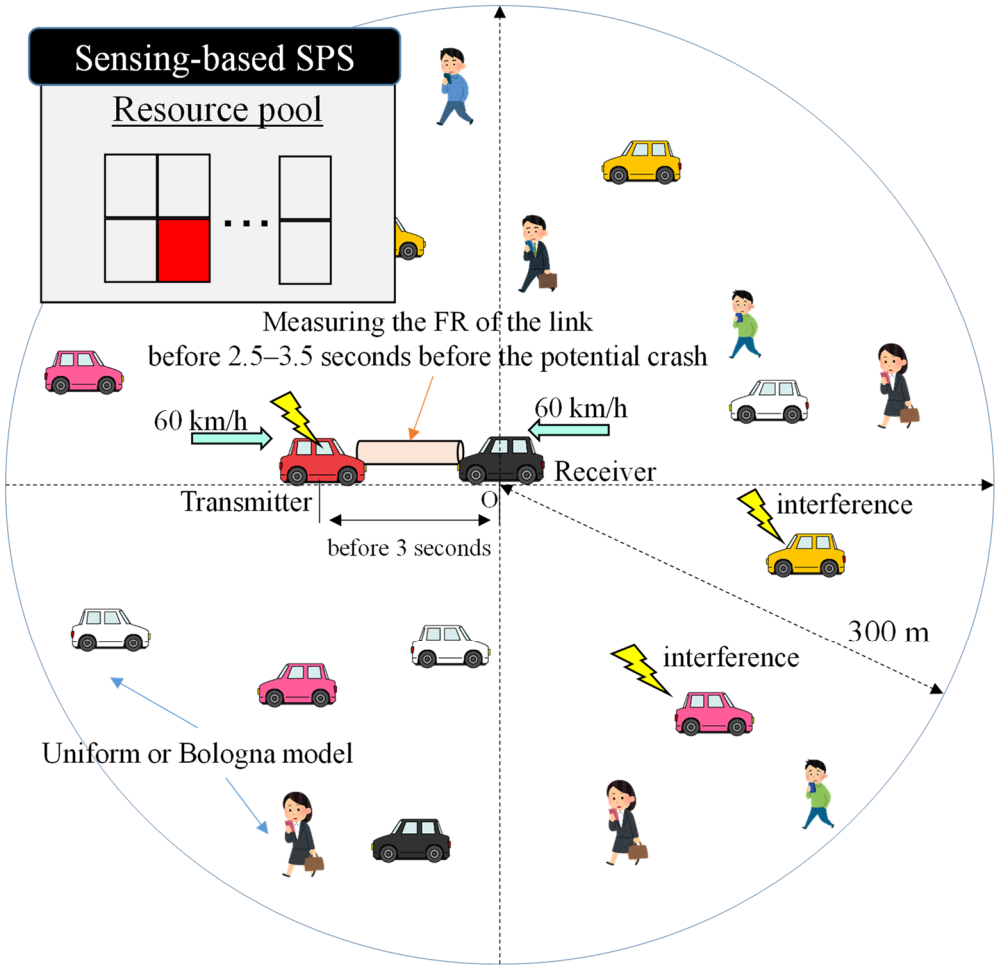


Fig. 47 The abstract image of the node distribution and communication behaviors before 3 seconds prior to the potential crash.

performance under the required reliability of the CWS and the feasibility of methods for channel congestion. The author mainly compared this metric of each method. Note that the author did not measure a maximum end-to-end latency of transmitted frames because sensing-based SPS suppresses the latency up to 100 milliseconds.

The author measured the FR of a node (called a target receiver) from a node (called a target transmitter). Fig. 47 presents the behavior of the two nodes before 3 seconds prior to their potential crash. As shown in Fig. 47, the two nodes frontally approached each other. Such a head-on crash scenario provides the longest distance during the warning period in other crash scenarios. Thus, the link undergoes the worst performance. The author distributed the other nodes within the range radius of 300 m from the center of the circle in Fig. 47. The surrounding nodes played a role in creating the channel congestion; specifically, they were competitors of the slot selections and interference for the target nodes. In Fig. 47, the target transmitter and the other two nodes used a slot at the same time.

The density of the nodes complied with the uniform model or Bologna models, building various crowded environments. The uniform model was one of the fundamental stochastic models and thus provided us with the average performance. Additionally, the model freely operated the number of nodes, allowing us to evaluate NAC; the author investigated the performance at the number of nodes from 60 nodes to 500 nodes. The Bologna models were based on Bologna data through the simulation of urban mobility (SUMO) simulator [82] [83]. The data are open location data in Bologna, Italy, available at http://sumo.dlr.de/wiki/Data/Scenarios. Many researchers have used these data to obtain realistic node distribution models [82] [83]. Thus, the model provided us with a realistic performance. From the Bologna data, the author selected the intersection shown in Fig. 48 (a). Fig. 48 (b) shows that the number of nodes within 300 m varied with time. The horizontal axis is the time from the beginning time of the data in seconds. The curve shows that the number of nodes was the highest at 3250 s, and the author can observe to distribute more nodes around the time than the other time.

All the nodes moved in their specified directions. The target nodes were assumed to move at 60 km/h in urban areas. The surrounding nodes moved as follows. In the uniform model, each of the speeds was either 3 km/h for pedestrians or 15 km/h, or 60 km/h for cars [88]. The directions were fixed at random. In the Bologna model, the speeds complied with the mobility of the nodes in the data. The locations were updated every 50 milliseconds, in contrast to Reference [88], which updated them every 100 milliseconds. The reason for using 50 milliseconds is that the smallest transmission period was 50 milliseconds in using the RT.

## B) Wireless Parameters

The author configured the parameters as listed in Table 8. At first, the author describes the bandwidth setting. The bandwidth was 10 MHz, divided into 50 RBPs per millisecond

[24]. The author assumed that bandwidth was used at the unit of a slot. Each slot has


(a) The geographical map of the target realistic node distribution model in Bologna, Italy.

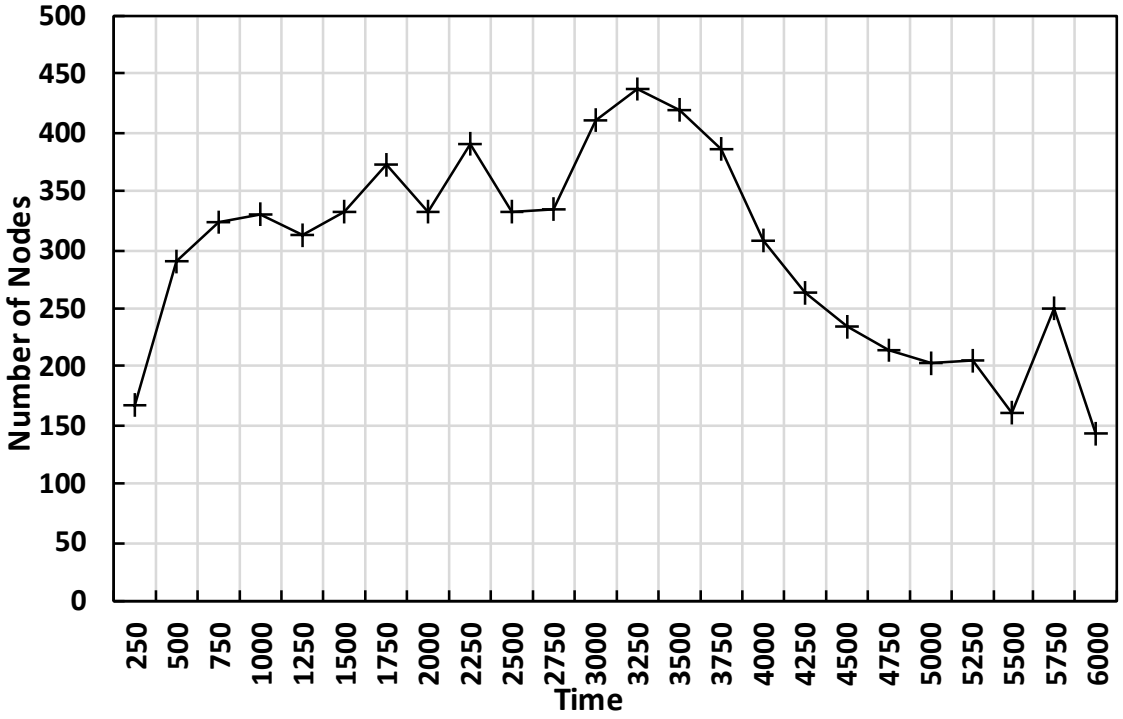


(b) The number of nodes in the Bologna model with time.

Fig. 48 The geographic and stochastic information of the Bologna model.

several RBPs. The number of occupied RBP depends on the used MCS. The author used two typical MCSs: MCS 4 as a low-index MCS and MCS 9 as a high-index MCS. The two MCSs present the relationship between the number of slots and the SINR threshold, as analyzed in the above section. Given the frame size of 190 bytes at the standard of CWS [23], each slot consumes 24 RBPs at MCS 4 and 12 RBPs at MCS 9 [90]. Thus, the system had two slots per millisecond at MCS 4 and four slots per millisecond at MCS 9. The number of slots was 2000 slots/s for MCS 4 and 4000 slots/s for MCS 9. In our simulations, all the nodes completely synchronized the timing of the slots by GNSS.

The channel model was as follows. The transmission power was set to 23 dBm [23]. The author assumed that power was divided into occupied RBPs [31]. The transmitted signals attenuated along to the WINNER+ B1 model [85], which METIS has recommended for mode 4 [86]. In particular, the author used the LOS model to create the most severe interference conditions at the node densities. In the model, the antenna height was 1.5 m [29]. In our simulations, the propagation model included log-normal shadowing gains with a deviation of 3 dB [23]. The gains were independent and identically distributed (i.i.d.) values between nodes. In each node, the decorrelation distance was 10 m [24] [88]. The shadowing gains were updated with updating locations [88], i.e., every 50 milliseconds. Also, the noise power per RB was set to −110 dBm [30] [91]. The author assumed that frames were correctly received under the simulated SINR was above the SINR threshold. The threshold was 2.7 dB for MCS 4 or 9.6 dB for MCS 9 [90].

Next, the author describes SPS-NOMA parameters. At first, nodes transmitted frames at 10 Hz, except for 20 Hz for the RT. The initial RSRP threshold was set to −110 dBm [22] by default, which is the same value as noise power. Also, each slot utilization counter was 5–15 times for 10 Hz at the standard. The author assumed the perfect channel estimation because of the following reasons. First, our main aim is to present the primary performance characteristics of the proposed method as the first step. The fundamental assumption supports the essential performance of SPS-NOMA; many related works [64]–[68] also assumed the perfect channel estimation to show the essential performance. Second, channel estimation techniques have advanced [92] and will improve the estimation accuracy in the future. The third reason is related to the collisions of reference signals, which cause channel estimation errors. Reference [87] assumed to use twelve orthogonal sequences for reference signals. Also, the ideal assumptions of related works [64]–[68] mean that their systems have prepared many reference signals enough to avoid collisions of reference signals. Based on the above works, our proposed method can also assume to be available to use similar numbers of the signals. Compared with the number of available reference signals, at most several nodes simultaneously share a slot because of at most 500 nodes per 100 slots at MCS 4 and the RT. In addition to the numbers of reference signals, the proposed method uses the sensing history to avoid the collisions of reference signals, as described in the above section. Finally, given the system has enough numbers of reference signals, the interference is expected to provide more dominant impacts to SIC performance degradation than collisions of reference signals.

Finally, the author describes how to measure the FR and the PDR. The author averaged 2000 outputs to guarantee the computational accuracy of these metrics; specifically, the sizes of the errors of the 95%-confidence interval were within $\pm 0.02$ in

Table 8 Summary of Wireless Parameters

| **Parameters for bandwidth** | **Values** |
|---|---|
| Carrier Frequency | 5.9 GHz |
| Bandwidth | 10 MHz (50 RBs) |
| Frame size | 190 bytes |
| MCS index | 4 or 9<br>(the default is 4) |
| The number of RBPs per slot | MCS 4: 24 pairs<br>MCS 9: 12 pairs |
| The number of subchannels | MCS 4: 2<br>MCS 9: 4 |
| **Parameters for channel** | **Values** |
| Transmission power | 23 dBm |
| Propagation model | WINNER+ |
| Shadowing model | Log-normal |
| Shadowing deviation | 3 dB |
| Noise power per RB | −110 dBm |
| SINR threshold | MCS 4: 2.7 dB<br>MCS 9: 9.6 dB |
| **Parameters for SPS-NOMA** | **Values** |
| Number of transmissions | 10 Hz |
| Initial RSRP threshold<br>(Default) | −110 dBm |
| Slot utilization counter | 5–15 |

all the plotted data. As reference values of computational accuracy of data, the author drew the error bar for each plotted data. Additionally, each simulation ran for 4.1 seconds to exclude the transition duration of the sensing-based SPS. Nodes generated the first frames within the first 100 milliseconds. During the next 3 seconds, nodes have executed their SPS procedures at least twice. After these durations, the FR during the last second was investigated.

# 3. Performance Evaluation of SPS-NOMA

The first subsection presents the impacts of the key factors and performance gains of SPS-NOMA in the uniform model. The next subsection highlights the practical performance gains of SPS-NOMA in the Bologna model.

## A) Performance Characteristics and Average Performance

### a). Slot Selection Mechanisms of Sensing-based SPS

This subsection focuses on the performance characteristics of SPS-NOMA for the sensing-based SPS mechanism. Fig. 49 presents the performance characteristics for the initial RSRP threshold at MCS 4 at 360 nodes. The horizontal axis is the initial RSRP threshold, and the vertical axis is the FR. Fig. 49 shows the performance trend of SPS-NOMA for the RSRP threshold discussed in the above section. The small thresholds, such as −110 dBm, were effective for the performance improvements. In the simulations, avoiding selecting slots used by near transmitters was more effective than decreasing the number of superposed signals.

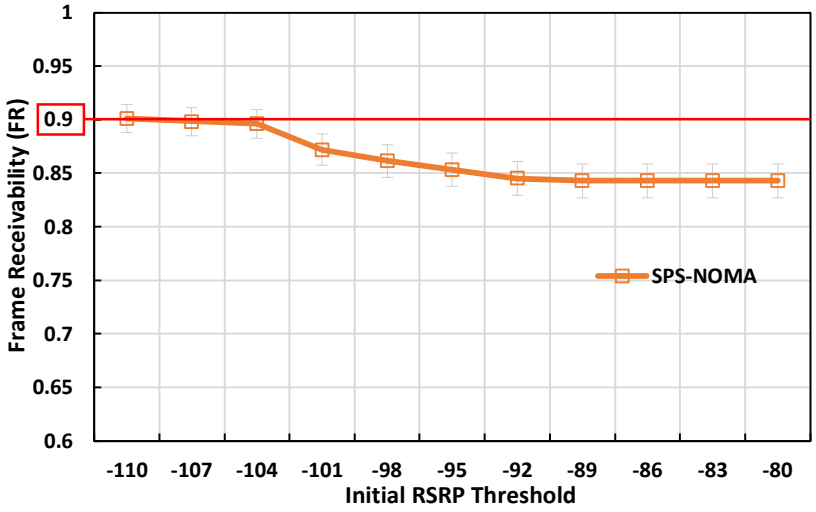


Fig. 49 The FR characteristics of SPS-NOMA for the initial RSRP threshold at 360 nodes.

Fig. 50 depicts the FR characteristics of SPS-NOMA and UL-NOMA with either of the slot selection mechanisms for the number of nodes at MCS 4. In other words, this graph shows the contributions of each mechanism in SPS-NOMA. The horizontal axis is the number of nodes, and the vertical axis is the FR. The label of RSRP-only or RSSI-only means methods implementing either of the slot selections. Fig. 50 highlighted that the RSRP mechanism was more dominant in the performance of SPS-NOMA than the RSSI mechanism. In UL-NOMA, the RSRP mechanism achieved an NAC of 360 nodes, which is the performance close to SPS-NOMA; the RSSI mechanism reached an NAC of 260 nodes. Thus, the RSRP mechanism was 38% larger NAC than the RSSI mechanism.

Fig. 51 shows the FR trends of each mechanism of UL-NOMA and OMA. The graph highlighted the performance gains of UL-NOMA in each mechanism compared with OMA at MCS 4. The axes are the same as in Fig. 50. UL-NOMA boosted the NAC of the original RSRP mechanism by 29% and the NAC of the original RSSI mechanism by 30%. In summary, SPS mechanisms and UL-NOMA are significant synergies.

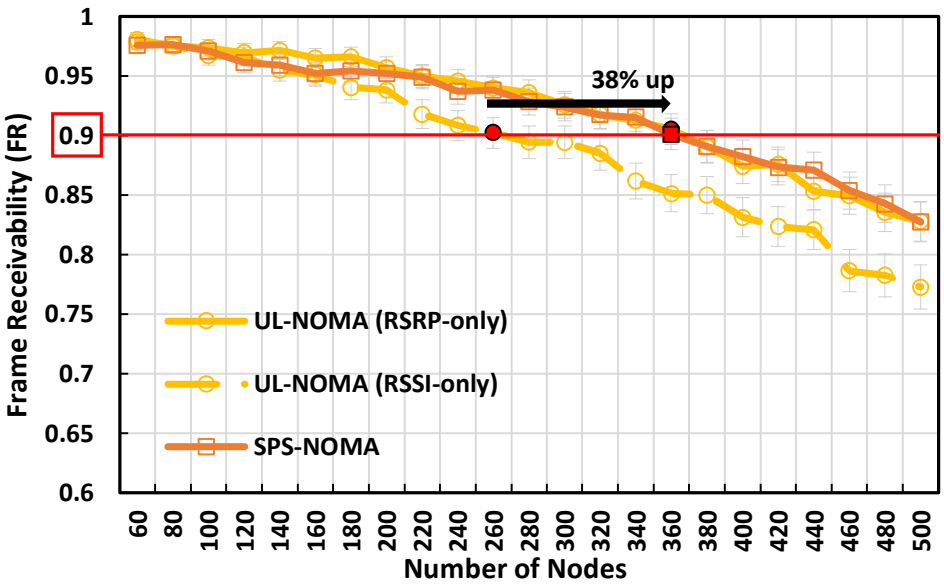


Fig. 50 The FR characteristics for slot selection mechanisms of sensing-based SPS at MCS 4 in the uniform model.

## b). MCS

Fig. 52 highlights the FR trends of SPS-NOMA for every MCS index in comparison with the current mode 4. This graph emphasized the positive and negative impacts of the choice of MCS for SPS-NOMA. The axes are the same as Fig. 50.

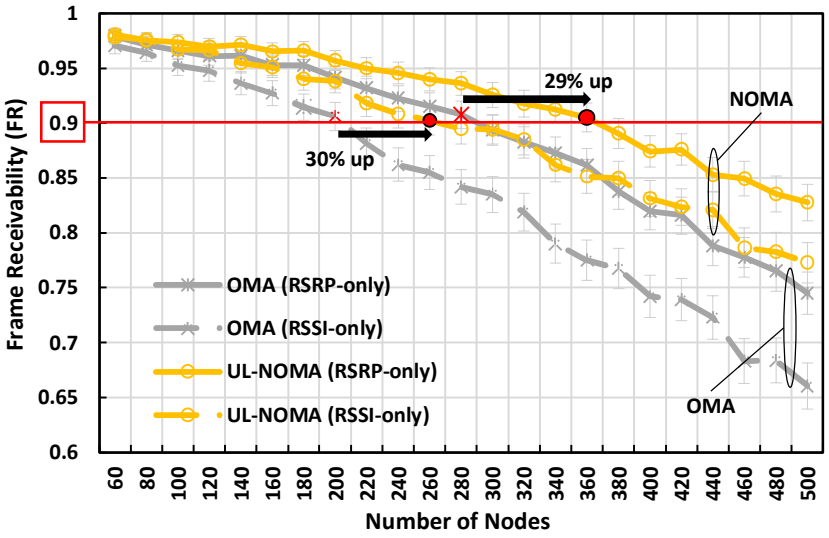


Fig. 51 The comparisons between OMA and NOMA every slot selection mechanism at MCS 4 in the uniform model.

At first, we can observe the trade-off of the choice of the MCS from Fig. 52. In MCS 4, the current mode 4 accommodated 260 nodes; SPS-NOMA accommodated 360 nodes. Thus, SPS-NOMA improved the performance of current mode 4 by 38%. In MCS 9, the current mode 4 achieved an NAC of 220 nodes, and SPS-NOMA achieved an NAC of 240 nodes. The performance gain was limited, and the improvement ratio was 9%. By comparing the performance gains for mode 4 at MCS 4 and 9, the author highlight that decreasing the SINR threshold contributes to more effective SIC decoding than decreasing the number of slots. Notably, these results demonstrated that congestion environments needed the ability to cover collisions, which has low-index MCSs.

Next, the author compares the performance of SPS-NOMA for the choice of MCS.

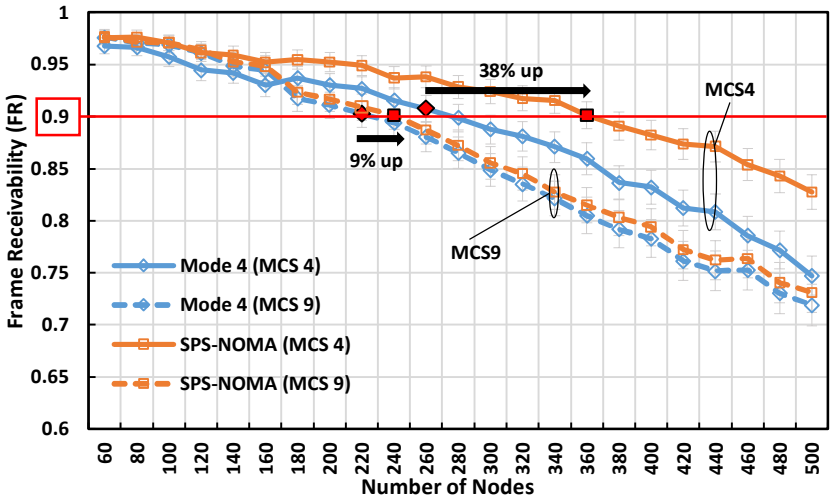


Fig. 52 The FR characteristics of SPS-NOMA with the two MCSs for the number of nodes in the uniform model.

Based on Fig. 52, using MCS 4 showed better performance than using MCS 9 for SPS-NOMA; the performance difference was 50%. Thus, SPS-NOMA recommended using MCS 4 to improve performance more.

### c). Redundant Transmission

Fig. 53 plots the FR characteristics of SPS-NOMA with/without RT. The axes are the same as in Fig. 50. In Fig. 53, we can observe the trend (the positive and negative impacts) of the RT, as discussed in the above section. In MCS 4, at small numbers of nodes, less than 320, the RT improves the FR above the method without the RT. However, at numbers of nodes more than 340, the negative impact of the RT was observed. As a result, the NAC decreased by 6% below the SPS-NOMA without the RT. At MCS 9, such a trend was also observed, as well as at MCS 4. The negative impact was represented at 360 nodes or more. In MCS 9, the method with the RT provided 8% more NAC than the method without the RT. Based on these results, amplifying the interference, i.e., the negative impact, was more dominant than the impact of selection diversity, i.e., the positive impact, especially in MCS 4. In the uniform model, the effects of the RT were limited for increasing the maximum NAC.

In Fig. 54, the author shows the FR and PDR trends in the RT. As a reference, the author plotted the PDR trend of the current mode 4 at MCS 9. The horizontal axis is the number of nodes. The vertical axis is the FR or PDR. This graph demonstrated that the RT at both MCSs showed much lower PDRs than mode 4 at MCS 9 overall. In other words, the negative impact of the redundancy reduced the reception reliability per frame, even in using SIC. In contrast, we can observe that the redundancy effects increased the reliability per time window by comparing the FR and PDR at the same MCSs.

Fig. 53 and Fig. 54 demonstrated that the RT improved the system-required

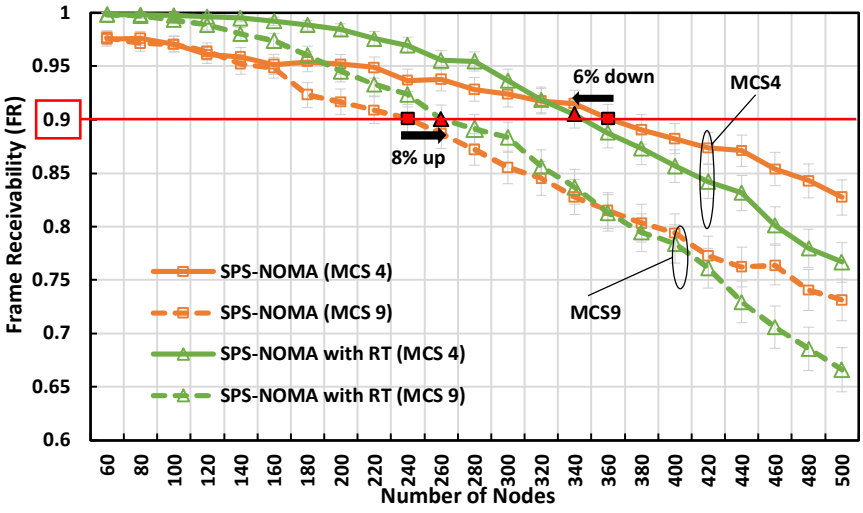


Fig. 53 The FR characteristics of SPS-NOMA with/without the RT for the number of nodes in the uniform model.

performance, especially in the conditions where the number of nodes is small. Comprehensively, SPS-NOMA increased the NAC of the current mode 4 by 38% at MCS 4 without the RT; at MCS 9, the improvement ratio was 18% with the RT.

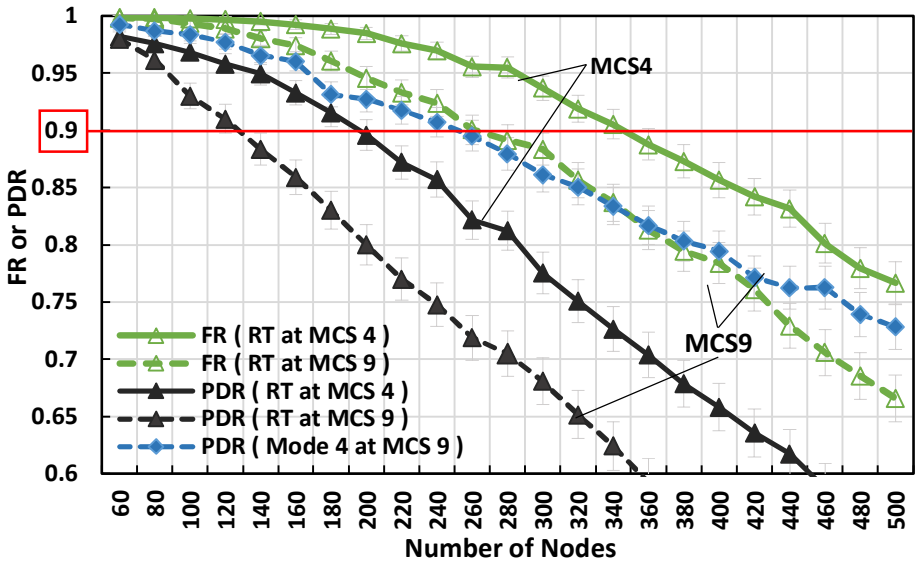


Fig. 54 The FR and PDR characteristics of SPS-NOMA with the RT at both MCSs and PDR characteristics of the current mode 4 at MCS 9 in the uniform model.

## B) Realistic Performance of SPS-NOMA

Fig. 55 plots the FR characteristics of SPS-NOMA and the current mode 4 in the Bologna model. This graph shows the practical performance of SPS-NOMA. The horizontal axis is time; the number of nodes varied with time, as shown in Fig. 48. The

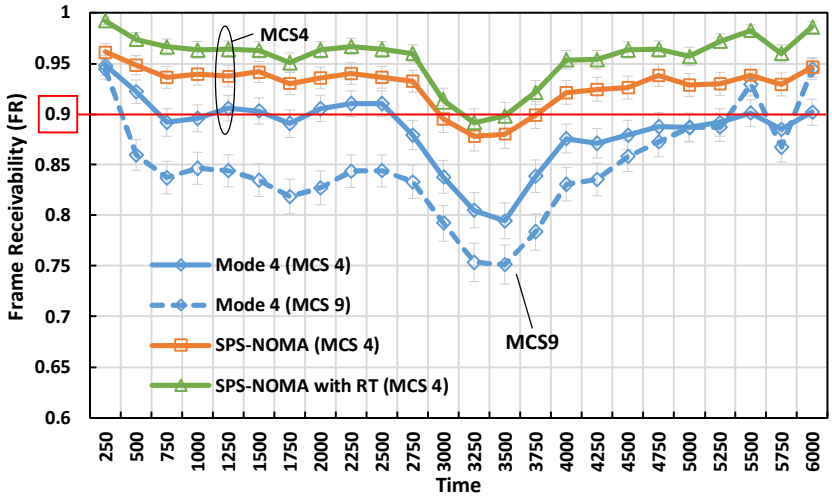


Fig. 55 The FR characteristics of SPS-NOMA with the time in the Bologna model.

vertical axis is the FR. To emphasize the effects of SPS-NOMA, the author plot the performance of SPS-NOMA at only MCS 4 and mode 4 at both MCSs.

First, the author describes the overall trends. In this evaluation, the SPS-NOMA with the RT showed consistently better performance than the other methods. SPS-NOMA without the RT followed the above method. These methods outperformed the current mode 4. Next, the author compares the number of situations that satisfied the QoS requirements. In mode 4, the number of satisfied situations was nine in MCS 4 and three in MCS 9. In contrast, SPS-NOMA without/with the RT satisfied the requirements in 20 or 22 situations, respectively. Particularly, SPS-NOMA with the RT addressed 144% more situations than the current mode 4 and satisfied the requirements in most situations in the Bologna models.

For example, the author shows the largest FR gain and the smallest gain between SPS-NOMA with the RT and mode 4 at MCS 4 under satisfying the QoS requirements. First, the SPS-NOMA provided the smallest gain at 250 s. Then, the mode 4 and the SPS-NOMA provided the FRs of 0.95 and 0.99, respectively; the gain was 5%. Also, the SPS-NOMA provided the largest gain at 3750 s in other situations, compared with the mode 4. At the time, the mode 4 and the SPS-NOMA achieved the FRs of 0.84 and 0.92, respectively; the gain was 10%, and the SPS-NOMA became to satisfy the QoS requirements.

Fig. 56 shows the FR and the PDR trends of the RT. The horizontal axis is time, and the vertical axis is the same as Fig. 54. As well as Fig. 54, the author referred to the PDR characteristics of the current mode 4 at MCS 9. The RT showed smaller PDR than mode 4 at MCS 9 in most situations, even in the Bologna model because of redundancy. In other words, at the level of reception reliability per frame, SIC was not useful to cover the negative impact of the redundancy; however, at the reception reliability per time window, the RT significantly supported to improve SIC gains. In conclusion, SPS-NOMA also

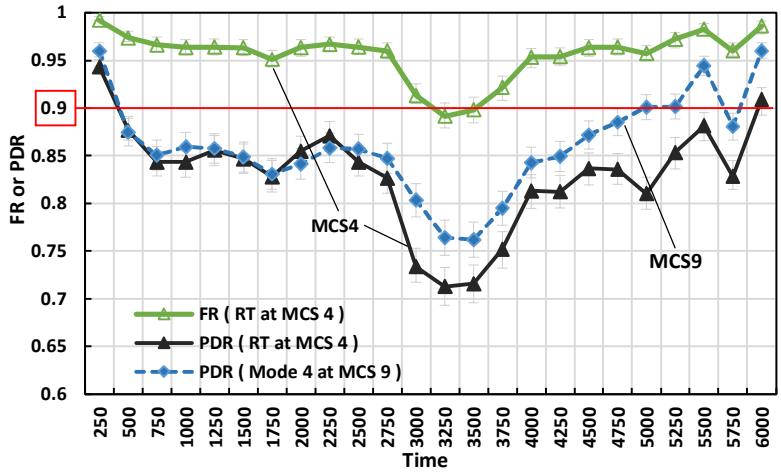


Fig. 56 The FR and PDR characteristics of SPS-NOMA with the RT at both MCSs and PDR characteristics of the current mode 4 at MCS 9 in the Bologna model.

advanced the performance of the current mode 4 in the realistic node distribution model. In particular, the RT mechanism was effective in practical uses.

# 4. Conclusion in Section VI

The author highlighted the performance gains of SPS-NOMA in the CWS to explore the next generation sidelink C-V2X. SPS-NOMA uses UL-NOMA in mode 4. In SPS-NOMA, multiple nodes simultaneously broadcast frames, and receivers decode the superposed signal by SIC. SPS-NOMA enables nodes to access the V2X channel more efficiently than the current mode 4. Our simulation results highlighted that SPS-NOMA outperformed mode 4 in the uniform node distribution model and realistic models. In the uniform model, SPS-NOMA boosted the NAC of mode 4 by 38%. In realistic cases, the proposed method satisfied the QoS requirements of the CWS in 144% more situations than the current mode 4. These results demonstrated that SPS-NOMA showed an excellent option for the potential extension of sidelink C-V2X mode 4.

# VII. Conclusion

This paper focused on the decentralized V2X in CWS to reduce traffic accidents in ITS. The current decentralized V2X has actively developed DSRC and PC5-based C-V2X mode 4. These technologies require no infrastructures to provide D2D communications. The advantage supports ITS in the early stages, in which infrastructures are too small for nodes to connect them anywhere. CWS requires nodes to obtain enough frames to warn potential traffic accidents.

The author challenged a channel congestion problem of the decentralized V2X in CWS, unsolved in related works. Such a problem occurs in crowded environments, like intersections. The problem causes frame collision errors more frequently than in non-crowded environments, and thus, CWS may fail to satisfy the QoS requirements. Few related works have focused on a congestion problem considering the QoS requirements. In particular, no related works have evaluated the performance of mode 4 with the QoS requirements. Additionally, some related works focused on DCC, but DCC reduces the number of transmitted frames (i.e., decreasing the number of received frames) to mitigate channel congestion. As a result, related works have essentially addressed no channel congestion for the QoS requirements.

To this end, the author studied the following three contents: evaluating the performance characteristics of mode 4 under channel congestion in CWS, proposing the decentralized cross-layer congestion controls for DSRC and PC5-based C-V2X mode 4 in CWS. Our main idea for congestion controls is efficient MAC protocols by cross-layer approaches with other layers without reducing the number of transmissions in V2X bandwidth, unlike the existing DCC methods.

In Section III, the author proposed a node-clustering method for DSRC, CLASES, an application-MAC cross-layer decentralized congestion control method. In CLASES, multiple nodes form a cluster, and then only each cluster head transmits frames of all the cluster members on behalf of members; data in frames of the members comply with estimated data from their past frames. The proposed method efficiently accesses a V2X channel and thus mitigates channel congestion. Through simulations in multiple points of view, the author highlighted that CLASES mitigates the channel congestion of DSRC efficiently; specifically, CLASES improved 27% better performance than the current DSRC. In Section III, the proposed method enables us to mitigate DSRC performance degradation due to channel congestion without losing the amount of information.

In Section IV, the author presented the performance degradation of mode 4 due to channel congestion because the degradation remained unknown. The author evaluated the performance in both fundamental and practical node density, strongly related to channel congestion. Through the simulations, mode 4 has experienced its channel congestion problem; especially, mode 4 achieved 55% lower performance than the QoS requirements

at a large intersection. Section IV highlighted that the performance degradation of the current mode 4 due to channel congestion.

In Sections V and VI, the author proposed a NOMA method for mode 4, called DB-NOMA, a physical-MAC cross-layer decentralized congestion control method. DB-NOMA has two types of NOMA. One of them is a frame relaying method with NOMA; each node broadcasts its own frame and the relayed frame of another node in a NOMA manner. The other is SPS-NOMA. In SPS-NOMA, each node selects a spectrum resource based on sensing-based SPS, a suitable slot selection for NOMA, and multiple nodes simultaneously transmit their frames in a NOMA manner. NOMA supports nodes to receive multiple frames at a spectrum resource simultaneously and thus mitigates channel congestion. Our simulation results highlighted that the proposed relaying method improved 94% better performance than the current mode 4, and SPS-NOMA boosted 38% better performance than the current mode 4. In Sections V and VI, the proposed method allows us to access spectrum resources more efficiently than the current mode 4 and improves channel congestion without decreasing the number of transmitted frames.

In conclusion, this paper achieved to mitigate channel congestion of decentralized V2X through decentralized cross-layer congestion control methods. First, this paper contributes to advancing wireless communications, ITS, and smart mobility. In particular, the author proposed new V2X congestion control approaches without decreasing the amount of transmitted information, unlike existing DCC methods. The simulation results highlighted the possibility of the proposed congestion control approaches. The proposed methods also allow supporting more diverse CWS situations than the current standards and thus advanced CWS developments practically for both V2X standards. For the further challenges, addressing more severe channel congestion is necessary because the proposed methods failed to meet the requirements in some intersections. Additionally, promoting practical uses of CWS is necessary through demonstration experiments. Second, this paper potentially suggests to extend the proposed methods for other applications on *smart city* or other wireless networks for the fifth-generation (5G) and further next-generation communications.

# Acknowledgments

The author sincerely thanks all people to support summarizing this thesis.

First, the author sincerely thanks Prof. Tutomu Murase, Prof. Tohru Ishihara, Prof. Yutaka Matsubara at Nagoya University, and Prof. Shigeo Shioda at Chiba University to advise me on this thesis. In particular, Prof. Tutomu Murase has instructed me to grow an independent researcher in wireless communications. He strongly supported me to get opportunities for discussing my research with other researchers, like Prof. Ji Yusheng in the National Institute of Informatics and Prof. Celimuge Wu at the University of Electro-Communications. Through such discussions, he has taught me the importance of joint research or collaborations with other researchers.

Second, the author sincerely thanks various researchers for discussing my research. In particular, Prof. Shioda, Prof. Yusheng, and Prof. Wu discussed it with me frequently. Prof. Shioda instructed me on effective ways for joint research. The author also thanks Prof. Eiji Okamoto in Nagoya Institute of Technology and Mr. Shinpei Yasukawa in NTT DOCOMO because they advised me on the wireless technologies. The author also thanks Prof. Suguru Kameda in Tohoku University and Prof. Nobuyoshi Komuro in Chiba University. They supported me to do research in Wireless Information Network Laboratory (WINLAB) at Rutgers University, USA. Finally, the author thank professors, students, and stuffs in WINLAB. In particular, Prof. Dipankar Raychaudhuri and Prof. Predrag Spasojevic gave me the opportunity of joint research. They strongly instructed me on how to study.

Third, the author sincerely thanks all members and graduated members in Murase and Shimada Laboratory at Nagoya University. Prof. Hajime Shimada and Prof. Yukiko Yamaguchi have supported me through communications in my daily life. Prof. Yukihiro Tadokoro advised my research and my course many times. Mrs. Junko Sakaguchi administratively supported my research. All students always discussed my research with me. Their professional knowledge inspired my thoughts.

Finally, the author sincerely thanks my family for supporting my life and health. My father, Tohru, financially supported me and made me relax through baseball, Shogi, and public bath when the author came back home. He initially disagreed with entering the doctoral course but finally supported it. My mother, Natsue, mentally supported me. She always cares about my health and advised me of better foods for my health. My sister, Rina, supported me to study hard. She told me about the appearance of our family through her photographs when she went back home. She also consulted her future career with me. Her attitude increases my research motivation. The author sincerely thanks them again.

# Reference

[1] Pakistan Today, 3 February 2017, http://www.pakistan-today.com.pk/2011/12/24/city/karachi/in-karachi-16562- more-vehicles-hit-the-roads-each-month/

[2] 4. Dawn News, 29 January 2017, http://www.dawn.com/ news/1083354

[3] Peden MM. World report on road traffic injury preven- tion, 2004, https://www.who.int/violence_injury_preven tion/publications/road_traffic/world_report/summary_en _rev.pdf

[4] A. Fitah, A. Badria, M. Moughit, and A. Sahel, "Performance of DSRC and WIFI for intelligent transport systems in VANET," Procedia Comput. Sci., vol. 127, pp. 360–368, 2018.

[5] L. Zhu, F. R. Yu, Y. Wang, B. Ning, and T. Tang, "Big Data Analytics in Intelligent Transportation Systems: A Survey," IEEE Trans. Intell. Transp. Syst., vol. 20, no. 1, pp. 383–398, 2019.

[6] Z. Xiong, H. Sheng, W. Rong, and D. E. Cooper, "Intelligent transportation systems for smart cities: a progress review," China Information Science, vol. 55, no. 12, pp. 2908– 2914, 2012.

[7] T. Zaheer, A. W. Malik, A. U. Rahman, A. Zahir, and M. M. Fraz, "A vehicular network–based intelligent transport system for smart cities," Int. J. Distrib. Sens. Networks, vol. 15, no. 11, 2019.

[8] T. ElBatt et al., "Cooperative collision warning using dedicated short range wireless communications," ACM VANET 2006, 2006.

[9] D. Bezzina, "Light Vehicle Platform Update," IVBSS 2008 Public, Meeting, Apr. 2008.

[10] U.S. Department of Transportation Announces Decision to Move Forward with Vehicle-to-Vehicle Communication Technology for Light Vehicles. Available online: https://www.auto-talks.com/u-s-department-transportation-announces-decision-move-forward-vehicle-vehicle-communication-technology-light-vehicles/ (accessed on May 2020).

[11] A. Kousaridas, D. Medina, S. Ayaz, and C. Zhou, "Recent advances in 3GPP networks for vehicular communications," IEEE CSCN 2017, pp. 91–97, 2017.

[12] ETSI, "ETSI TR 102 638 V1.1.1 (2009-06): Intelligent Transport Systems (ITS); Vehicular Communications; Basic Set of Applications; Definitions," ETSI, vol. 1, pp. 1–81, 2009.

[13] J. B. Kenney, "Dedicated short-range communications (DSRC) standards in the United States," IEEE, vol. 99, no. 7, 2011.

[14] D. Jiang et al., "Design of 5.9GHz DSRC-based Vehicular Safety Communication," IEEE Wireless Communications, vol. 13, no. 5, 2006.

[15] D. Jiang and L. Delgrossi, "IEEE 802.11p: Towards an international standard for wireless access in vehicular environments," IEEE VTC 2008, 2008.

[16] T. V. Nguyen, F. Baccelli, K. Zhu, S. Subramanian, X. Wu, "A Performance Analysis of CSMA Based Broadcast Protocol in VANETs, " IEEE INFOCOM 2013, 2013.

[17] G. Bansal, J. B. Kenney, and C. E. Rohrs, "LIMERIC: A Linear Adaptive Message Rate Algorithm for DSRC Congestion Control," IEEE Transactions on Vehicular Technology,

vol. 62, no. 9, pp. 4182–4197, 2013.

[18] T. Tielert, D. Jiang, Q. Chen, L. Delgrossi, and H. Hartenstein, "Design methodology and evaluation of rate adaptation based congestion control for Vehicle Safety," 2011 IEEE Vehicular Networking Conference, pp. 116–123, 2011.

[19] B. Cheng, A. Rostami, M. Gruteser, J. B. Kenney, G. Bansal, and K. Sjoberg, "Performance evaluation of a mixed vehicular network with CAM-DCC and LIMERIC vehicles," IEEE WoWMoM 2015, 2015.

[20] K. Wako, H. Onishi, F. Watanabe, F. Mlinarsky, T. Murase and K. Sasajima, "V2V communication quality with multi-antenna in field assessments and simulations," ICCVE, pp. 209-214, 2014.

[21] H. Ito, et al. "Crash warning for intersection and head-on car collision in vehicle-to-vehicle communication," ICCVE, 2015.

[22] 3GPP, "Evolved Universal Terrestrial Radio Access (E-UTRA); Physical layer procedures," 3GPP TS 36.213 version 14.2.0 Release 14, 2017.

[23] R. Molina-Masegosa and J. Gozalvez, "LTE-V for Sidelink 5G V2X Vehicular Communications: A New 5G Technology for Short-Range Vehicle-to-Everything Communications," IEEE Vehicular Technology Magazine, vol. 12, no. 4, pp. 30–39, 2017.

[24] A. Bazzi and S. Member, "Study of the Impact of PHY and MAC Parameters in 3GPP C-V2V Mode 4," IEEE Access, vol. 6, pp. 71685–71698, 2018.

[25] M. Gonzalez-Martin, M. Sepulcre, R. Molina-Masegosa, and J. Gozalvez, "Analytical Models of the Performance of C-V2X Mode 4 Vehicular Communications," IEEE Trans. Veh. Technol., vol. 68, no. 2, pp. 1155–1166, 2018.

[26] Y. Park, S. Weon, I. Hwang, H. Lee, J. Kim, and S. Member, "Spatial Capacity of LTE-based V2V Communication," ICEIC 2018, pp. 1–4, 2018.

[27] A. Nabil, V. Marojevic, K. Kaur, and C. Dietrich, "Performance Analysis of Sensing-Based Semi-Persistent Scheduling in C-V2X Networks," arXiv:1804.10788, 2018.

[28] B. Toghi, M. O. Mughal, H. N. Mahjoub, Y. P. Fallah, J. Rao, and S. Das, "Multiple Access in Cellular V2X: Performance Analysis in Highly Congested Vehicular Networks," arXiv:1809.02678, 2018.

[29] J. He, Z. Tang, Z. Fan, and J. Zhang, "Enhanced collision avoidance for distributed LTE vehicle to vehicle broadcast communications," IEEE Communication Letter, vol. 22, no. 3, pp. 630–633, 2018.

[30] G. Cecchini, A. Bazzi, B. M. Masini, and A. Zanella, "Performance comparison between IEEE 802.11p and LTE-V2V in-coverage and out-of-coverage for cooperative awareness," IEEE VNC 2018, pp. 109–114, 2018.

[31] A. Bazzi, B. M. Masini, and A. Zanella, "How many vehicles in the LTE-V2V awareness range with half or full duplex radios?," ITST 2017, pp. 1–6, 2017.

[32] V. Vukadinovic et al., "3GPP C-V2X and IEEE 802.11p for Vehicle-to-Vehicle Communications in Highway Platooning Scenarios," Ad Hoc Networks, vol. 74, pp. 17–29, 2018.

[33] A. Mansouri, V. Martinez, and J. Harri, "A First Investigation of Congestion Control for LTE-V2X Mode 4," 2019 15th Annu. Conf. Wirel. On-demand Netw. Syst. Serv. (WONS), pp. 56–63, 2019.

[34] P. Wendland, G. Schaefer, and R. S. Thoma, "LTE-V2X Mode 4: Increasing robustness and DCC compatibility with reservation splitting," 2019 8th IEEE Int. Conf. Connect. Veh.

Expo (ICCVE 2019), pp. 1–6, 2019.

[35] T. Hirai and T. Murase, "Node Clustering Communication Method With Member Data Estimation to Improve QoS of V2X Communications for Driving Assistance With Crash Warning," IEEE Access, vol. 7, pp. 37691–37707, 2019, doi: 10.1109/ACCESS.2019.2906392.

[36] Takeshi Hirai and Tutomu Murase, "Performance Evaluations of PC5-based Cellular-V2X Mode 4 for Feasibility Analysis of Driver Assistance Systems with Crash Warning," MDPI Sensors, vol. 20, no. 10, pp. 2950–2966, May 2020, doi: https://doi.org/10.3390/s20102950.

[37] Takeshi Hirai and Tutomu Murase, "Performance Evaluation of NOMA for Sidelink Cellular-V2X Mode 4 in Driver Assistance System with Crash Warning," IEEE Access, vol. 8, pp. 168321–168332, Sep. 2020, doi: 10.1109/ACCESS.2020.3023721.

[38] Takeshi Hirai and Tutomu Murase, "NOMA Concept for PC5-based Cellular-V2X mode 4 in Crash Warning System," IEEE VTC 2019-Fall, USA, Sep. 2019.

[39] Takeshi Hirai and Tutomu Murase, “Performance Characteristics of Sensing-based SPS of PC5-based C-V2X Mode 4 in Crash Warning Application under Congestion,” IEEE ITSC 2019, New Zealand, Oct. 2019.

[40] Takeshi Hirai and Tutomu Murase, "Practical Performance of Simple C-V2X Mode 4 using NOMA for Driver Assistant System with Crash Warning," IEICE SmartCom2019, New Jersey, Nov. 2019.

[41] R. Kawasaki, H. Onishi, T. Murase, “Performance evaluation on V2X communication with PC5-based and Uu-based LTE in Crash Warning Application,” IEEE GCCE 2017, pp. 1–2, 2017.

[42] S. Gamboa, R. Thanigaivel, and R. Rouil, “System level evaluation of UE-to-network relays in D2D-enabled LTE networks,” IEEE Int. Work. Comput. Aided Model. Des. Commun. Links Networks (CAMAD), 2019.

[43] Z. Velkoy, B.Spasenovski, et al., “Capture Effect in IEEE 802.11 Basic Service Area under Influence of Rayleigh Fading and Near/Far Effect,” IEEE PIMRC 2002, vol.1, pp. 172–176, 2002.

[44] X. Li and Q.-A. Zeng, “Capture effect in the IEEE 802.11 WLANs with rayleigh fading, shadowing, and path loss,” IEEE WiMob 2006, 2006.

[45] L. Bai, L. Zhao, and Z. Liao, “A Novel Cooperation Scheme in Wireless Sensor Networks *,” Communication Society, vol. 1, no. April, pp. 1889–1893, 2008.

[46] H. Su and H. H. Chen, “Cluster-based multi-channel communications protocols in vehicle ad hoc networks,” IEEE Wireless Communications, vol. 13, no. 5, pp. 44–50, 2006.

[47] T. Taleb and A. Benslimane, “Design guidelines for a network architecture integrating VANET with 3G & beyond networks,” IEEE GLOBECOM 2010, 2010.

[48] A. Benslimane, T. Taleb, and R. Sivaraj, “Dynamic clustering-based adaptive mobile gateway management in integrated VANET 3G heterogeneous wireless networks,” IEEE Journal on Selected Areas in Communications, vol. 29, no. 3, pp. 559–570, 2011.

[49] S. Ucar, S. C. Ergen, and O. Ozkasap, “Multihop-Cluster-Based IEEE 802.11p and LTE Hybrid Architecture for VANET Safety Message Dissemination,” IEEE Transactions on Vehicular Technology, vol. 65, no. 4, pp. 2621–2636, 2016.

[50] L.-C. Tung, J. Mena, M. Gerla, and C. Sommer, “A cluster based architecture for intersection collision avoidance using heterogeneous networks,” 2013 12th Annual Mediterranean Ad Hoc Network Workshop, pp. 82–88, 2013.

[51] W. R. Heinzelman, A. Chandrakasan, and H. Balakrishnan, “Energy-efficient communication protocol for wireless microsensor networks,” 33rd Annual Hawaii International Conference on System Sciences, 2000.

[52] S. K. Singh, M. P. Singh, A. Professor, and D. K. Singh, “A Survey of Energy-Efficient Hierarchical Cluster-Based Routing in Wireless Sensor Networks,” International Journal of Advanced Networking and Application, vol. 2, no. 2, pp. 570–580, 2010.

[53] O. Younis, S. Member, and S. Fahmy, “HEED : A Hybrid, Energy-Efficient, Distributed Clustering Approach for Ad Hoc Sensor Networks,” IEEE Transactions on mobile computing, vol. 3, no. 4, pp. 366–379, 2004.

[54] G. Ran, H. Zhang, and G. Shulan, “Improving on LEACH Protocol of Wireless Sensor using Fuzzy Logic,” Journal of Information &Computational Science, vol. 3, no. March, pp. 767–775, 2010.

[55] D. Kumar, T. C. Aseri, and R. B. Patel, “EEHC: Energy efficient heterogeneous clustered scheme for wireless sensor networks,” Computer Communications, vol. 32, no. 4, pp. 662–667, 2009.

[56] A. Ahlawat and V. Malik, “An Extended Vice-Cluster Selection Approach to Improve V Leach Protocol in WSN,” Advanced Computing and Communication Technologies, pp. 236–240, 2013.

[57] V. Loscri, G. Morabito, and S. Marano, “A two-levels hierarchy for low-energy adaptive clustering hierarchy (TL-LEACH),” IEEE VTC 2005, 2005.

[58] M. C. Domingo and R. Prior, “A distributed clustering scheme for underwater wireless sensor networks,” IEEE PIMRC, 2007.

[59] P. Basu, N. Khan, and T. D. C. Little, “A mobility based metric for clustering in mobile ad hoc networks,” Distributed Computing Systems Workshop, pp. 413 - 418, 2001.

[60] E. Souza, I. Nikolaidis, and P. Gburzynski, “A new Aggregate Local Mobility (ALM) clustering algorithm for VANETs,” IEEE International Conference on Communications, no. April, 2010.

[61] N. Maslekar, M. Boussedjra, J. Mouzna, and H. Labiod, “A stable clustering algorithm for efficiency applications in VANETs,” IWCMC 2011, pp. 1188–1193, 2011.

[62] S. A. Mohammad and C. W. Michele, “Using traffic flow for cluster formation in vehicular ad-hoc networks,” IEEE Local Computer Network. Conference, pp. 631–636, 2010.

[63] R. Chai, B. Yang, L. Li, X. Sun, and Q. Chen, “Clustering-based data transmission algorithms for VANET,” IEEE WCSP 2013, 2013.

[64] C. Chen, B. Wang, and R. Zhang, "Interference Hypergraph-Based Resource Allocation (IHG-RA) for NOMA-Integrated V2X Networks," IEEE Internet Things J., vol. 6, no. 1, pp. 161–170, 2019.

[65] J. Bin Kim, I. H. Lee, and J. Lee, "Capacity Scaling for D2D Aided Cooperative Relaying Systems Using NOMA," IEEE Wirel. Commun. Lett., vol. 7, no. 1, pp. 42–45, 2018.

[66] Y. Chen, L. Wang, Y. Ai, B. Jiao, and L. Hanzo, “Performance analysis of NOMA-SM in vehicle-to-vehicle massive MIMO channels,” IEEE J. Sel. Areas Commun., vol. 35, no. 12, pp. 2653–2666, 2017.

[67] T. Kim, S. Member, Y. Park, H. Kim, and S. Member, "Cooperative Superposed Transmission in Cellular-based V2V Systems," IEEE Trans. Veh. Technol., vol. 68, no. 12, p. 11888–11901, 2019.

[68] B. Di, L. Song, Y. Li, and Z. Han, “V2X Meets NOMA: Non-Orthogonal Multiple Access

for 5G-Enabled Vehicular Networks," IEEE Wirel. Commun., vol. 24, no. 6, pp. 14–21, 2017.

[69] Z. Wang, J. Hu, G. Liu, and Z. Ma, "Optimal Power Allocations for Relay-assisted NOMA-based 5G V2X Broadcast/Multicast Communications," 2018 IEEE/CIC ICCC, pp. 688–693, 2019.

[70] H. Jiang, Q. Cui, Y. Gu, X. Qin, X. Zhang, and X. Tao, "Distributed Layered Grant-Free Non-Orthogonal Multiple Access for Massive MTC," IEEE PIMRC 2018, 2018.

[71] M. Moriyama, K. Takizawa, M. Oodo, H. Tezuka, and F. Kojima, "Experimental Evaluation of UL-NOMA System Employing Correlated Receive Diversity," ICNC 2019, pp. 894–899, 2019.

[72] S. M. R. Islam, N. Avazov, O. A. Dobre, and K. S. Kwak, "Power-Domain Non-Orthogonal Multiple Access (NOMA) in 5G Systems: Potentials and Challenges," IEEE Commun. Surv. Tutorials, vol. 19, no. 2, pp. 721–742, 2017.

[73] Li, A. Benjebbour, X. Chen, H. Jiang, and H. Kayama, "Uplink Non-Orthogonal Multiple Access (NOMA) with Single-Carrier Frequency Division Multiple Access (SC-FDMA) for 5G systems," IEICE Trans. Commun., vol. E98B, no. 8, pp. 1426–1435, 2015.

[74] J. Zhao, Y. Liu, K. K. Chai, Y. Chen, and M. Elkashlan, "Joint Subchannel and Power Allocation for NOMA Enhanced D2D Communications," IEEE Trans. Commun., vol. 65, no. 11, pp. 5081–5094, 2017.

[75] T. Ute, Y. Watanabe, K. Sato, T. Fujii, T. Shimizu, and O. Altintas, "Poster: Multi-antenna successive interference cancellation to improve reliability of V2V communication," IEEE VNC 2018, pp. 29–30, 2018.

[76] Y. Watanabe, K. Sato, and T. Fujii, "Poster: A scheduling method for V2V networks using successive interference cancellation," IEEE VNC 2017, vol. 1, pp. 1–2, 2017.

[77] D. Zhang, Y. Liu, L. Dai, A. K. Bashir, A. Nallanathan, and B. Shim, "Performance Analysis of Decentralized V2X System with FD-NOMA," 2019 IEEE 90th Vehicular Technology Conference, pp. 1–6, 2019.

[78] T. Hirai, H. Ito, H. Onishi, T. Murase, "Node-Clustering in Vehicle-to-Pedestrian Communications for Crash Warning Applications," ITS World Congress 2016, 2016.

[79] Y. Park and H. Kim, "Collision control of periodic safety messages with strict messaging frequency requirements," IEEE Transactions on Vehicular Technology, vol. 62, no. 2, pp. 843–852, 2013.

[80] P. Bellavista, L. Foschini, and E. Zamagni, "V2X Protocols for low-penetration-rate and cooperative traffic estimations," IEEE VTC 2014, 2014.

[81] W. Zhou, T. Ying, L. Yang, Y. Yang, J. Yuan, and M. Du, "Design of an intelligent driving system simulation platform and its application," IEEE SSCI 2017, pp. 1–7, 2018.

[82] L. Bedogni, M. Gramaglia, A. Vesco, M. Fiore, J. Härri, and F. Ferrero, "The Bologna ringway dataset: Improving road network conversion in SUMO and validating urban mobility via navigation services," IEEE Transactions on Vehicular Technology, vol. 64, no. 12, pp. 5464–5476, 2015.

[83] L. Bieker et al., "Traffic Simulation for All: A Real World Traffic Scenario from the City of Bologna," SUMO Conference 2014, 2014.

[84] M. Behrisch, L. Bieker, J. Erdmann, D. Krajzewicz, "SUMO – Simulation of Urban MObility," 2010.

[85] Juha Meinilä et al., "D5.3: WINNER+ Final Channel Models," Wireless World Initiative

New Radio – WINNER+, 2010.

[86] METIS EU Project Consortium, “Initial channel models based on measurements,” ICT-317669-METIS/D1.2, 2014.

[87] C. Wang, Y. Chen, Y. Wu, and L. Zhang, "Performance Evaluation of Grant-Free Transmission for Uplink URLLC Services," IEEE VTC2017-Spring, 2017.

[88] 3GPP, “Study on LTE-based V2X Services; (Release 14),” 3GPP TS 36.885 v. 14.0.0, 2016.

[89] S. Y. Jung, H. R. Cheon, and J. H. Kim, "Reducing consecutive collisions in sensing based semi persistent scheduling for cellular-V2X," IEEE Veh. Technol. Conf., pp. 1–5, 2019.

[90] A. Bazzi, A. Zanella, and B. M. Masini, "Optimizing the Resource Allocation of Periodic Messages with Different Sizes in LTE-V2V," IEEE Access, vol. 7, pp. 43820–43830, 2019.

[91] L. F. Abanto-Leon, A. Koppelaar, and S. H. De Groot, “Enhanced C-V2X Mode-4 Subchannel Selection,” IEEE VTC, pp. 1–12, 2018.

[92] Y. Du et al., "Joint Channel Estimation and Multiuser Detection for Uplink Grant-Free NOMA," IEEE Wirel. Commun. Lett., vol. 7, no. 4, pp. 682–685, 2018.

# Research Achievements

① Peer-reviewed Journals (First Authors)

[1] Takeshi Hirai and Tutomu Murase, “Performance Evaluation of NOMA for Sidelink Cellular-V2X Mode 4 in Driver Assistance System with Crash Warning,” IEEE Access, vol. 8, pp. 168321–168332, Sep. 2020. (Impact Factor of 2019: 3.745).

[2] Takeshi Hirai and Tutomu Murase, “Performance Evaluations of PC5-based Cellular-V2X Mode 4 for Feasibility Analysis of Driver Assistance Systems with Crash Warning,” MDPI Sensors, vol. 20, no. 10, pp. 2950–2966, May 2020 (Impact Factor: 3.031).

[3] Takeshi Hirai and Tutomu Murase, “Node Clustering Communication Method With Member Data Estimation to Improve QoS of V2X Communications for Driving Assistance With Crash Warning,” IEEE Access, vol. 7, pp. 37691–37707, Mar. 2019 (Impact Factor of 2018: 4.098).

[4] Takeshi Hirai and Tutomu Murase, “Node-Clustering Communication Method to improve QoS in V2X Communications in Crash Warning Applications,” IEICE Communication Express, vol. 7, no. 10, pp. 376–381, Oct. 2018.

② Peer-reviewed International Conference Papers
【International conferences (First author)】

[5] Takeshi Hirai and Tutomu Murase, “Practical Performance of Naive PC5-based C-V2X Mode 4 using NOMA for Driver Assistant System with Crash Warning,” The 6th International Workshop on Smart Wireless Communications (IEICE SmartCom 2019), USA, Nov. 2019.

[6] Takeshi Hirai and Tutomu Murase, “Performance Characteristics of Sensing-based SPS of PC5-based C-V2X Mode 4 in Crash Warning Application under Congestion,” 2019 IEEE Intelligent Transportation Systems Conference (IEEE ITSC 2019), New Zealand, Oct. 2019.

[7] Takeshi Hirai and Tutomu Murase, “NOMA Concept for PC5-based Cellular-V2X mode 4 in Crash Warning System,” 2019 IEEE 90th Vehicular Technology Conference (IEEE VTC2019-Fall), USA, Sep. 2019.

[8] Takeshi Hirai and Tutomu Murase, “Frame Relaying for Low Rates of Received Frames in Crash Warning Application using V2X communication,” 25th World Congress on Intelligent Transport Systems (ITS World Congress 2018), AP-TP1271, Denmark, Sep. 2018.

[9] Takeshi Hirai and Tutomu Murase, “Effect of Estimation Error in Node-Clustering with V2X Communications for Crash Warning Applications,” IEEE International Conference on Consumer Electronics - Taiwan (IEEE 2018 ICCE-TW), Taiwan, May 2018.

【International conferences (Non-first author)】

[10] Kai Takahashi, Yuto Konuma, Shigeo Shioda, Takeshi Hirai, and Tutomu Murase, “Closed-Form Expressions of Performance Metrics of V2X Safety Communication in Urban Scenarios,” 2020 92nd IEEE Vehicular Technology Conference (IEEE VTC2020-Fall), Nov. 2020.

③ Non-reviewed Presentations

【Invited presentations (First author)】

[11] Takeshi Hirai and Tutomu Murase, “[Invited Lecture] Performance Evaluation on MAC Layer Protocol in Crash Warning Application using PC5-based Cellular-V2X mode4,” IEICE Technical Report, vol. 119, no. 221, NS2019-101, pp. 13-18, Aichi, Oct. 2019.

【Domestic conferences (First author)】

[12] Takeshi Hirai and Tutomu Murase, “NOMA for Infrastructure-less Cellular-V2X in Crash Warning System,” IPSJ FIT 2019, M-031, Okayama, Sep. 2019.

[13] Takeshi Hirai and Tutomu Murase, “Performance Evaluation on MAC Layer Protocol in Crash Warning Application using PC5-based Cellular-V2X mode4,” IEICE General Conference, BS-4-29, Tokyo, Mar. 2019.

[14] Takeshi Hirai, Tutomu Murase, “Performance Evaluation on MAC protocol of Infrastructure-less Cellular V2X Communication in Crash Warning Application,” The 81st National Convention of IPSJ, 7E-06, Fukuoka, Mar. 2019.

[15] Takeshi Hirai, Tutomu Murase, “QoS Improvement of V2X Communications for Crash Warning Applications by Combining Multiple SINR Improvement Methods,” IEICE Technical Report, IN2018-37, Miyagi, Sep. 2018.

[16] Takeshi Hirai, Tutomu Murase, “Performance Impact on Communication Quality with Considering Transient Periods of Organizing Clusters in Node-Clustering Communication Method in V2X for Crash Warning, 電気・電子・情報関係学会東海支部連合大会, C3-6, Aichi, Sep. 2018.

[17] Takeshi Hirai, Tutomu Murase, “Decentralized Congestion Control based on Characteristic of Crash Warning Applications in V2X Communications,” IPSJ DICOMO 2018, 3B-4, Fukui, July 2018.

【Domestic conference (Non-first author)】

[18] Kai Takahashi, Yuto Konuma, Shigeo Shioda, Takeshi Hirai, Tutomu Murase, “Performance Analysis of a V2X-Based Crash Warning System Using a Spatial Point Process,” IEICE General Conference, 2019, B-11-6, Mar. 2019.

[19] Kai Takahashi, Yuto Konuma, Shigeo Shioda, Takeshi Hirai, Tutomu Murase, “Performance Analysis of a V2X-Based Crash Warning Application Using a Spatial Point Process Model,” IEICE Technical Report, vol. 118, no. 466, IN2018-121, pp. 223-228, Okinawa, Mar. 2019.

④ Fellowships and Awards
【Fellowships】

[1] 平井健士, 日本学術振興会特別研究員 (DC2),

“衝突事故警告システムにおける混雑した帯域でも高品質な電力重畳型車車間通信の検討”
2020 年 4 月.

【Awards】

[2] 平井健士, 電子情報通信学会学術奨励賞
“Performance Evaluation on MAC Layer Protocol in Crash Warning Application using PC5-based Cellular-V2X mode4”
2020 年 3 月.

[3] 平井健士, 電子情報通信学会ネットワークシステム研究会英語セッション奨励賞,
“Performance Evaluation on MAC Layer Protocol in Crash Warning Application using PC5-based Cellular-V2X mode4”
2019 年 10 月.

[4] Takeshi Hirai, IEEE VTS Tokyo Chapter 2019 Young Researcher's Encouragement Award,
“NOMA Concept for PC5-based Cellular-V2X mode 4 in Crash Warning System”
2019 年 9 月.

[5] 平井健士, 電子情報通信学会東海支部学生研究奨励賞受賞
2018 年 6 月.

[6] 平井健士, 日本学生支援機構奨学金返還免除, 全額
2018 年 6 月.

[7] 平井健士, 名古屋大学ホシザキ奨学金 (給付型), 月額 12 万円
2018 年度–2019 年度, 2018 年 6 月.

⑤ Research Grants
【Grants for research】

[1] 平井健士, 日本学術振興会特別研究員奨励金(DC2), 令和 2 年度
「衝突事故警告システムにおける混雑した帯域でも高品質な電力重畳型車車間通信の検討」
助成金額 1,000 千円, 研究代表者.

[2] 平井健士, 村瀬勉, 塩田茂雄, 計宇生, 策力木格, 日立財団倉田奨励金, 令和 2 年度
「安全安心な自律飛行ドローンシステムを構築するための車両間無線通信性能の発展に関する研究」
助成金額 1,000 千円, 研究代表者.

【Grants for studying abroad】

[3] 平井健士, トビタテ！留学 JAPAN, 令和元年度
「米国ラトガース大学 Wireless Information Network Laboratory (WINLAB)への留学助成」
助成金額 570 千円, 研究代表者.

【Travel grants for international conference】

[4] 平井健士, スズキ財団令和元年度研究者海外研修助成, 令和元年度
「国際会議論文 “NOMA Concept for PC5-based Cellular-V2X mode 4 in Crash Warning System”に対する 2019 IEEE 90th Vehicular Technology Conference (IEEE VTC2019-Fall)への海外渡航費助成」
助成金額 150 千円, 研究代表者.

[5] 平井健士, 立石科学技術振興財団 2019 年度後期国際交流助成, 令和元年度
「国際会議論文 “Performance Characteristics of Sensing-based SPS of PC5-based C-V2X Mode 4 in Crash Warning Application under Congestion”に対する 2019 IEEE Intelligent Transportation Systems Conference (IEEE ITSC 2019)への海外渡航費助成」
助成金額 287 千円, 研究代表者.

[6] 平井健士, 電気通信普及財団海外渡航旅費援助, 平成 30 年度
「国際会議論文 “Frame Relaying for Low Rates of Received Frames in Crash Warning Application using V2X communication”に対する 25th World Congress on Intelligent Transport Systems (ITS World Congress 2018)への海外渡航費助成」
助成金額 290 千円, 研究代表者.

【Grants for journal publications】

[7] 平井健士, 中部電気利用基礎研究振興財団出版助成, 令和 2 年度
「IEEE Access 論文 “Performance Evaluation of NOMA for Sidelink Cellular-V2X Mode 4 in Driver Assistance System with Crash Warning”に対する論文出版

費助成」
助成金額 120 千円, 研究代表者.

[8] 平井健士, エディテージ研究費 2018 年 11 月分英文校正グラント, 平成 30 年度
「研究論文英文添削費用助成」
助成金額 50 千円, 研究代表者.

[9] 平井健士, 中部電気利用基礎研究振興財団出版助成, 平成 30 年度
「IEICE Communication Express (IEICE ComEx)論文 “Node-Clustering Communication Method to improve QoS in V2X Communications in Crash Warning Applications”の論文出版費助成」
助成金額 41 千円, 研究代表者.

⑥ Patents

[1] 平井健士, 村瀬勉,「グループ通信方式」特開 2017-146790 (特願 2016-028142), 2017 年 8 月.